Biogeochemistry Across Spatiotemporal Scales: The Role of Reactive Interfaces in Modulating Landscape Scale Contaminant Fluxes

by

Frederick Yiu-Sum Cheng

A thesis
presented to the University of Waterloo
in fulfillment of the
thesis requirement for the degree of
Doctor of Philosophy
in
Civil Engineering

Waterloo, Ontario, Canada, 2022

Examining Committee Membership

The following served on the Examining Committee for this thesis. The decision of the Examining Committee is by majority vote.

External Examiner	Erin Hotchkiss Associate Professor Department of Biological Sciences Virginia Polytechnic Institute and State University
Supervisor	Nandita Basu Professor Department of Civil and Environmental Engineering Department of Earth and Environmental Sciences University of Waterloo
Internal Member	James Craig Associate Professor Department of Civil and Environmental Engineering University of Waterloo
Internal-External Member	Philippe Van Cappellen Professor Department of Earth and Environmental Sciences University of Waterloo
Internal-External Member	Maria Strack Professor Department of Geography and Environmental Management University of Waterloo

Author's Declaration

This thesis consists of material all of which I authored or co-authored: see Statement of Contributions included in the thesis. This is a true copy of the thesis, including any required final revisions, as accepted by my examiners. I understand that my thesis may be made electronically available to the public.

Statement of Contributions

The various chapters in my dissertation had contributions from different research collaborators and co-authors:

Chapter 2: Danyka Byrnes, and Drs. Kimberly Van Meter and Nandita Basu contributed to the research of this chapter. The following chapter is based on the following published article:

Cheng, F., Van Meter, K., Byrnes, D., and Basu, N. 2020. Maximizing US nitrate removal through wetland protection and restoration. Nature. doi:10.1038/s41586-020-03042-5

N.B.B., K.J.V.M. and F.Y.C. conceived the study. N.B.B., F.Y.C. and K.J.V.M. developed the wetland N removal models. F.Y.C. ran simulations for current wetland N removal, and K.J.V.M. carried out the wetland restoration simulations and cost analysis. D.K.B., K.J.V.M. and N.B.B. provided N input data for the model simulations.

Chapter 3: The following chapter is written based on a prepared manuscript, that has not been submitted for peer-review with my co-authors Junehyeong Park, Dr. Mukesh Kumar and Dr. Nandita Basu.

N.B.B. and F.Y.C. conceived the study. M.K. and J.P. processed and provided the remote sensing data for the wetlandscapes. N.B.B., and F.Y.C. developed the wetland hydrologic and N removal models. F.Y.C. ran simulations for current wetland N removal.

Chapter 4: Drs. Heather Preisendanz, Michael Mashtare, Linda Lee, and Nandita Basu contributed to the research of this chapter. The following chapter is based on the following published article:

Cheng, F., Preisendanz, H., Mashtare, M., Lee, L., and Basu, N. 2021. Nevertheless, they persisted: Can hyporheic zones increase the persistence of estrogens in streams? Water Resources Research. doi:10.1029/2020WR028518

F.Y.C., and N.B.B. conceived of the study. F.Y.C. and N.B.B. conducted the data analysis and developed the estrogen hyporheic zone model. F.Y.C. ran simulations and calibration of the model. M.M., H.G., and L.L. collected the hydrologic and water quality data and analyzed the samples.

Chapter 5: The following chapter is written based on a prepared manuscript, that has not been submitted for peer-review with my co-authors Dr. Nandita Basu and Dr. Amilcare Porporato.

N.B.B. and F.Y.C. conceived the study. F.Y.C., N.B.B. developed the modelling framework with major inputs from A.P. Analysis of the model was conducted by F.Y.C. F.Y.C and N.B.B. wrote the manuscript.

Abstract

The intensification of agricultural and urban activities has been accompanied by increased fluxes of nutrients to inland and coastal waters, leading to concerns of eutrophication and drinking water contamination. Certain areas in the landscape can intercept, remove or retain nutrients and other contaminants at much higher rates than the overall landscape. While there has been extensive work documenting the extremely dynamic behaviour of these ***reactive interfaces***, watershed-scale models are unable to explicitly capture the spatiotemporal heterogeneity of reactive interfaces. In this thesis, I developed methodologies to explicitly represent different reactive interfaces across the upland-stream continuum using a combination of data synthesis and deterministic modelling.

In Chapter 2, I quantify the role of wetlands in retaining nitrogen (N) at the watershed across the US at the annual time scale. Here, I combined spatially explicit datasets of nitrogen surplus and wetland location to demonstrate that current N removal by US wetlands is limited by a spatial disconnect between high-density wetland areas and N hotspots. Simulations of wetland restoration scenarios also showed that spatially targeting areas of high N surplus can greatly increase N retention compared to current practices.

I further explore the behaviour of wetland N retention with a focus on sub-annual temporal dynamics in Chapter 3. Using a reduced complexity model with thirty years of remotely sensed wetland inundation levels across eight wetlandscapes in the US, I show that the consideration of transient hydrologic dynamics can increase N retention estimates compared to steady-state models. This effect was more apparent in smaller, isolated wetlands, where the limited outflows of water limited the loss of N and increased the time for denitrification in the wetland.

Next, I explore another common reactive interface found in agroecosystems: the hyporheic zone (HZ). While the HZ is often considered a sink for agricultural contaminants such as nitrogen, its role in modulating other contaminants is less clear. In Chapter 4, I developed a mechanistic HZ model to quantify the fate and transport of estrogen, an emerging contaminant in agroecosystems. Using the model, I show that the HZ actually functions as a source and increases the temporal persistence of estrogens in the stream network.

Finally, I developed a coupled CN biogeochemical model to a humid water balance model to further our understanding of water fluctuations on nitrogen fluxes in Chapter 5. While the water table is commonly ignored in CN modeling, I show that consideration of water table fluctuations modify the CN export by modulating the redox conditions and altering the transport mechanisms and should not be ignored.

My results show that reactive interfaces have complex spatiotemporal behaviours driven by the interactions between the hydrological and biogeochemical processes. Through the use of data synthesis and deterministic modelling, I quantify various environmental factors that contribute to the functionality of reactive interfaces and developed methodologies that can help decision makers predict and mitigate the contaminant fluxes from agroecosystems to protect our water resources.

Acknowledgements

This research has been financially supported by the University of Waterloo, NSERC's generous scholarship, and the AGU Horton Research Grant. I have been very fortunate to have gone through my time here at Waterloo with little worry about finances.

I would like to thank Nandita Basu for being an amazing mentor since I was an undergraduate co-op student and all the way through my PhD journey. One of the main reasons that I was willing to stay at Waterloo for both my graduate degrees was because I knew she would provide the type of guidance and support that would let me grow as a researcher. Coming up with new ideas and solutions was always a joy and I will miss our regular chats. In addition to always providing invaluable insight to my academic problems and questions, your care and interest in me beyond research meant the world to me.

Finally, while the Waterloo chapter of my career might finally be over after 12 years, I couldn't have gone through it without the support of so many people there. First, there was the Basu Lab which started with only three graduate students when I joined as a co-op student, and grew to a bustling group with the amazing people today and everyone that's joined and moved on in-between. Special thanks to my office mates Kim, Darcy, and Danyka were instrumental in keeping me sane. Next, the awesome administrative staff of CEE and especially Lisa was always there to help and make my life easier. Finally, there was my ballroom family Kyra, Venessa, and François – no words can express how much you've all helped me throughout my PhD, but especially during the pandemic.

Finally, I am grateful to my family for supporting me throughout my degree and reminding me to work a bit less. My last thanks go to my mom, who couldn't be here to see me through my degree, but I hope I've made you proud.

Table of Contents

List of Figures

List of Tables

Chapter 1

Introduction

In the last century, intensification of agricultural activities to support growing global populations has come at a significant environmental cost (Anderson et al., 2002). Globally, loading of agricultural contaminants such as nutrients and emerging contaminants into the environment has been greatly accelerated with increased commercial fertilizer use and large-scale livestock operations (Gruber & Galloway, 2008), with growing evidence that these along with other perturbations are exceeding the planet's capacity to maintain human and ecosystem health (Steffen et al., 2015). For example, excess nutrients from agricultural fields have been linked to increasing occurrences of eutrophication, harmful algal blooms and the development of large hypoxic zones in inland and coastal waters (Rabalais et al., 2010; Smith, 2003). To combat eutrophication, numerous plans to have been developed to mitigate nitrogen and phosphorus loads for water bodies worldwide, including Lake Erie in Canada, the Gulf of Mexico in the USA, the Mediterranean and Baltic Seas in Europe, and the East China Sea (Selman & Greenhalgh, 2009). Although there have been successes in controlling point sources of contaminants (e.g. urban wastewater treatment plants), non-point source pollution - especially that from agricultural lands - continues to pose a significant challenge (Carey & Migliaccio, 2009; Schoumans et al., 2014). Thus, there remains a critical need to better understand the transport and retention of agricultural contaminants across the landscape to better develop management solutions to reduce these fluxes from agroecosystems.

Biogeochemical processes within the landscape can naturally retain and transform agricultural non-point source pollution and thus have the capacity to protect downstream waters. It is increasingly

recognized that certain features in the landscape are more effective at processing contaminants due to significantly greater biogeochemical rates than their surroundings (McClain et al., 2003; Mitsch et al., 2005; Seitzinger et al., 2006). Such high reactivity zones often occur at the interface between two landscape elements – for example, the water table between the saturated and unsaturated zones in the subsurface (Holden & Fierer, 2005), the riparian zone between a stream and its upland (Mayer et al., 2007), and the hyporheic zone between the stream and its sediment (Harvey et al., 2013; Zarnetske et al., 2012). These ***reactive interfaces*** in the landscape are characterized by steep gradients in chemical, physical and biological properties and enhanced biogeochemical activity (**Figure 1.1**). McClain et al. (2003) referred to RIs as spatially localized 'hotspots' that are effective at removing contaminants due to the confluence of relatively high levels of contaminant input, and the appropriate environmental conditions (e.g. redox levels, temperature, substrate availability) for biogeochemical reactions.

In agroecosystems, many best management practices are implemented to create or enhance reactive interfaces that will attenuate the export of agricultural contaminants to the environment – for example, constructed wetlands or vegetated buffer strips facilitate nitrate uptake and denitrification (Jordan et al., 2011; Verhoeven et al., 2006), and drainage ditches enhance P sedimentation and sorption (Macrae et al., 2003; Smith & Huang, 2010). While these management strategies are becoming more prevalent, there remains a need to better understand the biogeochemical functioning of these reactive interfaces under transient climatic and management conditions. Additionally, it is important to recognize that reactive interfaces do not stand alone in the environment, but are part of a larger reactive transport network in the landscape. However, our understanding of this larger integrated system is limited, and there is a strong need to both characterize and quantify the impact of cascades of reactive interfaces across the field-stream continuum. Such enhanced science-based understanding is critical to better predict the behaviour of RIs and thus to guide the development and implementation of BMPs on a wider scale. In this thesis, my goal is to advance the quantitative understanding of coupled biogeochemical processes mediated by RIs in agroecosystems using parsimonious models.

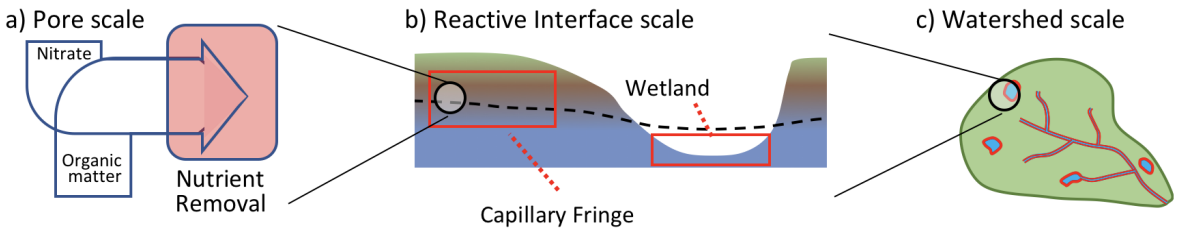

Figure 1.1.1 Reactive interfaces in agroecosystems: From pore scale (a) to the reactive interface scale (b) and the watershed scale (c).

1.1 Research Needs

1.1.1 Reactive Interfaces in Agroecosystems

Previous research on RIs has primarily focused on field-scale hotspot identification by quantifying reaction rates at discrete points in time (Bernhardt et al., 2017). What is often missed in these studies is that hotspots can exhibit a range of behaviour or even contrasting responses through time as a function of changing environmental conditions (Krause et al., 2017). For example, sediments in wetlands can act as a sink of phosphorus during high-flow conditions, but as a source during low-flow conditions (Dupas et al., 2015; Nair et al., 2015). In the riparian zone, CO_2 production may increase when the soil is wetted if soil was initially very dry (Harms & Grimm, 2012); however, if the soil is wet at the start, increases in saturation can suppress the activity of aerobic bacteria and lower the CO_2 flux (Vidon, 2017). To address this issue, Bernhardt et al. (2017) argued that these landscape features should be conceptualized as "control points" that have variable biogeochemical rates and can even switch between nutrient sources and sinks as a function of various system thresholds. While field-scale studies have established the fluctuating behaviour of RIs, most watershed models that incorporate the effects of RIs like riparian buffers and wetlands still consider them ubiquitously as sinks (Krause et al., 2017).

Also lacking from the literature is an understanding of the spatial arrangement of these hotspots that would enable scaling from the individual RI to the ecosystem scale. Bernhardt et al. (2017) proposed that modelling or statistical approaches that use the process understanding gained from decades of

hotspot research and enable scientists to scale up the aggregated functioning of RIs to the ecosystem scale is required. My research aims to address this need by developing a deterministic modelling framework that attempts to integrate the spatiotemporal patterns of RI biogeochemical functioning at the catchment scale.

The focus of this thesis will be on three major RIs: 1) the ***water table,*** where nutrient and carbon rich water from the oxic unsaturated zone meets the anoxic saturated groundwater in the subsurface, 2) ***wetlands***, saturated areas in the landscape that act as an interface between groundwater and surface water pathways that are large stores of organic carbon and receptors of nutrients, and 3) the ***hyporheic zone***, where sediment-groundwater-surface water interactions occur in the stream. These RIs are zones of extremely dynamic hydrological fluctuations and sharp gradients of redox and chemical concentrations that enhance biogeochemical processes both spatially and temporally. The three RIs chosen for this thesis are commonly found in agroecosystems and span the upland-stream continuum.

1.1.2 Reactive Transport Modelling of Nutrients in Watersheds

Current watershed-scale models that quantify nutrient dynamics lack the ability to explicitly represent reactive interfaces (Krause et al., 2017). A recent meta-analysis found that commonly used watershed nutrient export models (e.g. SWAT, INCA, etc.) typically discretize the landscape into representative areas such as a hydrologic response units (HRU) (Wellen et al., 2015). While often sufficient for the purposes of modelling streamflow, this aggregation of landscape characteristics into effective parameters over wide spatial scales prevents the model from capturing the heterogeneity and hotspot behaviour of reactive interfaces (Bracmort et al., 2006). First, all RIs within the HRUs (riparian buffers, wetlands, etc.) are often treated as temporally static units with annual percent removal rates that are also spatially unvarying. In addition, the representation of BMPs is typically based on empirical nutrient retention rates estimated from field studies, and scenario analyses provide estimates of the watershed scale effectiveness of BMPs (Alexander et al., 2002; Wade et al., 2002; Wagena et al., 2017). The lack of a process-based understanding of nutrient removal in these models make it difficult to differentiate the behaviour of different sub-groups of RIs (e.g. upland soil vs riparian soil, large wetland vs small wetland etc.). Thus, explicitly representing the cascade of RIs along the upland to stream continuum in watershed models can improve confidence in watershed scale predictions of BMP effectiveness.

The need to more explicitly incorporate the complexities of RI behaviour into catchment-scale models is now increasingly being recognized by many researchers (Krause et al. 2017). It has been argued that one of the main reasons RIs are not explicitly represented in catchment biogeochemical models is because of the difficulty in integrating processes across ecosystem boundaries (such as between wetlands and their upland areas, or between groundwater and streams). In a recent review of river representation in watershed models, Helton et al. (2011) showed that many current modelling approaches of river biogeochemistry lack the transient but critical connections to the underlying hyporheic zone, the surrounding riparian zones, or floodplains in watershed models. The other complexity in effectively integrating RIs into watershed models arises from the temporal dynamics of reactive interfaces that lead to their behaviour changing over time (from sources, to mere transporters, to sinks) as a function of hydrologic and other controls. For example, Wollheim et al. (2017) have shown that infrequent, but intense, flood events can cause significant amounts of organic carbon to be 'shunted' through the river network, thus bypassing nutrient removal processes in the hyporheic zone. A few studies have, however, have tried to quantify the aggregate watershed response of RIs. Pinay et al. (2015), for example, have proposed a conceptual framework that combines high-resolution geomorphic data to identify potential denitrification zones in the landscape with known hydrologic flow paths. Within their framework, they propose the use of dimensionless numbers (the Damkohler and Peclet numbers) to quantify the ratio between reaction and transport timescales and determine the extent of denitrification. However, they do not consider dynamic effects such as fluctuating water tables on the RI - effects that can flip RIs between source and sink behaviour. Focusing on the hyporheic zone, Gomez-Velez and Harvey (2015) were the first to provide a deterministic modelling framework to predict denitrification potential across the entire stream network in the Mississippi River basin. They used a novel approach where hyporheic residence times were estimated by using river bedform morphology, and denitrification potential was estimated by comparing hyporheic residence times to reaction times. However, they only explored the sink function of the hyporheic zone, while it has been shown that for elements like P the hyporheic zone can act as both source and sink (Palmer-Felgate et al., 2010; Withers & Jarvie, 2008). My goal is to build on this body of work and develop methodologies to explicitly represent reactive interfaces at the watershed scale across the upland-stream continuum and further our quantitative understanding of the coupled biogeochemical and hydrological processes at these interfaces.

1.1.3 Objectives

The overall objective of my research is to quantify the role of reactive interfaces in modulating landscape-scale biogeochemical fluxes, with a specific focus on both natural and managed RIs in agroecosystems. This dissertation focuses on several agricultural contaminants (namely carbon, nitrogen and estrogen), but the results may be relevant to a broader suite of contaminants that can be found in agroecosystems. The dissertation will be structured through the following four objectives:

Objective 1: Quantify the role of wetlands in retaining nitrogen at the continental scale and the impact of different restoration strategies for optimal N retention.

Objective 2: Quantify the role of wetland size, climate, and downstream connectivity on nitrogen retention at the sub-annual scale.

Objective 3: Quantify the role of hyporheic zone characteristics on the spatial and temporal persistence of estrogens in stream networks.

Objective 4: Quantify the role of rainfall and water table fluctuations in controlling carbon-nitrogen dynamics at the water table, with a specific focus on humid ecosystems under intensive agriculture.

Chapter 1 References

Alexander, R. B., Johnes, P. J., Boyer, E. W., & Smith, R. A. (2002). A comparison of models for estimating the riverine export of nitrogen from large watersheds. *Biogeochemistry*, *57–58*(1), 295–339. https://doi.org/10.1023/A:1015752801818

Anderson, D. M., Glibert, P. M., & Burkholder, J. M. (2002). Harmful algal blooms and eutrophication: Nutrient sources, composition, and consequences. *Estuaries*, *25*(4), 704–726. https://doi.org/10.1007/BF02804901

Bernhardt, E. S., Blaszczak, J. R., Ficken, C. D., Fork, M. L., Kaiser, K. E., & Seybold, E. C. (2017). Control Points in Ecosystems: Moving Beyond the Hot Spot Hot Moment Concept. *Ecosystems*. https://doi.org/10.1007/s10021-016-0103-y

Bracmort, K., Arabi, M., Frankenberger, J., Engel, B., & Arnold, J. (2006). Modeling long-term water quality impact of structural BMPs. *Transactions of the ASABE*, *49*(2), 367–374.

Carey, R. O., & Migliaccio, K. W. (2009). Contribution of Wastewater Treatment Plant Effluents to Nutrient Dynamics in Aquatic Systems: A Review. *Environmental Management*, *44*(2), 205–217. https://doi.org/10.1007/s00267-009-9309-5

Dupas, R., Gruau, G., Gu, S., Humbert, G., Jaffrézic, A., & Gascuel-Odoux, C. (2015). Groundwater control of biogeochemical processes causing phosphorus release from riparian wetlands. *Water Research*, *84*, 307–314. https://doi.org/10.1016/j.watres.2015.07.048

Gomez-Velez, J. D., Harvey, J. W., Cardenas, M. B., & Kiel, B. (2015). Denitrification in the Mississippi River network controlled by flow through river bedforms. *Nature Geoscience*, *8*(12), 941–945. https://doi.org/10.1038/ngeo2567

Gruber, N., & Galloway, J. N. (2008). An Earth-system perspective of the global nitrogen cycle. *Nature*, *451*(7176), 293–296. https://doi.org/10.1038/nature06592

Hannah, R., D'Aco, V. J., Anderson, P. D., Buzby, M. E., Caldwell, D. J., Cunningham, V. L., et al. (2009). Exposure assessment of 17α-ethinylestradiol in surface waters of the United States and Europe. *Environmental Toxicology and Chemistry*, *28*(12), 2725–2732. https://doi.org/10.1897/08-622.1

Harms, T. K., & Grimm, N. B. (2012). Responses of trace gases to hydrologic pulses in desert floodplains. *Journal of Geophysical Research: Biogeosciences*, *117*(G1). https://doi.org/10.1029/2011JG001775

Harvey, J. W., Böhlke, J. K., Voytek, M. A., Scott, D., & Tobias, C. R. (2013). Hyporheic zone denitrification: Controls on effective reaction depth and contribution to whole-stream mass balance: Scaling hyporheic flow controls on stream denitrification. *Water Resources Research*, *49*(10), 6298–6316. https://doi.org/10.1002/wrcr.20492

Helton, A. M., Poole, G. C., Meyer, J. L., Wollheim, W. M., Peterson, B. J., Mulholland, P. J., et al. (2011). Thinking outside the channel: modeling nitrogen cycling in networked river ecosystems. *Frontiers in Ecology and the Environment*, *9*(4), 229–238. https://doi.org/10.1890/080211

Holden, P. A., & Fierer, N. (2005). Microbial Processes in the Vadose Zone. *Vadose Zone Journal*, *4*(1), 1–21. https://doi.org/10.2136/vzj2005.0001

Jordan, S. J., Stoffer, J., & Nestlerode, J. A. (2011). Wetlands as sinks for reactive nitrogen at continental and global scales: A meta-analysis. *Ecosystems*, *14*(1), 144–155. https://doi.org/10.1007/s10021-010-9400-z

Krause, S., Lewandowski, J., Grimm, N. B., Hannah, D. M., Pinay, G., McDonald, K., et al. (2017). Ecohydrological interfaces as hot spots of ecosystem processes. *Water Resources Research*, *53*(8), 6359–6376. https://doi.org/10.1002/2016WR019516

Macrae, M. L., English, M. C., Schiff, S. L., & Stone, M. A. (2003). Phosphate retention in an agricultural stream using experimental additions of phosphate. *Hydrological Processes*, *17*(18), 3649–3663. https://doi.org/10.1002/hyp.1356

Mayer, P. M., Reynolds, S. K., McCutchen, M. D., & Canfield, T. J. (2007). Meta-Analysis of Nitrogen Removal in Riparian Buffers. *Journal of Environment Quality*, *36*(4), 1172. https://doi.org/10.2134/jeq2006.0462

McClain, M. E., Boyer, E. W., Dent, C. L., Gergel, S. E., Grimm, N. B., Groffman, P. M., et al. (2003). Biogeochemical hot spots and hot moments at the interface of terrestrial and aquatic ecosystems. *Ecosystems*, *6*(4), 301–312. https://doi.org/10.1007/s10021-003-0161-9

Mitsch, W. J., Day, J. W., Zhang, L., & Lane, R. R. (2005). Nitrate-nitrogen retention in wetlands in the Mississippi River Basin. *Ecological Engineering*, *24*(4), 267–278. https://doi.org/10.1016/j.ecoleng.2005.02.005

Nair, V. D., Clark, M. W., & Reddy, K. R. (2015). Evaluation of Legacy Phosphorus Storage and Release from Wetland Soils. *Journal of Environmental Quality*, *44*(6), 1956–1964. https://doi.org/10.2134/jeq2015.03.0154

Palmer-Felgate, E. J., Mortimer, R. J. G., Krom, M. D., & Jarvie, H. P. (2010). Impact of Point-Source Pollution on Phosphorus and Nitrogen Cycling in Stream-Bed Sediments. *Environmental Science & Technology*, *44*(3), 908–914. https://doi.org/10.1021/es902706r

Pinay, G., Peiffer, S., De Dreuzy, J.-R., Krause, S., Hannah, D. M., Fleckenstein, J. H., et al. (2015). Upscaling Nitrogen Removal Capacity from Local Hotspots to Low Stream Orders' Drainage Basins. *Ecosystems*, *18*(6), 1101–1120. https://doi.org/10.1007/s10021-015-9878-5

Rabalais, N. N., Díaz, R. J., Levin, L. A., Turner, R. E., Gilbert, D., & Zhang, J. (2010). Dynamics and distribution of natural and human-caused hypoxia. *Biogeosciences*, *7*(2), 585–619. https://doi.org/10.5194/bg-7-585-2010

Schoumans, O. F., Chardon, W. J., Bechmann, M. E., Gascuel-Odoux, C., Hofman, G., Kronvang, B., et al. (2014). Mitigation options to reduce phosphorus losses from the agricultural sector and improve surface water quality: A review. *Science of The Total Environment*, *468–469*, 1255–1266. https://doi.org/10.1016/j.scitotenv.2013.08.061

Seitzinger, S., Harrison, J. A., Böhlke, J. K., Bouwman, A. F., Lowrance, R., Peterson, B., et al. (2006). Denitrification across landscapes and waterscapes: A synthesis. *Ecological Applications*, *16*(6), 2064–2090. https://doi.org/10.1890/1051-0761(2006)016[2064:DALAWA]2.0.CO;2

Selman, M., & Greenhalgh, S. (2009). *Eutrophication: Policies, Actions, and Strategies to Address Nutrient Pollution* (3) (p. 16).

Smith, D. R., & Huang, C. (2010). Assessing Nutrient Transport Following Dredging of Agricultural Drainage Ditches. *Transactions of the ASABE*, *53*(2), 429–436. https://doi.org/10.13031/2013.29583

Smith, V. H. (2003). Eutrophication of freshwater and coastal marine ecosystems a global problem. *Environmental Science and Pollution Research*, *10*(2), 126–139. https://doi.org/10.1065/espr2002.12.142

Steffen, W., Richardson, K., Rockström, J., Cornell, S. E., Fetzer, I., Bennett, E. M., et al. (2015). Planetary boundaries: Guiding human development on a changing planet. *Science*, *347*(6223), 1259855. https://doi.org/10.1126/science.1259855

Verhoeven, J., Arheimer, B., Yin, C., & Hefting, M. (2006). Regional and global concerns over wetlands and water quality. *Trends in Ecology & Evolution*, *21*(2), 96–103. https://doi.org/10.1016/j.tree.2005.11.015

Vidon, P. (2017). Not all riparian zones are wetlands: Understanding the limitation of the “wetland bias” problem. *Hydrological Processes*, *31*(11), 2125–2127. https://doi.org/10.1002/hyp.11153

Wade, A. J., Durand, P., Beaujouan, V., Wessel, W. W., Raat, K. J., Whitehead, P. G., et al. (2002). A nitrogen model for European catchments: INCA, new model structure and equations. *Hydrology and Earth System Sciences*, *6*(3), 559–582. https://doi.org/10.5194/hess-6-559-2002

Wagena, M. B., Bock, E. M., Sommerlot, A. R., Fuka, D. R., & Easton, Z. M. (2017). Development of a nitrous oxide routine for the SWAT model to assess greenhouse gas emissions from agroecosystems. *Environmental Modelling & Software*, *89*, 131–143. https://doi.org/10.1016/j.envsoft.2016.11.013

Wellen, C., Kamran-Disfani, A.-R., & Arhonditsis, G. B. (2015). Evaluation of the Current State of Distributed Watershed Nutrient Water Quality Modeling. *Environmental Science & Technology*, *49*(6), 3278–3290. https://doi.org/10.1021/es5049557

Withers, P. J. A., & Jarvie, H. P. (2008). Delivery and cycling of phosphorus in rivers: A review. *Science of The Total Environment*, *400*(1), 379–395. https://doi.org/10.1016/j.scitotenv.2008.08.002

Wollheim, W. M., Mulukutla, G. K., Cook, C., & Carey, R. O. (2017). Aquatic Nitrate Retention at River Network Scales across Flow Conditions Determined Using Nested In Situ Sensors. *Water Resources Research*, n/a-n/a. https://doi.org/10.1002/2017WR020644

Zarnetske, J. P., Haggerty, R., Wondzell, S. M., Bokil, V. A., & González-Pinzón, R. (2012). Coupled transport and reaction kinetics control the nitrate source-sink function of hyporheic zones. *Water Resources Research*, *48*(11), n/a-n/a. https://doi.org/10.1029/2012WR011894

Chapter 2

Maximizing US Nitrate Removal Through Wetland Protection and Restoration

Chapter 2 Abstract

Growing populations and agricultural intensification have led to elevated riverine nitrogen (N) loads, groundwater contamination, and increases in the incidence of coastal hypoxia.[1] While recent work has pointed to the potential for individual wetlands to improve water quality,[2–9] little is known regarding current magnitudes of wetland N removal at the landscape scale. Here, we use National Wetland Inventory data and 5-km grid-scale estimates of N inputs and outputs to demonstrate that current N removal by U.S. wetlands (~ 860 ± 160 ktons of N y^{-1}) is limited by a spatial disconnect between high-density wetland areas and N hotspots. Our model simulations suggest that a spatially targeted, 10% increase in U.S. wetland area (5.1 million ha) would double wetland N removal. This increase would provide an estimated 54% decrease in N loading in nitrate-impacted watersheds such as the Mississippi River Basin. The costs of this increase in area would be approximately US$3.3 billion annually across the U.S.—nearly twice the cost of wetland restoration on non-agricultural, undeveloped land, but providing approximately 40 times more N removal. These results suggest that water quality improvements should be considered when creating policy regarding wetland restoration and protection.

2.1 Introduction

Increased nutrient loads have led to an increasing incidence of harmful algal blooms (HABs) and coastal hypoxia, from the Chesapeake Bay and Gulf of Mexico in North America, to the Baltic Sea in Europe and the South China Sea in Asia.[1] Low oxygen levels in these hypoxic zones limit biodiversity, degrade ecosystem function, and negatively impact coastal economies.[10] In a warming climate, it is expected that hypoxic zones will grow larger and persist for longer periods, making it of even greater import to decrease export of excess nutrients from intensively managed landscapes to coastal waters.[11]

In the U.S., the policy response to problems of coastal hypoxia as well as groundwater nitrate contamination has focused on a range of interventions to reduce nitrogen (N) loads, from wastewater treatment plant upgrades to on-farm reductions in fertilizer application, construction of riparian buffers, and use of cover crops.[2] Interest has also grown in the use of wetlands to improve water quality, and, in particular, to reduce N loading to downstream waters.[3–7] Since 1989, the USDA alone has spent more than $4.2 billion on wetland restoration and protection, especially through the Conservation Reserve Program and Wetland Reserve Program.[12,13]

Wetland restoration efforts, however, are often carried out in an ad hoc manner, focusing on simply maximizing restored wetland area, or achieving "No Net Loss" of wetland area – a U.S. policy objective initially established in 1989.[14–16] Also, because wetlands provide a host of ecosystem services, from flood prevention and carbon sequestration to provision of critical habitats, restoration projects may focus on a more general reestablishment of ecosystem structure and function rather than on targeted interventions to improve water quality.[17]

Although most studies of wetland N removal have focused on the individual wetland scale, there have increasingly been attempts to estimate more landscape-scale effects.[3,18] Jordan et al. have estimated that U.S. wetlands currently remove approximately 5,800 ktons of N y^{-1}.[19] Mitsch et al. have estimated that restoring 2.2 million ha of wetlands in the Mississippi River Basin would reduce nitrate loading to the Gulf of Mexico by 40%,[4–6] while Fennessy and Craft [9] suggest that 1.3 million ha would be sufficient to achieve this goal. While providing important foundational estimates of the importance of wetlands to surface water quality, these studies have been limited by a lack of spatially explicit N input data. Instead, these studies have assumed mean N loading rates across large

watersheds to quantify N retention, with no explicit consideration of spatial variability in N loading across heterogeneous landscapes.[9,19] Given that N removal by wetlands is known to be a strong function of N loading,[3,4,19] this omission leads to a gap in current understanding of the contribution of wetlands to water quality across diverse land use and management. Other important recent work has attempted, at smaller watershed scales, to estimate wetland N removal through a direct consideration of the spatial positioning of individual wetlands along the river network and the hierarchical network effects of nested wetland catchments.[20,21] This approach, however, is limited by a need for extensive water quality sampling as well as an explicit mapping of wetland connectivity to the river network that does not easily allow for consideration of upland, geographically isolated wetlands.[18,20,22]

In the present study, we use a newly developed dataset of landscape N surplus values, calculated at a 5-km grid scale for the contiguous U.S., to estimate spatially varying N inputs to the more than 30 million individual wetlands included in the U.S. National Wetlands Inventory (NWI) (**Fig. 2.1**). The N inputs to individual wetlands are then used to estimate N removal as a function of wetland size, thus providing spatially varying, continental U.S.-scale estimates of N removal from current wetlands. Here, wetland N removal is defined as the difference between N inputs and N outputs across a wetland and includes both temporary, e.g. plant uptake, and permanent, e.g. denitrification, removal processes.

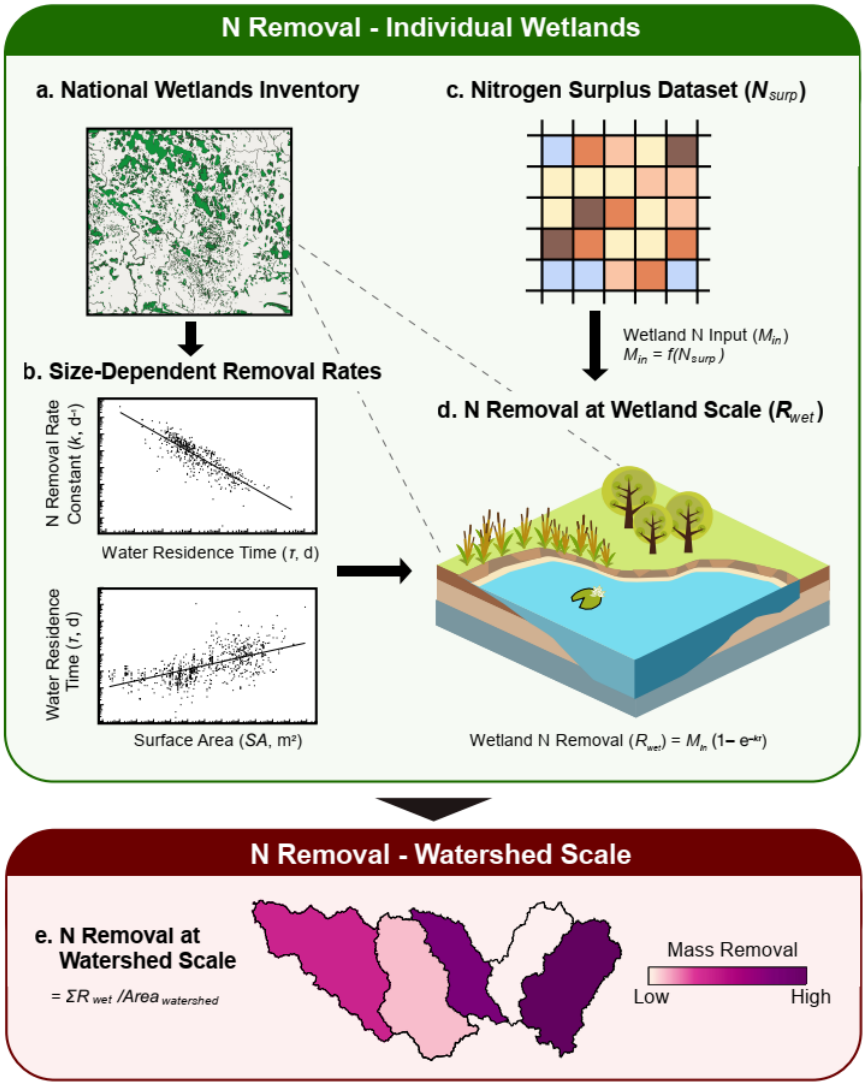

Figure 2.1 A conceptual figure demonstrating our approach to estimating wetland N removal across the U.S. (a). National Wetland Inventory (NWI) is used to identify the locations and sizes of individual wetlands (**b)** Size-dependent removal rates and residence times are estimated for each wetland as a function of surface area. Such estimates are based on a previous study demonstrating that, despite the complexity and heterogeneity of wetland N removal processes across diverse landscapes, there exists a remarkably consistent, inverse relationship between the N removal rate constant and wetland surface area (see Methods). (**c)** Grid-scale N surplus values are used to estimate N mass inputs to individual wetlands as a function of surplus N, catchment area and fraction of N surplus that enters the wetland. (**d)** Wetland N removal is estimated as the product of the incoming N load and the percent removal. (**e)** Watershed-scale N removal is estimated as a summation of N removal from individual wetlands within the watershed.

We next use a modeling approach to simulate spatially explicit scenarios of wetland restoration and to estimate the potential for enhanced wetland N removal across the U.S. In our analysis, we ask the following questions: (i) What is the magnitude of N being removed by current wetlands? (ii) How would a loss of these wetlands impact water quality? (iii) How can we spatially target wetland restoration efforts to maximize N removal and meet goals for water quality? (iv) What would be the costs associated with such restoration?

In **Fig. 2.2a**, we show wetland densities across the contiguous U.S. based on aggregation of NWI wetland areas to the HUC-8 watershed scale. The highest wetland densities in the U.S. are currently found along the Gulf of Mexico (from the Texas playas to Florida's cypress swamps), in the Prairie Pothole Region of Minnesota and North Dakota, and along the eastern seaboard (including the Delmarva and Carolina Bays).

Areas with high wetland densities theoretically have the potential for high rates of N removal, as wetland soils are rich in organic carbon and are frequently anoxic, making them hotspots for denitrification.[23] Our calculations, which take into account relationships between wetland surface area, water residence times, and denitrification rate constants, demonstrate that percent N removal varies widely across HUC-8 watersheds, from minimum values of < 0.05 across large areas of the arid western U.S., to as high as 0.52 in areas of Florida and Minnesota, where wetland densities are high (**Fig. 2.2b**).

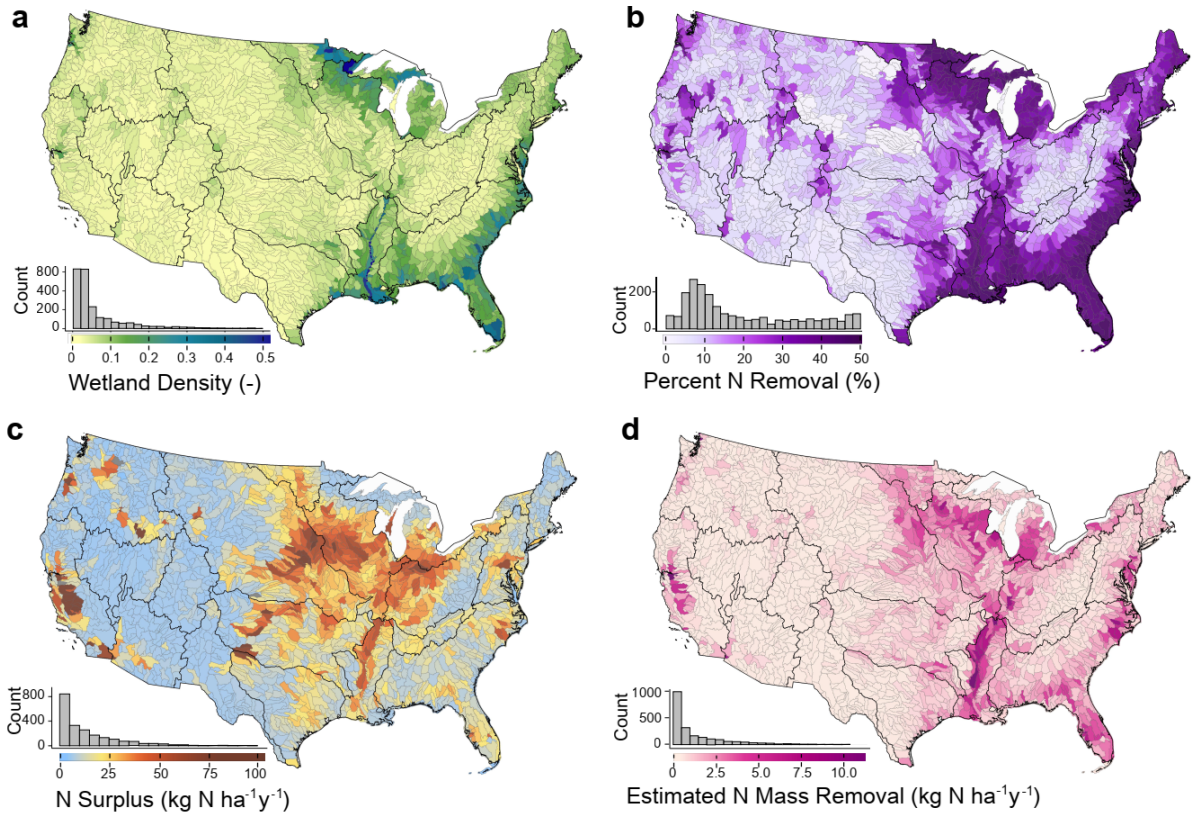

Figure 2.2 Wetland densities, N surplus magnitudes, and wetland N removal across the contiguous U.S. (a) Wetland density (-); (b) Percent wetland N removal; (c) N surplus magnitudes (kg ha^{-1} y^{-1}); (d) Estimated N mass removal by wetlands (kg ha^{-1} y^{-1}). All results aggregated to the HUC-8 scale; (c) and (d) are normalized by watershed area; (b) and (d) are median values from Monte Carlo simulations.

The percent N removal, however, tells only part of the story. The magnitude of N that is actually removed is inherently dependent on the amount of surplus N present within wetland catchment areas. In the present study, the N removal magnitudes of existing wetlands were estimated as the product of the percent removal for individual wetlands and the incoming N load from its upstream catchment area. N surplus magnitudes, which were calculated as the difference between anthropogenic N inputs (N fertilizer, atmospheric N deposition, manure N, biological N fixation of leguminous crops) and non-hydrologic N outputs (crop N production) (**Fig. 2.2c**), vary across regions, with the highest magnitudes being seen in the Upper Mississippi River Basin (**Extended Data Fig. 1 in Appendix A**).

Our results suggest that wetlands across the U.S. are currently removing approximately 860 ± 160 ktons of anthropogenic N y^{-1}, a total that represents approximately 8% of the current landscape N surplus for the contiguous U.S. Areas with the highest removal rates occur in areas where relatively high wetland densities intersect with high-N surplus areas, primarily in HUC-8 watersheds bordering the Mississippi River in Missouri, Arkansas, and Kentucky (**Fig. 2.2d, Extended Data Fig. 2 in Appendix A**). Notably, our results suggest that U.S.-scale wetland N removal masses are an order of magnitude less than the previously estimated 5,800 ktons removal,[19] thus demonstrating the importance of spatially explicit N surplus values in making these estimates.

The maps of current N surplus magnitudes (**Fig. 2.2b**) and wetland densities (**Fig. 2.2a**) suggest that areas with the highest levels of excess N generally have relatively low wetland densities. Indeed, classification of U.S. watersheds based on wetland densities and N surplus magnitudes demonstrates a clear disconnect between nutrient source zones and potential N removal sites (**Fig. 2.3a**). The majority of U.S. HUC-8 watersheds (41%) can be considered "low-input" systems, with both a low N surplus (< 8 kg ha^{-1} y^{-1}) and low wetland densities (< 10% wetland area). Another 8% of watersheds are also low-input, but they have more wetlands (> 10% wetland area), meaning that the wetland N removal potential in these systems is high in relation to surplus N. Importantly, however, we find that 38% of watersheds with N surplus magnitudes in the upper quartile (> 8 kg ha^{-1} y^{-1}) actually fall in the *lowest* quartile for wetland density (< 10% wetland area). These "wetland-limited" watersheds cover an area of approximately 861,000 km^2, nearly 40% of the contiguous U.S. (**Fig. 2.3b**), and the N surplus from this area constitutes approximately 70% of the contiguous U.S. landscape N surplus.

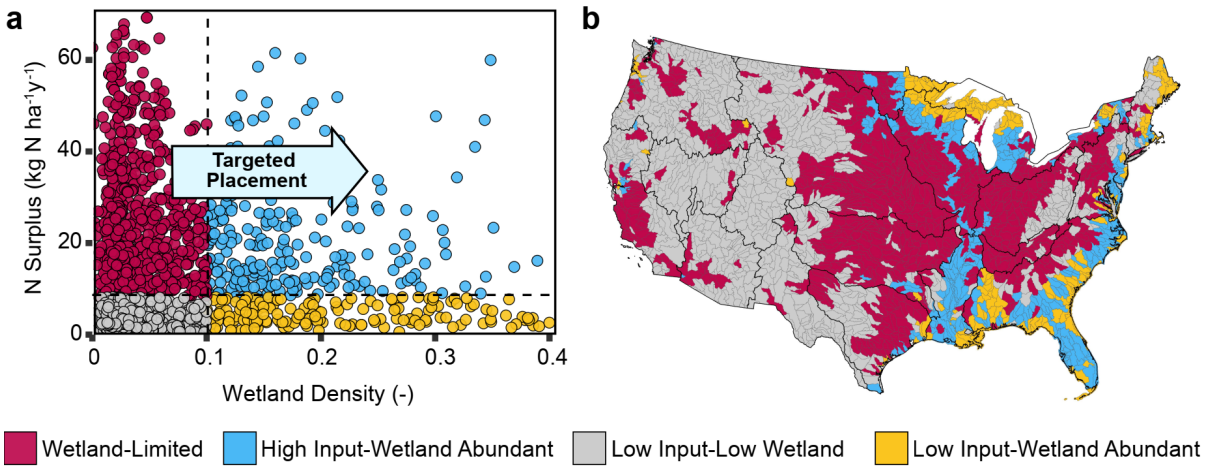

Figure 2.3 Spatial relationships between N source areas and existing wetlands. The figure demonstrates a lack of wetlands in areas that could benefit most from enhanced N removal. (**a**) Each point represents a HUC-8 watershed classified based on relative magnitudes of N surplus and wetland density: (i) Wetland-Limited (red), (ii) High Input-Wetland Abundant (blue), (iii) Low Input-Low Wetland (grey), (iv) Low Input-Wetland Abundant (yellow). The horizontal dashed line corresponds to the mean watershed N surplus magnitude (8 kg ha^{-1} y^{-1}), and the vertical dashed line to a watershed wetland density of 10%. (**b**) Spatial distribution of the four watershed types.

This large "wetland-limited" area of the U.S. suggests that wetland restoration in high-N surplus areas has a strong potential to maximize water quality benefits. To test this hypothesis, we carried out simulations for three wetland restoration scenarios. Under the first scenario (Random Placement, SC1), wetlands are placed randomly across the landscape. Under the second scenario (No Ag Land Loss, SC2) wetlands are placed only on non-agricultural lands, to minimize loss of productive cropland, and under the third scenario (Targeted Restoration, SC3), wetlands are preferentially placed in areas with the highest N surplus values so as to maximize wetland N removal. Under all scenarios, wetland restoration is capped within each grid cell, such that the sum of all wetland areas and wetland contributing areas does not exceed the total area of the cell. As such, no nesting of wetland catchments is assumed. For each scenario, simulations are run across a range of increases in wetland area to estimate resulting increases in wetland N removal and also associated costs (**Fig. 2.4**).

Our results indicate that for all three scenarios, N removal increases linearly up to an approximately 15% increase in wetland area (**Fig. 2.4a**), with the highest removal levels being seen for the Targeted Restoration scenario (SC3). Above a 15% increase in wetland area, rates of increase in N removal for the Targeted scenario begin to flatten as restoration efforts move outside of areas with the highest N

Surplus magnitudes. Costs for the three restoration scenarios also increase in a near-linear fashion (**Fig. 2.4b**), with the higher costs of targeted restoration being driven by higher land-rental costs for prime agricultural land. However, though the costs for Targeted Restoration are nearly double those required for restoration on non-agricultural land, the targeted approach provides approximately 40 times more wetland N removal (**Fig. 2.4b**).

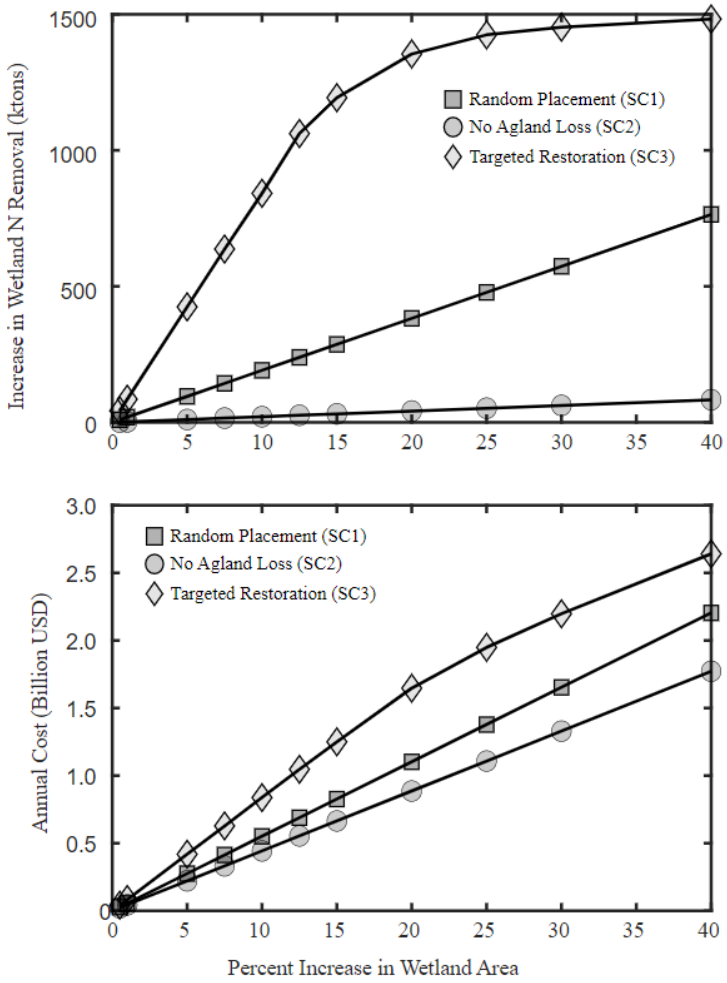

Figure 2.4 Estimated N mass removal and costs for the three wetland restoration scenarios. (**a**) Targeted Restoration (SC1) results in the greatest increase in N Removal over current levels with increases in wetland area; (**b**) Estimated wetland restoration costs scale approximately linearly with wetland area for all three scenarios, with higher costs for Targeted Restoration due to higher land rental costs for prime agricultural land.

In **Fig. 2.5**, we show more detailed results for the simulations providing a 10% increase in wetland area. The 10% increase was chosen to explore a restoration agenda that is ambitious—approximately 5 times more restored wetland area than that supported in the USDA Wetland Reserve Program—but for which associated costs are not outside the bounds currently allotted to water quality improvements.[24,25] The three modeled scenarios result not just in different N removal magnitudes, but also very different spatial distributions for the restored wetlands (**Fig. 2.5**). Under the Random Placement scenario, we see an almost uniform distribution of new wetlands across the contiguous U.S. In contrast, with Targeted Restoration, we see higher densities of restored wetlands in areas with the highest levels of agricultural production, and N removal is also concentrated in these high-input areas. With this 10% increase in wetland area, targeted restoration results in a more than 90% increase in N removal above current levels, constituting an additional 809 ± 395 ktons N removal across the contiguous U.S. This removal magnitude is approximately 4.3 times greater than that achieved with random placement, and 40 times greater than that with no loss of agricultural land, thus quantitatively demonstrating the value of the targeted approach.

With a wetland restoration landscape optimized for N removal, we find that great strides can be taken towards achieving policy goals for water quality in N-impacted watersheds (**Extended Data Table S1 in Appendix A)**. In the Mississippi River Basin, for example, our results show that current wetlands remove approximately 439 ktons of N y^{-1}. In comparison, approximately 868 ktons of N y^{-1} are delivered to the catchment outlet at the St. Francisville station, meaning that without current wetlands, Mississippi River N loads could be 51% higher than they are at present (~1300 ktons N y^{-1}). Under our targeted restoration scenario, a 10% increase in wetland area for the U.S. results in a 22% increase in wetland area for the Mississippi River Basin, as wetlands are preferentially placed in areas with high N surplus values. These restored wetlands would contribute to an additional 467 ktons y^{-1} of N removal, providing an approximately 54% decrease in N loading to Gulf and taking us more than halfway toward the current policy goal of a 60% reduction in riverine N loads.[26] While recent work has suggested it could take on the order of 30 years to achieve the desired reductions in N loading due to the presence of legacy N in soil and groundwater,[26,27] wetland restoration in many ways presents a fast-track solution, allowing for the capture and removal of both current-year and legacy N before it reaches downstream waters.

As noted above, such gains have an associated cost. Our analysis suggests that a targeted, 10% increase in U.S. wetland area would cost on the order of $3.3 billion—nearly twice the cost of wetland restoration on non-agricultural land—and would require removing 3.9 million ha of cropland (2% of total cropland area) from agricultural production.[28] While these costs are substantial, they are in line with current expenditures to achieve water quality goals.[15] For example, in Iowa, a corn belt state estimated to contribute from 11-52% of the total N load to the Gulf of Mexico, annual costs for conservation measures to improve water quality–including reductions in fertilizer use, the planting of cover crops, and construction of bioreactors as well as wetland restoration–are already estimated to be as high as $1.4 billion.[29,30]

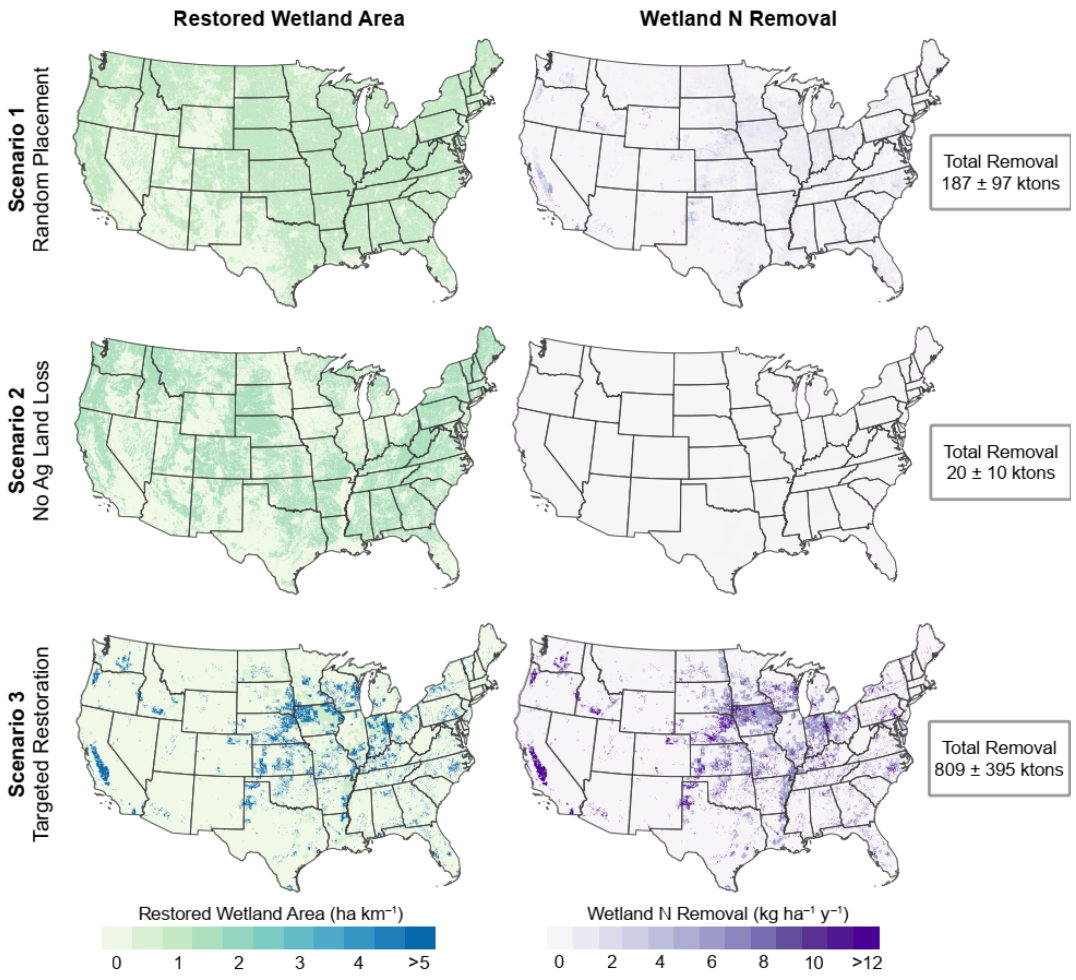

Figure 2.5 Wetland restoration simulation results for a 10% increase in wetland area. Total N removal values represent wetland N removal over and above current wetland N removal. Results show that with equivalent increases in wetland area, the Targeted Restoration scenario (SC3) maximizes wetland N removal, thus providing the greatest water quality benefit.

Our refined estimates of wetland N removal first indicate that current wetlands remove 860 ± 160 ktons of N y^{-1}, which is an order of magnitude less than previous estimates. This lower estimate arises due to our spatially explicit consideration of the preferential loss of wetlands in areas of intensive agricultural production, where fertilizer application and livestock production lead to N runoff and high stream N concentrations.[31] Our simulations, based on a newly developed high-resolution N surplus dataset, suggest that targeted restoration efforts could provide outsized reductions in N loads—in the Mississippi River Basin alone, a 22% increase in wetland area could decrease N

delivery to the coast by more than 40%. Importantly, these results not only corroborate earlier work by Mitsch et al.,[4] who predicted similar possible N removal magnitudes, but also move beyond previous finding by providing, for the first time, a spatially explicit "blueprint" for targeted restoration, suggesting priority areas for wetland restoration at a 5-km grid scale. These results provide critical context to discussions of wetland restoration and water quality that are especially important today, when a new Clean Water Act rule is reducing protections offered to existing wetlands.[32]

Of course, every watershed is different, and there are countless practical and policy-related challenges to carrying out targeted restoration. There is a strong need for watershed-scale solutions that consider and balance potential water quality benefits along with farmer attitudes and the need for agricultural production. These watershed solutions are not 'one size fits all,' as they require a detailed knowledge of past, current, and future land use and N loading along with an active dialogue between water authorities and land owners. However, watershed planners today have more access than ever to high-resolution data that can expedite the creation of watershed-specific solutions through interactions with local stakeholders.[33] The current results, which provide spatially varying estimates of potential water quality benefits from wetland restoration, create an important context for such dialogues and represent a fundamental step towards a more nuanced, landscape-scale understanding of the current and potential role of wetlands in improving water quality and reducing coastal eutrophication.

2.2 Methods

In the following, we provide details regarding our underlying datasets, analytical methods, and modeling approach to provide estimates of current wetland N removal, simulations of potential N removal under developed scenarios, and associated cost estimates.

N Surplus Calculations and Data Sources

The 2017 landscape N surplus was calculated using a soil surface N balance approach, an approach that is commonly used to to assess the impacts of agriculture—and agricultural policy—on the environment.[34,35] With the soil surface approach, all relevant N input, output, and loss terms are explicitly taken into account for a given land area at the soil surface:[35]

$$NS = DEP + FERT + BNF + MAN - CROP \quad \textbf{(Eq. 2.1)}$$

where *NS* is the N surplus, *DEP* is atmospheric N deposition, *FERT* is fertilizer N application, *BNF* is biological N fixation, *MAN* is livestock N excretion (urine and manure), and *CROP* includes both crop N uptake and consumption of pasture N by foraging livestock.

All N mass balance data was obtained from the TREND-nitrogen dataset.[36,37] N inputs (*DEP, FERT, BNF, MAN*) and outputs (*CROP*) were estimated at a U.S. county scale using crop and livestock data from the USDA Census of Agriculture,[38] atmospheric deposition data from the National Atmospheric Deposition Program,[39] and fertilizer data from USGS and USDA.[40,41] For additional details, see Byrnes.[37]

County-scale N surplus values were downscaled to the 5-km grid scale using the NLCD 2016 Land Cover raster. NLCD land cover was aggregated from 30-m to 5-km grid cells based on the dominant land cover designation for each 5-km grid cell. County-scale agricultural N inputs and outputs (fertilizer, crop biological fixation, manure production, and crop production) were then allocated equally to the agricultural grid cells within the county boundaries. Land use for areas labeled as pasture/hay or cultivated crops was considered to be agricultural. Atmospheric N deposition was considered to be distributed evenly across all grid cells within a county. The grid-scale landscape N surplus was calculated by adding N inputs and outputs for each 5-km grid cell.

N Removal - Individual Wetlands

Nitrogen (N) removal by wetlands across the U.S. was estimated as a function of N removal rates and estimated N surplus magnitudes, which determine the maximum mass of N potentially available to the wetlands for removal. Removal rates were estimated as a function of the wetland size, based on a meta-analysis of 178 wetlands across the world. Spatial data for individual wetlands was obtained from the National Wetlands Inventory (NWI), which comprises data for approximately 30 million upland and riparian wetlands across the contiguous U.S.[42] Although it is well documented that the NWI underestimates the presence of small wetlands, it remains the most comprehensive, seamless, and consistent national-scale database.[7]

The upscaling methodology developed in the current study is based on a previous empirical analysis of relationships between wetland N removal, wetland size, and water residence times that included a global meta-analysis of measured nitrogen removal data from 178 wetlands.[3] The study found that N removal rates in individual wetlands vary across a wide range, from 0.01 to 7200 g m^{-2} y^{-1}, with a median removal rate of 110 g m^{-2} y^{-1} and a median removal efficiency of 48%. These estimates of N removal are similar to those reported in other meta-analyses found in the literature.[19,43]

The wide range of estimates for N removal arises from the complexities of N removal processes in wetlands and creates challenges for upscaling individual wetland data to regional and continental scales. Wetland N removal can occur via temporary (e.g. plant uptake, burial) and permanent (e.g. denitrification) removal processes, and these processes depend on a variety of factors including nutrient loading, wetland area, residence time, wetland types, plant biomass, substrate availability and constraints on microbial metabolism.[19,44] Despite such complexity and the heterogeneity of processes across the hundreds of wetlands studied, the meta-analysis showed a remarkably consistent and significant inverse relationship ($p<0.001$) between the first-order N removal rate constant in individual wetlands, k [T^{-1}], the wetland residence time τ [T], and surface area, SA [L^2] (**Extended Data Fig. 3 in Appendix A**).[3] The authors hypothesized that the consistency of the relationship arises due to strong hydrologic controls on biogeochemical processing and validated their hypothesis using a sediment-water model that links major nutrient removal processes with wetland size.[3] Specifically, they showed that the inverse relationship can be attributed to the lower ratio of reactive sediment area to water volume for larger wetlands, which reduces the opportunity for nitrate in the water column to come into contact with denitrifying bacteria in the sediment.[3]

The relationships between k and τ, and between τ and SA, developed by Cheng and Basu are used in our study to estimate wetland N removal rates as a function of wetland size and nutrient loading.[3] The relationships were developed for both total N and nitrate-N, and were not found to be significantly different, possibly because nitrate dominates total N in most impacted systems. Due to a lack of ability to capture N speciation at this scale, we have used the estimates for TN in our analysis.

Following this approach, the percent wetland N removal, $\rho_{wet,i}$ (%), of each of the 30 million upland and riparian wetlands, i, in the National Wetlands Inventory (**Fig. 2.2**) was estimated as a function of

the removal rate constant (k_i; d^{-1}) and water residence times (τ_i; d) for that wetland, using first order removal rate kinetics:[3,45]

$$\rho_{wet,i} = (1 - \exp(-k_i \tau_i))*100 \quad \textbf{(Eq. 2.2)}$$

Removal rate constants, k_i, and residence times, τ_i, for the NWI wetlands were estimated using the empirical relationships developed by Cheng and Basu between these variables and wetland surface area, SA_i, with wetland surface area being obtained from the NWI database.[3]

$$\tau_i = a\,(SA_i)^{\,b} \quad \textbf{(Eq. 2.3)}$$

$$k_i = c\,(\tau_i)^{\,d} \quad \textbf{(Eq. 2.4)}$$

where a, b, c, and d are the coefficients and exponents of the empirically derived relationship.

The N removal by the individual wetlands, $R_{wet,i}$ (kg y^{-1}), was then estimated as the product of the N input to these wetlands ($M_{in,i}$; kg y^{-1}) and the percent wetland N removal $\rho_{wet,i}$ (%).

$$R_{wet,i} = M_{in,i}\,(\rho_{wet,i}/100) \quad \textbf{(Eq. 2.5)}$$

Spatially varying N inputs to the wetlands were estimated based on the area-normalized N surplus of the corresponding HUC, $N_{s,i}$ (kg-N ha^{-1} y^{-1}), the contributing area (ha) of each wetland, CA_i, and a reduction factor, γ, that quantifies the fraction of the N surplus that enters each wetland via flow through surface or subsurface pathways.[2]

$$M_{in,i} = \gamma\, N_{s,i}\, CA_i \quad \textbf{(Eq. 2.6)}$$

The reduction factor γ represents the fraction of the N surplus in the wetland's catchment area that can potentially enter the wetland, assuming that the rest is either retained in soils and groundwater, or denitrified in upstream soils, ditches and wetlands. The range of values employed for the γ term (0.3-0.5) is based on both monitoring- and modeling-based literature estimates of soil and watershed denitrification rates. The catchment area of each wetland was estimated by assuming a catchment area

to wetland area ratio of α, with values of α based on empirically determined relationships between wetland catchment area and wetland surface area.[46] The empirical distribution of α values is based on catchment delineation for more than 30,000 wetlands using high-resolution lidar data in the North American Prairie Pothole Region.[46] We used the geometric mean and standard deviation of the data to bound α in our Monte Carlo analysis. Future refinements of this methodology would involve delineating the watersheds of all current U.S. wetlands, which will become possible in the future as high-resolution data becomes available for other regions.

In wetland-dense areas, wetland catchment areas are nested, and the sum of wetland catchment areas can sometimes be greater than the total watershed area A_{wshd} ($\Sigma CA_i > A_{wshd}$). In these cases, wetland contributing areas were rescaled by multiplying individual wetland areas by a correction factor ($=A_{wshd} / \Sigma CA_i$), such that $\Sigma CA_i = A_{wshd}$. This rescaling was done to ensure that mass is conserved in the model calculations; in other words, we ensure that the mass of N entering the wetlands is not greater than the mass of N available within the watershed for removal. Following this approach, as the percent area intercepted by wetlands in a watershed would increase, the N removal by wetlands in the watershed would also increase.[21] One limitation of this approach to wetland-rich areas is that upgradient wetlands reduce nitrate, and thus the M_{in} to a downstream wetland should be ideally reduced due to the presence of a wetland in its contributing watershed.[20] Our model takes this into account implicitly, rather than explicitly, through the reduction factor γ. Advancement of this methodology would involve a network-scale assessment of the role of upstream wetlands in mass delivery to downstream wetlands that relies on detailed information of the network structure of the 30 million wetlands at the continental U.S. scale.

N Removal - Watershed Scale

The N removal by wetlands at the HUC-8 watershed scale (**Fig. 2.2D**) was estimated by aggregating the N removal of all wetlands within the watershed, and then normalizing by watershed area:

$$R_{wet,i} = (\gamma N_s CA_i) \ (\rho_{wet,i}/100) \qquad \textbf{(Eq. 2.7)}$$

The percent wetland N removed in each HUC-8 watershed, ρ_{wshd} (%), (**Fig. 2.2B**) was estimated as the sum of the percent wetland N removal for all wetlands in that watershed, weighted by their respective contributing areas:

$$\rho_{wshd} = \frac{\sum_i^n \rho_{wet,i} CA_i}{A_{wshd}} \quad \textbf{(Eq. 2.8)}$$

where $\rho_{wet,i}$ is the percent N removal of an, individual wetland, *i,* (% (from **Eq. 2.3**); CA_i is the catchment area of the wetland, *i,* (km^2), *n* is the number of wetlands in the watershed, and A_{wshd} is the total watershed area (km^2).

Parameter Ranges and Uncertainty Analysis

Monte Carlo simulations were used to characterize the uncertainty associated with estimates of N removal, as a function of the uncertainties associated with *k, τ*, wetland contributing area, and the fraction of N surplus that is intercepted by the wetland.[47] The ranges of values used for each parameter are provided in **Extended Data Table 2 in Appendix A**. The Latin hypercube sampling (LHS) technique, a form of stratified Monte Carlo sampling, was used to generate 500 parameter sets from these ranges, assuming a uniform distribution across each range.[48] LHS allows for strategic and efficient sampling of the parameter space, thus allowing for relatively fewer simulations to be run while still effectively assessing uncertainty across parameter ranges.[48] We conducted 500 Monte Carlo simulations to obtain median and interquartile range values to provide estimates of N removal.

Simulations of Wetland Restoration

Three wetland restoration scenarios were simulated. The three scenarios had the following stipulations: (SC1) Random Placement; (SC2) No Loss of Agricultural Land; and (SC3) Targeted Restoration in areas with the highest N surplus values. Simulations for each scenario were carried out for a range of increases in wetland area, up to a 40% increase in area. Simulations were carried out at a 5-km grid scale. Land cover at this scale was obtained from the NLCD 2016 land cover raster, with data being upscaled from a 30-m to a 5-km grid scale based on the modal land cover designation for each cell. No placement of new/restored wetlands was allowed in any of the simulations in areas with

the following land cover designations: (1) open water; (2) developed land (open space, low intensity, medium intensity, high intensity); (3) barren land; (4) shrubland; (5) wetland.

In the simulations, wetlands of varying size were selected randomly for placement from an empirically derived power-law distribution of wetland size, with a maximum size of 10 ha.[3,49] Random placement was allowed in any grid cell with qualifying land cover until the sum of all catchment areas and wetland areas reached a maximum of 25 km^2, the total area of the cell. Random placement of restored wetlands stopped when the total restored area across the contiguous U.S. reached 5.1 million ha.

The simulated N removal, $R_{wet,i}$ (kg y^{-1}), for each wetland was calculated using **Eq 2.5**, with N surplus values at the 5-km grid-scale. The k and τ values are calculated as shown in **Eq. 2.2** and **Eq. 2.3**, above, using mean coefficient and exponent values (**Extended Data Table 2 in Appendix A)**. The ratio of catchment area, CA_i, to wetland area for each restored wetland was assumed to be 8.4 (range 3-20) based on the geometric mean of empirically determined relationships between wetland catchment area and wetland surface area.[46] Simulated N removal was summed to the 5-km grid scale for presentation in **Fig. 2.5**.

The LHS stratified sampling technique was used to estimate uncertainty for the three simulation scenarios. The ranges for all parameters were the same as those used in the Monte Carlo simulations for current wetland removal and are given in **Extended Data Table 2 in Appendix A**. We conducted 50 Monte Carlo simulations to obtain mean and standard deviation values for N removal magnitudes for all three scenarios to obtain uncertainty values associated with a 10% increase in wetland area.

While it is known that recently restored wetlands may not provide the same levels of denitrification as undisturbed wetlands, often due to low availability of organic carbon,[50] note that the meta-analysis used for calculation of denitrification rate constants included a large proportion of restored and constructed wetlands. Accordingly, the range of N removal predicted through the Monte Carlo simulations should take into account an appropriate range of potential removal magnitudes. There may, however, be time lags associated with achieving the predicted removal rates.

Wetland Restoration Cost Calculations

The costs for construction of new or restored wetlands were calculated using a cost-based decision support framework for wetland restoration.[15,51] This framework includes area-dependent costs associated with design, construction and maintenance, annualized over a 50-year management horizon at a real discount rate of 4%.". It also includes land rental costs, which vary by state and are established to cover the opportunity costs for land removed from agricultural production.[51] Land rental costs for cropland and pastureland were obtained at a state level from the Quick Stats 2.0 database (http://quickstats.nass.usda.gov).

The costs of restoring 1 ha of wetland on cropland and pastureland for each of the 48 states in the contiguous U.S. are shown in **Extended Data Fig. 4 in Appendix A**. Land rental costs for cropland are, in the mean, more than five times greater than those for pastureland (cropland, \$274 ± 156 ha^{-1}); pastureland, \$51 ± 156 ha^{-1}), due to the greater loss of agricultural productivity when converting cropland. Accordingly, the rental costs for cropland account for a greater proportion of the total annualized costs (cropland, 47 ± 13%; pastureland, 16 ± 7%) associated with wetland construction and maintenance, depending upon land rental costs in individual states.

For the SC1 (Random Placement) and SC3 (Targeted Restoration) scenarios, state-specific land rental costs for cropland and pastureland were used. For the SC2 simulation (no loss of agricultural area) land rental costs were assumed to be zero, to provide the most conservative estimates of cost differences between the SC2 and SC3 scenarios. Estimated costs shown in Fig. 4 (main text) and in **Extended Data Fig. 4 in Appendix A**, are given in 2017 U.S. dollars. Note that the costs estimated herein are for constructed nutrient retention wetlands, as exemplified by the USDA CREP wetland program. In our analysis, we do not distinguish between costs for construction of a new wetland and those for restoration of a drained wetland. As costs for constructed wetlands in some regions could be greater than those for wetland restoration, the costs presented herein can be considered an upper bound on possible costs.

Watershed N Loads and Wetland N Removal

N loading at the catchment outlet for a selection of major U.S. nitrate-impacted rivers was calculated using USGS water quality data compiled by Oelsner et al.[52] Annual loads were calculated using flow and modeled daily concentrations. The reported loads in **Extended Data Table 1 in Appendix A** are average annual loads for the period 2002 to 2012. Wetland N removal for both existing and simulated wetlands was calculated by summing N removal magnitudes for individual wetlands and aggregating to the boundaries of the selected watersheds.

Chapter 2 References

1. Diaz, R. J. & Rosenberg, R. Introduction to environmental and economic consequences of hypoxia. *Int. J. Water Resour. Dev.* **27**, 71–82 (2011).

2. Van Meter, K. J., Basu, N. B. & Van Cappellen, P. Two Centuries of Nitrogen Dynamics: Legacy Sources and Sinks in the Mississippi and Susquehanna River Basins. *Global Biogeochem. Cycles* **31**, 2016GB005498 (2017).

3. Cheng, F. Y. & Basu, N. B. Biogeochemical hotspots: Role of small water bodies in landscape nutrient processing. *Water Resour. Res.* **53**, 5038–5056 (2017).

4. Mitsch, W. J. *et al.* Reducing Nitrogen Loading to the Gulf of Mexico from the Mississippi River Basin: Strategies to Counter a Persistent Ecological Problem. *Bioscience* **51**, 373–388 (2001).

5. Mitsch, W. J. & Day, J. W. Restoration of wetlands in the Mississippi–Ohio–Missouri (MOM) River Basin: Experience and needed research. *Ecol. Eng.* **26**, 55–69 (2006).

6. Verhoeven, J. T. A., Arheimer, B., Yin, C. & Hefting, M. M. Regional and global concerns over wetlands and water quality. *Trends Ecol. Evol.* **21**, 96–103 (2006).

7. Cohen, M. J. *et al.* Do geographically isolated wetlands influence landscape functions? *Proc. Natl. Acad. Sci. U. S. A.* **113**, 1978–1986 (2016).

8. Thorslund, J. *et al.* Wetlands as large-scale nature-based solutions: Status and challenges for research, engineering and management. *Ecol. Eng.* **108**, 489–497 (2017).

9. Fennessy, S. & Craft, C. Agricultural conservation practices increase wetland ecosystem services in the Glaciated Interior Plains. *Ecol. Appl.* **21**, S49–S64 (2011).

10. Altieri, A. H. *et al.* Tropical dead zones and mass mortalities on coral reefs. *Proc. Natl. Acad. Sci. U. S. A.* **114**, 3660–3665 (2017).

11. Fennel, K. & Testa, J. M. Biogeochemical Controls on Coastal Hypoxia. *Ann. Rev. Mar. Sci.* **11**, 105–130 (2019).

12. Hansen, L. *et al. Targeting Investments To Cost Effectively Restore and Protect*. https://www.ers.usda.gov/webdocs/publications/45347/51895_err183.pdf?v=0 (2015).

13. Brinson, M. M. & Eckles, S. D. U.S. Department of Agriculture conservation program and practice effects on wetland ecosystem services: a synthesis. *Ecol. Appl.* **21**, S116–S127 (2011).

14. Zedler, J. B. Wetlands at your service: reducing impacts of agriculture at the watershed scale. *Front. Ecol. Environ.* **1**, 65–72 (2003).

15. Zimmerman, E. K., Tyndall, J. C. & Schulte, L. A. Using Spatially Targeted Conservation to

Evaluate Nitrogen Reduction and Economic Opportunities for Best Management Practice Placement in Agricultural Landscapes. *Environ. Manage.* **64**, 313–328 (2019).

16. Creed, I. F. *et al.* Enhancing protection for vulnerable waters. *Nat. Geosci.* **10**, 809–815 (2017).

17. Moreno-Mateos, D., Power, M. E., Comín, F. A. & Yockteng, R. Structural and functional loss in restored wetland ecosystems. *PLoS Biol.* **10**, e1001247 (2012).

18. Golden, H. E. *et al.* Non-floodplain Wetlands Affect Watershed Nutrient Dynamics: A Critical Review. *Environ. Sci. Technol.* **53**, 7203–7214 (2019).

19. Jordan, S. J., Stoffer, J. & Nestlerode, J. A. Wetlands as Sinks for Reactive Nitrogen at Continental and Global Scales: A Meta-Analysis. *Ecosystems* **14**, 144–155 (2011).

20. Czuba, J. A., Hansen, A. T., Foufoula-Georgiou, E. & Finlay, J. C. Contextualizing Wetlands Within a River Network to Assess Nitrate Removal and Inform Watershed Management. *Water Resour. Res.* **54**, 1312–1337 (2018).

21. Hansen, A. T., Dolph, C. L., Foufoula-Georgiou, E. & Finlay, J. C. Contribution of wetlands to nitrate removal at the watershed scale. *Nat. Geosci.* (2018) doi:10.1038/s41561-017-0056-6.

22. Czuba, J. A. & Foufoula-Georgiou, E. A network-based framework for identifying potential synchronizations and amplifications of sediment delivery in river basins. *Water Resour. Res.* **50**, 3826–3851 (2014).

23. Van Cleemput, O., Boeckx, P., Lindgren, P.-E. & Tonderski, K. Denitrification in wetlands. in *Biology of the nitrogen cycle* 359–367 (Elsevier, 2007).

24. Jeffrey Ferris, J. S. Primary Land Retirement Programs for Promoting Farmland Conservation. (2009).

25. Rabotyagov, S. S. *et al.* Cost-effective targeting of conservation investments to reduce the northern Gulf of Mexico hypoxic zone. *Proc. Natl. Acad. Sci. U. S. A.* **111**, 18530–18535 (2014).

26. Van Meter, K. J., Van Cappellen, P. & Basu, N. B. Legacy nitrogen may prevent achievement of water quality goals in the Gulf of Mexico. *Science* **360**, 427–430 (2018).

27. Van Meter, K. J., Van Cappellen, P. & Basu, N. B. Response to Comment on 'Legacy nitrogen may prevent achievement of water quality goals in the Gulf of Mexico'. *Science* vol. 365 (2019).

28. Materials and methods are available as supplementary materials at the Science website.

29. Hayes, D. J., Kling, C. L. & Lawrence, J. D. *Economic Evaluation of Governor Branstad's Water Quality Initiative*. https://governor.iowa.gov/sites/default/files/documents/ISU%20CARD%20Economic%20Evalu

ation.pdf (2016).

30. Jones, C. S., Nielsen, J. K., Schilling, K. E. & Weber, L. J. Iowa stream nitrate and the Gulf of Mexico. *PLoS One* **13**, e0195930 (2018).

31. Dahl, T. E. *Wetlands Losses in the United States, 1780's to 1980's*. (U.S. Department of the Interior, Fish and Wildlife Service, 1990).

32. Ward, A. S. New Clean Water Act Rule Leaves U.S. Waters Vulnerable - Eos. *Eos* https://eos.org/opinions/new-clean-water-act-rule-leaves-u-s-waters-vulnerable (2020).

33. Tomer, M. D. & Nelson, J. A. Measurements of landscape capacity for water detention and wetland restoration practices can inform watershed planning goals and implementation strategies. *J. Soil Water Conserv.* (2020) doi:10.2489/jswc.2020.00110.

34. Salo, T. & Turtola, E. Nitrogen balance as an indicator of nitrogen leaching in Finland. *Agric. Ecosyst. Environ.* **113**, 98–107 (2006).

35. Bouwman, A. F., Van Drecht, G. & Van der Hoek, K. W. Global and regional surface nitrogen balances in intensive agricultural production systems for the period 1970-2030. *Pedosphere* **15**, 137–155 (2005).

36. Byrnes, D. K., Van Meter, K. J. & Basu, N. B. The Trajectories Nutrient Dataset for Nitrogen (TREND-nitrogen: County-Scale N Mass Balance Data for the Contiguous US, 1930-2017. (2020) doi:forthcoming.

37. Byrnes, D. K., Van Meter, K. J. & Basu, N. B. Long-term shifts in U.S. nitrogen sources and sinks revealed by the new TREND-nitrogen dataset (1930-2017). *Global Biogeochem. Cycles* (2020) doi:10.1029/2020GB006626.

38. USDA-National Agricultural Statistics Service. Census of Agriculture. (2020).

39. National Atmospheric Deposition Program. NADP Total Deposition Maps. http://nadp.slh.wisc.edu/committees/tdep/tdepmaps/ (2018).

40. USDA ERS - Fertilizer Use and Price. https://www.ers.usda.gov/data-products/fertilizer-use-and-price.aspx.

41. Brakebill, J.W., Gronberg, J.M. *County-Level Estimates of Nitrogen and Phosphorus from Commercial Fertilizer for the Conterminous United States, 1987-2012 - ScienceBase-Catalog*. https://www.sciencebase.gov/catalog/item/5851b2d1e4b0f99207c4f238 (2019).

42. U.S. Fish and Wildlife Service. National Wetlands Inventory. (2019).

43. Land, M. *et al.* How effective are created or restored freshwater wetlands for nitrogen and phosphorus removal? A systematic review. *Environmental Evidence* **5**, 9 (2016).

44. Fisher, J. & Acreman, M. C. Wetland nutrient removal: a review of the evidence. (2004).

45. Spieles, D. J. & Mitsch, W. J. The effects of season and hydrologic and chemical loading on nitrate retention in constructed wetlands: a comparison of low- and high-nutrient riverine systems. *Ecol. Eng.* **14**, 77–91 (1999).

46. Wu, Q. & Lane, C. R. Delineating wetland catchments and modeling hydrologic connectivity using lidar data and aerial imagery. *Hydrol. Earth Syst. Sci.* **21**, 3579–3595 (2017).

47. Mishra, S. Uncertainty and sensitivity analysis techniques for hydrologic modeling. *Journal of hydroinformatics* **11**, 282–296 (2009).

48. Muleta, M. K. & Nicklow, J. W. Sensitivity and uncertainty analysis coupled with automatic calibration for a distributed watershed model. *J. Hydrol.* **306**, 127–145 (2005).

49. Van Meter, K. J. & Basu, N. B. Signatures of human impact: size distributions and spatial organization of wetlands in the Prairie Pothole landscape. *Ecol. Appl.* **25**, 451–465 (2015).

50. Theriot, J. M., Conkle, J. L., Reza Pezeshki, S., DeLaune, R. D. & White, J. R. Will hydrologic restoration of Mississippi River riparian wetlands improve their critical biogeochemical functions? *Ecol. Eng.* **60**, 192–198 (2013).

51. Tyndall, J. & Bowman, T. Iowa Nutrient Reduction Strategy Best Management Practice cost overview series. https://www.nrem.iastate.edu/bmpcosttools/ (2016).

52. Oelsner, G. P. *et al. Water-quality trends in the nation's rivers and streams, 1972–2012—Data preparation, statistical methods, and trend results*. http://pubs.er.usgs.gov/publication/sir20175006 (2017) doi:10.3133/sir20175006.

Chapter 3

Disconnectivity Matters: The Outsized Role of Small Ephemeral Wetlands in Landscape-Scale Nutrient Retention

Chapter 3 Abstract

Wetlands protect downstream waters by filtering excess nitrogen (N) generated from agricultural and urban activities. Small ephemeral wetlands, often known as geographically isolated wetlands (GIWs), are hotspots of N retention but have received fewer legal protections due to their apparent isolation from jurisdictional waters. Here, we hypothesize that the isolation of the GIWs make them more efficient N filters, especially when considering transient hydrologic dynamics. We use a reduced complexity model with thirty years of remotely sensed monthly wetland inundation levels in 3,700 GIWs across eight wetlandscapes in the US to show how consideration of transient hydrologic dynamics can increase N retention by 91%, with greater retention magnification for the smaller wetlands. This effect is more pronounced in semi-arid systems such as the prairies in North Dakota, where transient assumptions lead to 1.9 times more removal, compared to humid landscapes like the North Carolina Pocosins where transient assumptions only lead to 1.4 times more retention. Our results highlight how GIWs have an outsized role in retaining nutrients, and this service is enhanced due to their lack of hydrologic connectivity which must be protected to maintain the integrity of downstream waters.

3.1 Introduction

Wetland protection and restoration has been recognized as one of the most promising strategies for mitigating nutrient pollution (Mitsch *et al.*, 2005; Quin, Jaramillo and Destouni, 2015; Hansen *et al.*, 2018). Wetlands retain excess nutrients from agricultural and urban runoff and protect downstream waters (McClain *et al.*, 2003; Marton *et al.*, 2015; Cheng and Basu, 2017). In particular, the anoxic conditions and high organic carbon content in wetlands promotes the removal of nitrogen (N) through denitrification (Martínez-Espinosa *et al.*, 2021). Indeed, wetlands in the United States have been estimated to remove more reactive N than all other aquatic ecosystems combined, in addition to providing other ecosystem services such as carbon sequestration and biodiversity enhancement (Baron *et al.*, 2013; Thorslund *et al.*, 2017; Cheng *et al.*, 2020; Canning *et al.*, 2021).

Prioritization of wetland restoration requires an understanding of how different types of wetlands across the landscape perform different services (Cohen *et al.*, 2016). The effectiveness of N retention in a wetland varies widely across the landscape, with retention magnitudes ranging from 0.002-9048 g N/m^2/year and retention rates ranging between 30-40% of N inputs (Jordan, Stoffer and Nestlerode, 2011; Land *et al.*, 2016; Cheng and Basu, 2017). Retention rates have been found to correlate strongly with inputs from the landscape, wetland size and water residence times (Saunders and Kalff, 2001, Powers, Tank and Robertson, 2015; Arheimer and Wittgren, 2002; Cheng and Basu, 2017). These field studies focus on the dynamics in individual wetlands, while the N retention potential of wetlandscapes can be modeled as a function of N retention in individual wetlands, as well as the distribution and connectivity of wetlands across the landscape. Hansen et al. (2021) used a coupled model to explore N retention dynamics in the Le Sueur River Basin in the Minnesota River basin, and found restoration of floodplain wetlands to be the most cost-effective strategy for N retention. Evenson et al. (2021) found that restoring 2% of the area of the Upper Mississippi River Basin to wetlands can reduce the outlet N loads by 12%. Cheng et al. (2020) estimated N removal in over 30 million wetlands across the contiguous US, and found that a targeted 10% increase of current wetland area in zones of the highest nitrogen inputs can reduce N loads to the Gulf of Mexico by 40%.

An important class of wetlands is geographically isolated wetlands (GIWs), defined as wetlands that are completely surrounded by uplands and lack a persistent surface water connection to navigable streams and may contain water for only part of the year (Tiner, 2003). GIWs span many wetland

types and hydrogeomorphic settings (e.g., prairie potholes in Midwestern US and Central Canada, vernal pools of New England and eastern Canada, Delmarva and Carolina Bays, playas of southwestern US and Mexico, cypress domes of southeastern coastal plain in US), and have traditionally received less protection due to their apparent disconnectivity from downstream navigable waters (Lane and D'Amico, 2016; Creed *et al.*, 2017). GIWs are generally smaller than most riparian wetlands (Cohen *et al.*, 2016), and contain water for only a part of the year. They typically receive seasonal water inputs through snowmelt or intense storms and lose water over the next few months through evapotranspiration or groundwater recharge (Tiner, 2003; Morgan, Hayashi and Cey, 2021). From a biogeochemical perspective, GIWs often receive the first flush of solutes from the landscape (Cohen and Brown, 2007) and the lack of direct connection to the river network increases processing times and nutrient retention, making them landscape biogeochemical hotspots (Winter and LaBaugh, 2003; Marton *et al.*, 2015). However, while the lack of apparent connection to surface waters increases their ability to be most effective as nutrient filters, it is this lack of connection that excludes them from the Clean Water Act and makes them most vulnerable to loss (Marton *et al.*, 2015; Creed *et al.*, 2017).

The nutrient retention potential of GIWs is a function of their inundation characteristics that drives water residence times and reaction dynamics (Cheng *et al.*, 2020); yet most studies that quantify these services focus on a fixed wetland area often derived from national scale wetland inventories like the National Wetlands Inventory in the US. There is currently a lack of quantitative understanding of the temporal dynamics of water storage in small ephemeral GIWs, and how such dynamics can potentially affect their nutrient retention potential. In a recent paper, Park et al. (2022) used thirty years of satellite imagery to explore the seasonal dynamics of water storage in ten wetland regions across the US. The authors observed that the source of water in the wetlands (snowmelt or rain-fed) were correlated to distinct seasonal patterns of inundation across the wetlandscapes. Our objective is to build on this work and explore the linkages between water storage and nutrient retention dynamics. Specifically, we focus on the following questions: (1) What is the role of inundation dynamics on nutrient retention in wetlands? (2) How does the inundation-retention relationship vary as a function of wetland size? (3) How does wetland size and climate interact to alter these relationships for different wetlandscapes?

3.2 Methods

3.2.1 Wetland Inundation and Bathymetry Data

We modeled nitrogen retention dynamics in eight wetland regions of the continental US representing different climate and geomorphology: California vernal pools, prairie potholes in North Dakota, basin wetlands in Minnesota, Maine vernal pools, cypress domes in Florida, Texas playa lakes, North Carolina Pocosins, coastal plain wetlands in Georgia, and Nebraska sandhills. Within each of these eight landscapes, a 1000 km^2 rectangular region was selected based on the presence of a high density of NWI wetlands, and infrequent gaps in GSW data (Park et al., 2022). GIWs were then derived within the selected rectangular regions using the National Wetlands Inventory (NWI) and National Hydrography Dataset (NHD), following the methodology outlined in Park et al. (2022) and Lane and D'Amico (2016). First, using the NWI dataset, riverine, marine, and estuarine wetlands were excluded, and only the palustrine and lacustrine wetlands included. Next, to specifically focus on GIWs, we used the NHD to create 10 m buffer polygons for rivers, all NHD lakes larger than 8 ha, other water bodies larger than 1.5 ha, and other flowlines or features. All palustrine and lacustrine wetlands that intersect with the 10m NHD buffered polygons were removed, and the remaining were classified as GIWs for the remaining analysis. Further details of the methods for extracting GIWs are provided by Park et al. (2022).

Once GIWs were identified, we characterized the inundation dynamics of the GIWs using the Global Surface Water dataset that was derived from Landsat imagery and contains monthly observations of surface water body extent (Pekel *et al.*, 2016). By intersecting the boundaries of the identified GIWs with the Global Surface Water dataset, we were able to develop a monthly time series of wetland inundated areas between 1985 to 2015. The method led to the characterization of 3698 GIWs across the eight wetlandscapes, with the greatest density of GIWs in the 1000 km^2 block in North Dakota (2395 GIWs), and much fewer GIWs in the vernal pools and the North Carolina pocosins (**Table 3.1**).

Next, the bathymetric relationships (area-depth-volume) of the GIWs were derived to convert observed wetland inundated areas to monthly volume estimates. This was determined using the 1/3rd arc-second USGS DEM cropped to the GIW extent, and starting from the top of the wetland incrementally determining the areas and volumes at each vertical increment using the rasterio python

package. Starting at the maximum extent and elevation, the volume of each DEM pixel within the wetland boundary was calculated as the pixel size multiplied by the difference in elevation. These volumes were then integrated to estimate the total volume of the wetland at this maximum extent. This procedure was repeated by decreasing the maximum extent in 10,000 equal intervals until the lowest elevation of the wetland.

Table 3.1 Summary of GIWs and wetlandscape characteristics used in analysis

State	Wetland Type	Aridity Index (AI = PET/P)	Number of GIWs Identified	Total Wetland Years of Record
CA	Vernal Pools	2.90	27	392
FL	Cypress Domes	1.33	250	1287
GA	Coastal Plain	1.26	35	392
MN	Basin Wetlands	1.21	48	54
NE	Sandhills	3.17	864	574
NC	Pocosins	1.23	27	504
ND	Prairie Potholes	2.31	2395	12570
TX	Playa Lakes	4.71	52	589

3.2.2 Transient Wetland N Retention Dynamics

A reduced complexity model was developed to estimate temporal fluctuations in N retention dynamics in a wetland as a function of time-varying inflows and outflows (**Figure 3.1**). Assuming well-mixed conditions within the wetland, the rate of change of nitrogen mass M [M] within the wetland was described as:

$$dM/dt = C_{in}Q_{in} - Mk - MQ_{out}/V \quad (3.1)$$

where C_{in} is the concentration of nitrogen in the runoff from the contributing area [M/L^3], Q_{in} is the volume of water entering the wetland from its contributing area [L^3/T], Q_{out} is the volume of water that is leaving the wetland as recharge or surface outflow [L^3/T], V is the ponded wetland volume [L^3], and k is a first order N retention rate constant [T^{-1}] that describes the temporary (e.g. plant uptake, burial) and permanent (e.g. denitrification) processes that contribute to N retention in wetlands.

Using a meta-analysis approach, previous studies have found that N retention rates vary across a wide range of values, with a median removal efficiency of 48% (Cheng and Basu, 2017) and up to 2,486

g/m^2/yr (Land *et al.*, 2016). Despite such wide variability, the meta-analysis of 178 wetlands by Cheng and Basu (2017) highlighted a significant inverse relationship between k (1/d) and the wetland inundated surface area SA (m^2). The study further showed that the inverse relationship can be attributed to the higher ratio of reactive sediment area to water volume in smaller wetlands that increases the opportunity for nitrate in the water column to come in contact with the sediments. While Cheng and Basu focused primarily on steady state dynamics, as a wetland dries up over the course of a season, the surface area decreases, further increasing the retention rate constant. In our dynamic modeling framework we used time varying surface areas SA (m^2) of the wetlands from remotely sensed data (**Section 3.2.2**) to estimate time varying k (d^{-1}) values:

$$k = 0.51\ SA^{-0.28},\ r^2 = 0.52 \tag{3.2}$$

Remotely sensed wetland inundation data was also used to estimate the time-varying wetland volumes, as well as inflows and outflows Q_{in} and Q_{out} from the wetland. Specifically, we used estimated monthly ponded volumes of the wetland (V), and available data for rainfall, evapotranspiration and runoff to estimate the inflows and outflows with the following mass balance (Liebe *et al.*, 2009):

$$dV/dt = (P - ET)SA_{max} + Q_{in} - Q_{out} \tag{3.3}$$

where P is the direct precipitation rate on the wetland (m/d), ET is the evapotranspiration rate from the wetland surface (m/d), and SA_{max} is the maximum inundated surface area of the wetland over the 30 years of available remote sensing data. Although the ponded area of the wetland changes over time, we assumed direct precipitation to be intercepted by the maximum area. Additionally, though direct ET occurs only from the inundated area, we used the maximum surface area to estimate the overall ET flux, given ET in the moist margins of the wetland can induce losses from the ponded area through local groundwater exchange (Hayashi, van der Kamp and Rosenberry, 2016). Monthly precipitation (P), evapotranspiration (ET) and runoff (Q) rates were available from the TerraClimate dataset (Abatzoglou *et al.*, 2018). For each month between 1985 to 2015, a spatially averaged value of P, PET, AET, Q was used for each wetlandscape as inputs for the hydrologic model.

Given that both Q_{in} and Q_{out} are unknowns in **Eq. 3.3**, we used the gridded runoff data (mm/month) from the TerraClimate dataset and several assumptions to estimate them (**Figure 3.1**). First, we

assumed a catchment area to wetland area ratio of 8.2 based on the geometric mean of 33,000 wetland catchment delineations conducted by Wu and Lane (2017), and estimated Q_{in}' (m^3/month) as the product of Q from the TerraClimate Dataset and the catchment area of the wetland. We estimated changes in the wetland inundated volume (dV) for each wetland and for each month from the satellite data. For each monthly timestep, when the total water inputs to the wetland was greater than the observed change in volume ($Q_{in}'+(P - ET)*SA_{max} \geq dV/dt$), outflow was estimated as the difference between the total water inputs and the change in volume ($Q_{out} = (Q_{in}'+(P - ET)*SA_{max} – dV/dt)$ and Q_{in} was assumed to be equal to Q_{in}'. Conversely, when the total water inputs are less than the observed change in water volume ($Q_{in}'+(P - ET)*SA_{max} < dV/dt$), and Q_{out} was assumed to be zero while Q_{in}' was increased to meet the observed change in volume (see **Figure 1**). These estimates are of course uncertain, and can be refined using better site specific information. However, our goal was not to develop an exact model for a particular landscape, but rather to explore how consideration of inundation dynamics can alter N retention patterns in these small, ephemeral wetlands across the landscape.

We assumed the concentration C_{in} to be temporally invariant to better isolate the effects of hydrologic variability on N retention within the wetland. We did consider C_{in} to vary as a function of wetland size, given that small wetlands are often located in upland areas adjacent to nitrogen sources (e.g. agricultural land) and intercepts the highest concentrations of N (Arheimer and Wittgren, 2002), whereas large wetlands intercept larger areas with more dilute concentrations. Here, we used a concentration of 30 mg/L for C_{in} of the smallest wetlands and the largest wetlands receiving 0.3 mg/L, and a linear interpolation on a logarithmic scale to determine the input concentrations across wetland sizes. It should be noted that the relative N retention of a wetland, which is the focus of this study, is actually independent of the input concentration when C_{in} is temporally invariant. In reality, the chemodynamic relationship between C_{in} and the flow Q can vary between landscapes and over time (Musolff *et al.*, 12/2015), and future work should focus on quantifying how these dynamics impact N retention.

The coupled hydrologic and N retention model (**Equations 3.1 and 3.3**) were numerically solved with the forward Euler method using a daily time step to ensure model stability for each wetland and

year. To accommodate the smaller time step, linear interpolation was used to convert the wetland volume time series to a daily time scale; similarly, the monthly fluxes from the TerraClimate dataset were assumed to be constant over the month.

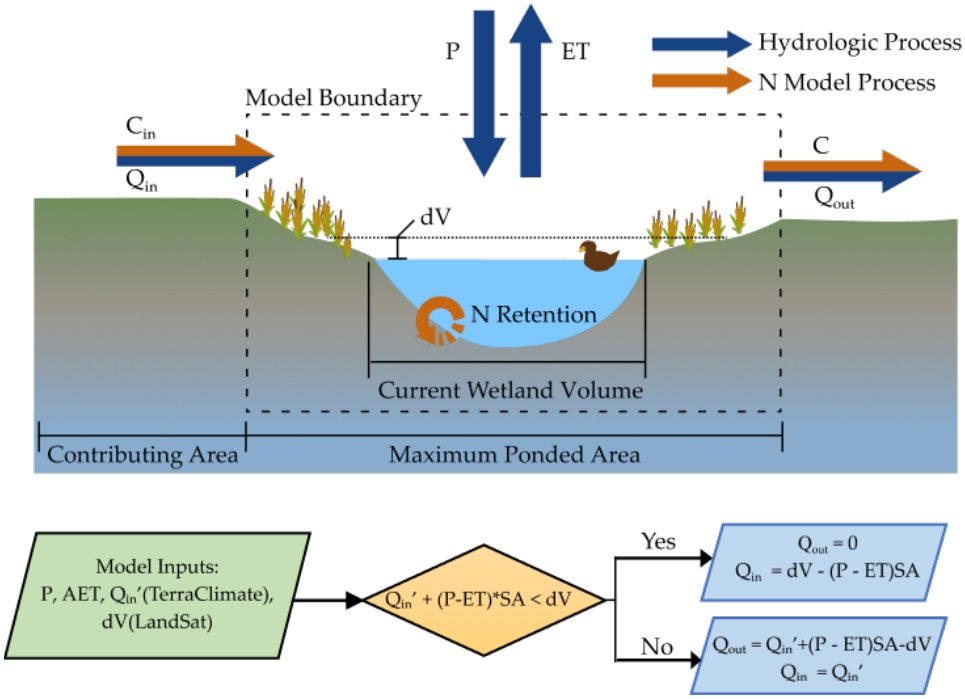

Figure 3.1 Hydrologic and N retention modelling. A coupled hydrologic-nitrogen retention model was used to estimate 30 years of N retention dynamics of all identified GIWs across the wetlandscapes.

3.2.3 N Retention under Steady and Transient Scenarios

We modeled each of the 3698 wetlands in the eight wetlandscapes ranging for all available years, with a total of 16,362 wetland-years modeled. As there was a significant amount of hydrologic variability between years, we did not temporally aggregate the results, and the subsequent analyses in this study are based on wetland-years of data. The percent N retained for each wetland-year was calculated by normalizing the N mass retained (from solving **Eq. 3.1**) by the N mass input to the wetland. For analyses relating to wetland size, each wetland year was assigned to a size bin based on the observed maximum annual wetland area for that year, with the wetland size bin increasing in increments of 0.5 on a logarithmic scale (i.e. $10^{2.5}$-10^{3}, 10^{3}-$10^{3.5}$, etc.). To compare the results from

our transient model to typical steady state, flow-through wetland models used in other watershed scale studies, we estimated the fractional nitrogen retention R_{ss} using a common first-order retention model for lentic water bodies under well-mixed conditions (Vollenweider, 1975):

$$R_{ss} = k\tau_{ss} \ / (1 + k\tau_{ss}) \tag{3.3}$$

where k is the same first order effective retention used in **Eq 3.1** and is a function of wetland area, and τ_{ss} is the hydraulic residence time (d). The steady-state hydraulic residence time (τ_{ss}, in days) was estimated for each wetland using an empirical relationship based on a meta-analysis of lentic water bodies: $\tau_{ss} = 1.51 \text{ X } SA^{0.23}$ ($r^2 = 0.4$, where SA is the size of wetland (m^2) (Cheng and Basu, 2017). To compare residence times between the two flow models, an effective residence time τ_{TS} was calculated for the transient state models using **Eq 3.3,** given the annual percent N retention R_{TS} and the median N retention rate constant k.

Finally, the Damkohler number Da (-) was estimated for the steady and transient models using **Eq. 3.3**, with the annual retention R where $Da = k\tau = \tau/\tau_{reaction}$. The Da is a dimensionless number that captures the chemical reaction and water residence timescales, where $Da > 1$ indicates that the system is has sufficiently large residence times to allow for more nutrient retention, while $Da < 1$ indicates that the water and nutrients are flowing through the system at faster timescales than the reaction timescales and thus limiting nutrient retention (Oldham, Farrow and Peiffer, 2013).

3.3 Results and Discussion

3.3.1 Effect of flow transience on nitrogen retention in wetlands

We first explored the behavior of prairie pothole wetlands in the North Dakota region to quantify how flow transience controls N retention. Incorporation of transient flow dynamics increased the median estimated N retention from 44% (steady state) to 80% (transient) of the N entering the wetlands (**Figure 3.2a**). When disaggregated by size, N retention increases with wetland size under the steady state scenario, from 38% for small wetlands ($10^{2.5}$- 10^3 m^2) to 50% for large wetlands ($10^{5.5}$-10^6 m^2). Interestingly, the relationship between N retention and size is reversed under the transient scenario, with greater N retention (88%) in the smaller wetlands compared to the larger ones (71%) (**Figure**

3.2b). This dependence of N retention on size and flow transience can be attributed to differences in flow dynamics between the small and large wetlands.

Small wetlands ($< 10^{3.5}$ m^2) in the prairie pothole region (PPR) have a median hydroperiod (time with water in wetland) of four months (**Figure 3.2c**), and typically fill up during the spring freshet and dry up over the summer months (Hayashi et al., 2016). Such seasonal wetting-drying dynamics imply that a large proportion of water entering the wetland leaves as evapotranspiration. Our flow analysis highlights that in these small wetlands, only 28% of the water that comes in as snowmelt or runoff actually leaves as groundwater or surface water outflow (Q_{out}), while the remaining 72% of water leaves as evapotranspiration (**Figure 3.2d**). This is consistent with field studies in the PPR that have found that in small wetlands over 80% of the water can leave the system as ET, when considering losses in both the wetland and the surrounding uplands (Sloan, 1972; Hayashi, van der Kamp and Rosenberry, 2016). Large wetlands ($> 10^{4.5}$ m^2), on the other hand, often have water for the entire year, and a greater proportion of incoming water leaves as lateral fluxes (43%) compared to ET (**Figure 3.2d**). The greater proportion of ET in small wetlands most likely contributes to a more terminal behavior for N retention in these small ephemeral systems.

To explore the effect of downstream disconnectivity, we compared the residence times and retention rate constants in small and large wetlands as a function of flow transience. Empirical studies have highlighted that the N retention rate constant k increases with decreasing wetland size (**Eq. 3.2**), and this occurs due to a greater reactive surface area per unit volume for smaller wetlands (Cheng and Basu, 2017). As a small wetland dries up over the course of a season, the reactive surface area to volume ratio increases, and this can increase the retention rate constant even further. Residence times are also a function of wetland size and flow transience. For the steady state assumption, residence times increase as a function of wetland size (Cheng and Basu, 2017), and the combined effect of a negative k-SA and a positive τ-SA relationship contributes to an increase in the percent N retention with increasing size (**Figure 3.2b**). Transient systems are more complicated since a large proportion of the water entering the system might only leave the system through evapotranspiration, implying that the N is retained within the system in the vegetation. Thus, water residence time is different from the nitrogen residence time. We estimated the effective nitrogen residence time (**Figure 3.2e**) in the transient scenario by using the removal efficiency estimated from the transient model (**Figure 3.2b**) and the k-SA (**Eq. 3.2**) relationship. The effective residence time in the transient scenario is greater

than the steady state scenario, and the τ-*SA* relationship shows a unique U-shaped behavior, with the smallest and largest wetlands having the largest effective residence times. While residence times in larger wetlands are larger because of their larger volume to lateral outflow flow ratio, residence times in smaller wetlands are larger under the transient scenario due to the terminal nature of their flow dynamics. Indeed, median residence times in the smaller wetlands are ~60 days which corresponds to the smaller hydroperiods of these systems (**Figure 3.2c**), such that water that enters only leaves through ET, and the nitrogen is retained within the vegetation. Effective residence times in these small, ephemeral systems can be 20 times greater than under steady state assumption, while the residence-times ratio between the transient and steady state scenarios for the larger wetlands are ~1 (**Figure 3.2f**).

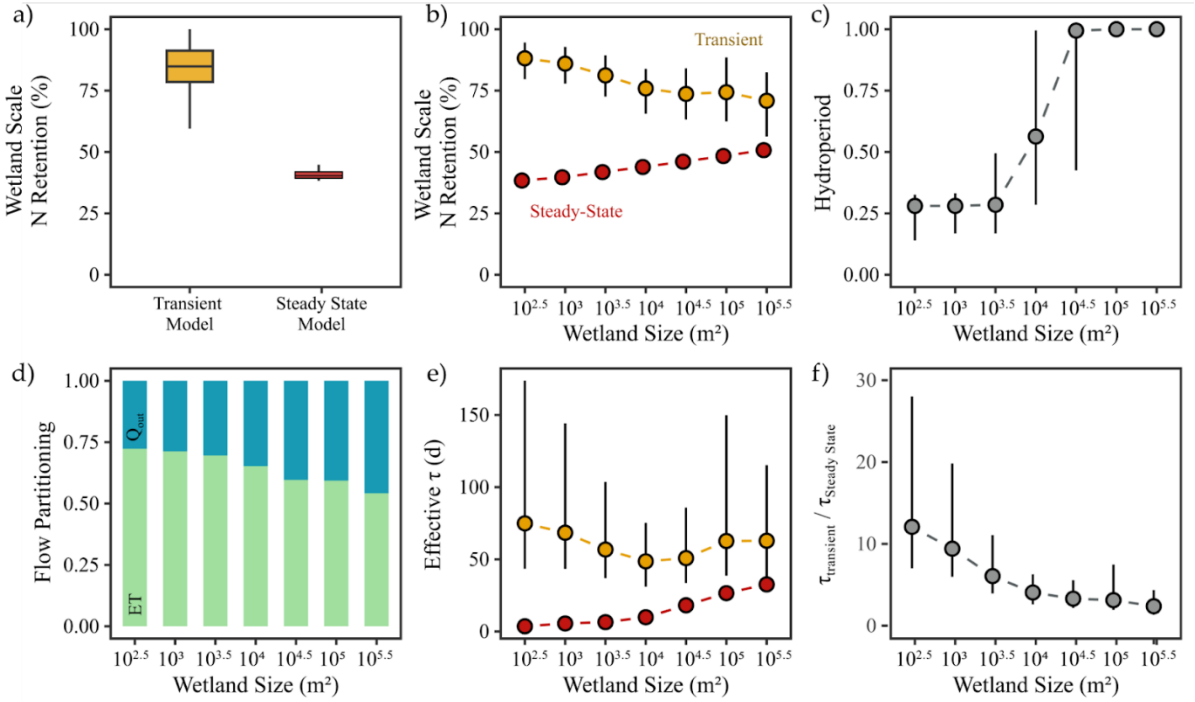

Figure 3.2 Size dependent relationships of wetland behavior in North Dakota. Distinct patterns of N retention were observed across wetland size and flow assumption: a) Percent N retention of all GIWs in landscape; b) Percent N retention of GIWs grouped by size. Differences in N retention were driven by differences in hydrologic behavior, and summarized in the following metrics: c) Hydroperiod; d) Flow partitioning of hydrologic inputs (P and Q_{in}) leaving wetland as lateral outflows (Q_{out}) and ET; e) Effective residence time (τ); f) Ratio of modeled transient hydraulic residence time (τ_{TS}) to steady-state hydraulic residence time (τ_{SS}). The box extent and horizontal lines in 2a show the interquartile range and median, with the whisker showing the maximum/minimum values. The

bounds in figures 2b to f show the interquartile range and the inner point is the median value of the results.

3.3.2 Effect of climate variability and inundation dynamics on N retention

To further explore the impact of hydroclimatic variability on wetland N retention, we expanded the analysis from North Dakota to seven other wetlandscapes across the US. We found wetland inundation dynamics to be strongly driven by climate and wetland size. In the semi-arid prairie pothole pothole region (PPR) of North Dakota (aridity index AI = 2.31), wetlands are frozen during the winter months and have peak inundation levels in April (**Figure 3.3a and 3.3b**). This behavior is typical of snowmelt driven systems like the basin wetlands of Minnesota, prairie potholes in North Dakota and Nebraska Sandhills (Park *et al.*, 2022). The climate drivers are further modified by wetland size, where small wetlands in the PPR typically fill up during the spring snowmelt and dry up over the summer months (**Figure 3.3a**) while large wetlands often lose only a smaller proportion of their total volume during summer and never completely dry up (**Figure 3.3b**). This is in contrast to wetlands in the more rainfed, humid systems like the pocosins in North Carolina (AI = 1.23), have water for most of the year in both small and large wetlands, albeit the smaller wetlands have greater drawdown magnitude compared to its volume (**Figure 3.3c** and **Figures 3.3d**).

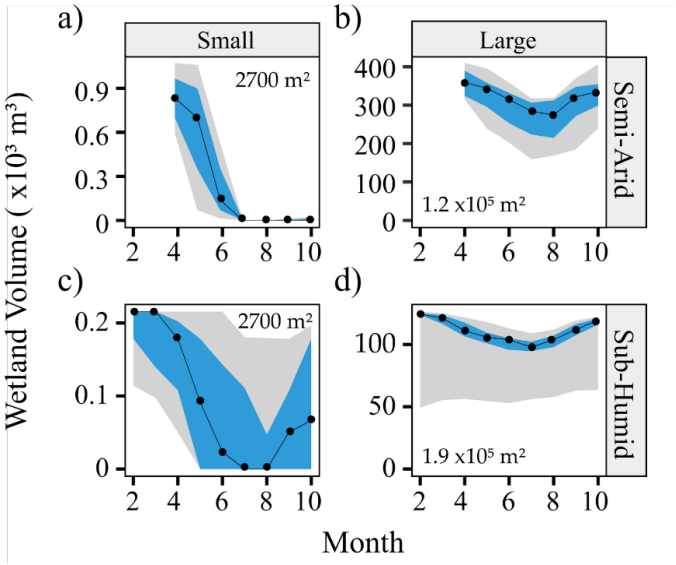

Figure 3.3 Regime curves of volume for example small (maximum area between $10^{2.5}$ to 10^{3} m^2) and large (10^{5} to $10^{5.5}$ m^2) wetlands in North Dakota and North Carolina. The black lines are median volumes for the period of record, the blue bands show the 25th-75th percentile, and the gray band shows the 5th-95th percentile. The maximum area of the individual wetlands is indicated in the figure.

This pattern is consistent across the hydroperiods in all eight wetlandscapes (black lines in **Figure 3.4**), with smaller wetlands in semi arid landscapes (regions with AI > 2, i.e. TX, NE, CA, ND) being more ephemeral (shorter hydroperiods), while humid landscapes have a greater proportion of more permanent wetlands. For example, the median hydroperiod for the largest size class (10^5 - $10^{5.5}$ m^2) in the Texas playas (aridity index = 4.71) is 6.8 months, while for the more humid North Carolina wetlands (AI = 1.23), the median hydroperiods for all wetlands > $10^{3.5}$ m^2 is one year, indicating that a greater proportion of the wetlandscape is composed of more permanent wetlands.

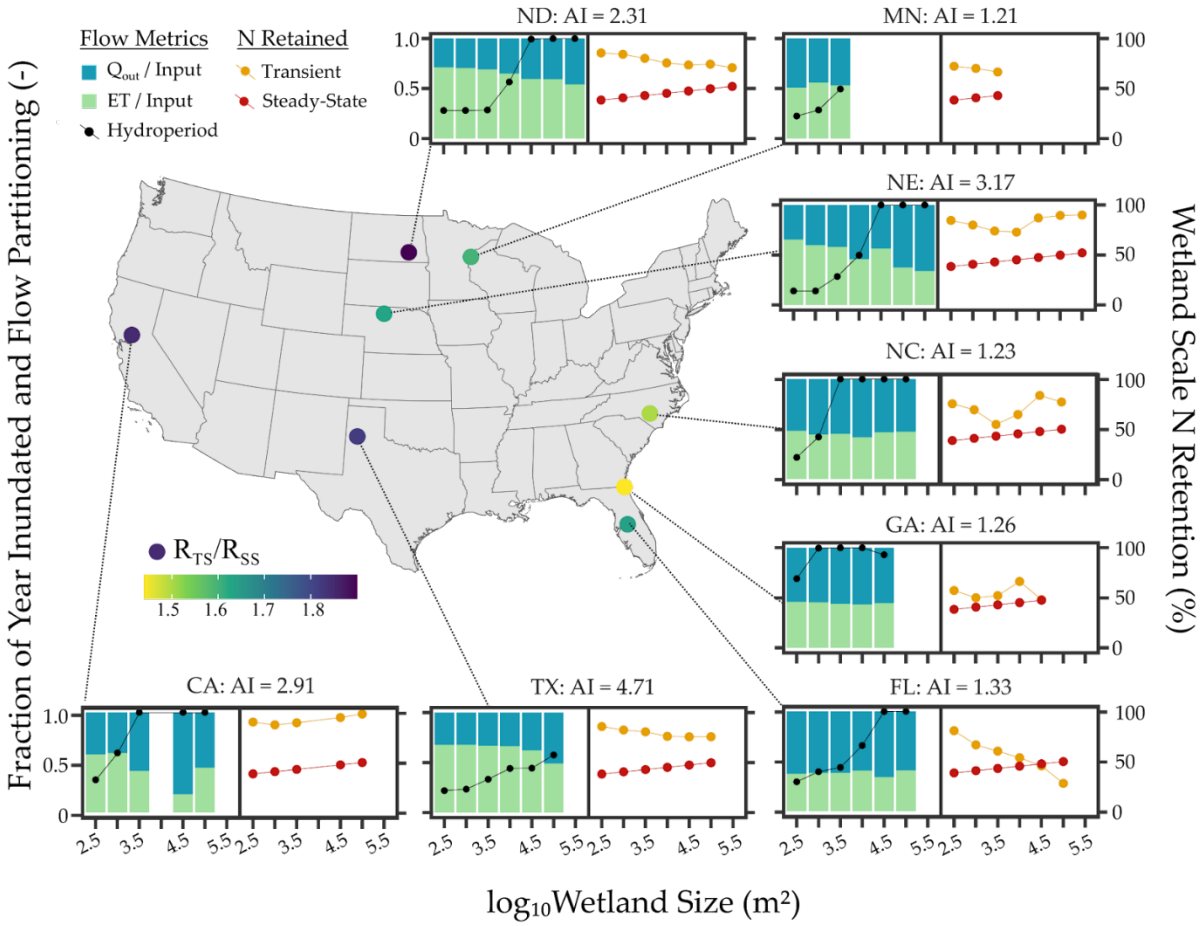

Figure 3.4 Differences in hydrologic behavior across wetlandscapes are apparent in the hydroperiod (black points) and partitioning of hydrologic inputs as outflow (blue bars) and ET (light green bars) and cause variability in the modeled transient N retention (yellow points). The N retention using the steady-state assumption is shown as the red points. Map inset shows the locations of the wetlandscapes, with the colored points indicating the ratio of the median transient and steady state N retention.

Evapotranspiration dominates the water partitioning in the semi-arid wetlandscapes (regions with AI > 2, i.e. TX, NE, CA, ND), and typically accounts for greater than 50% of the incoming water (green bars in **Figure 3.4**), with smaller wetlands having a greater proportion of ET fluxes. For example, ET loss accounted for 68% of the inflows in the small playas in Texas, but only 48% of the inflows for the larger playa wetland. More humid regions with aridity indices closer to 1 (FL, GA, NC, MN) have a greater proportion of lateral fluxes compared to ET, and no discernible flow partitioning differences with wetland size (**Figure 3.4**). These wetlands may have extended periods when inflows to the wetland exceed evapotranspiration and allow for more continuous surface outflows regardless of wetland size.

Finally, these differences translate to different patterns of N retention. While for most wetlands, the transient assumption leads to greater estimated N retention compared to the steady state assumption, the difference is greater for the semi-arid wetlandscapes, like the prairie potholes in North Dakota compared to the more humid wetlands in Georgia (**Figure 3.4**). Overall, N retention percentages for the semi-arid systems are 1.63 to 1.82 times greater in the transient compared to the steady state scenario, while for the humid systems N retention is only 1.43 to 1.65 times greater in the transient scenario (**Figure 3.5**). Of course, differences in the N retention patterns between wetlandscapes cannot be completely explained by aridity alone. For example North Carolina and Florida wetlands have similar AI values, but different N retention dynamics (**Figure 4**), and this can be attributed to differences in temporal patterns of rainfall, as well as differences in landscape attributes that drive N retention. While the patterns of N retention dynamics across humid and semi arid systems is interesting, the exact magnitudes should be interpreted with caution, especially for regions with relatively few wetlands, making the size dependent patterns less reliable. Furthermore, it is important to note that the residence time estimation in the steady state scenario is based on an empirical relationship, and is thus invariant across the different wetlandscapes, while the transient scenarios are driven by the local inundation dynamics from remote sensing datasets. Despite these limitations, our analyses highlight that small, ephemeral wetlands have a greater potential to sequester nutrients and protect downstream waters, and this difference is more significant in semi-arid systems.

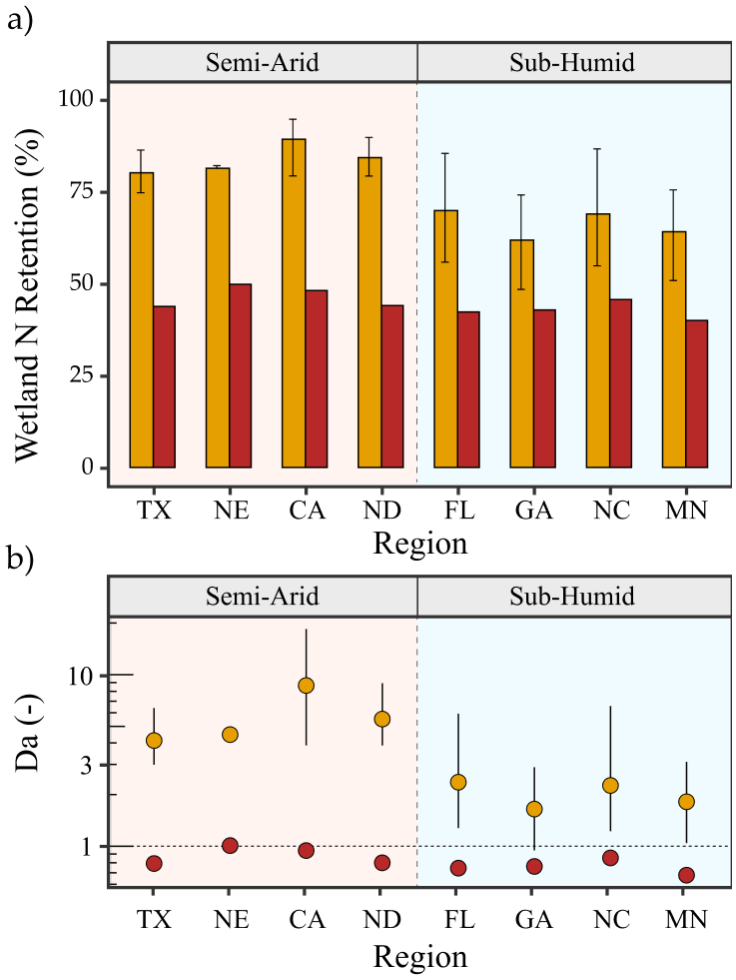

Figure 3.5 Regional estimates of N retention across different wetlandscapes. (A) Percent N retained in each wetlandscape. Transient flow assumptions (gold) removes more N than steady-state assumptions (red). Bars show the median annual removal and bounds indicate the upper and lower quantiles. Ranges shown on the yellow bars are the interquartile range estimates. (B) Damkohler numbers of wetlands in each wetlandscape. Wetlands with Da <1 are considered to be transport dominated, and Da > 1 to be dominated by biogeochemical processes.

3.4 Summary and Conclusions

The ability of wetlands to retain excess nutrients and protect downstream waters is a function of their hydrologic dynamics that drive nutrient inputs and processing rates. There is currently a lack of understanding on how temporal hydrologic dynamics drive nutrient retention patterns in wetlands across large spatial scales. Here, we develop a novel methodology to connect satellite-driven estimates of temporal wetland inundation dynamics to their nutrient retention potential, across

thousands of geographically isolated wetlands (GIWs) in eight US wetlandscapes. We show how small, ephemeral GIWs, especially in semi-arid landscapes, can be disconnected from their uplands for parts of the year due to high evapotranspiration rates, and this disconnectivity increases nitrogen retention time and retention potential. Indeed, when transient dynamics are considered N retention potential can increase by 1.8 times in semi-arid wetlandscapes in the prairie potholes in North Dakota, or the Texas playas, while consideration of transient dynamics only contributed to 1.5 times increase in nutrient retention in the more humid wetlands like the pocosins in North Carolina.

Our study has a few key novel aspects. From a methodological perspective, our work demonstrates the first use of remote sensing data in wetlands across thousands of wetlands for water quality modeling. As such datasets are becoming more common, future research can refine such methodologies and also provide more validation using site specific datasets. From a wetland management perspective our work highlights how the disconnectivity of the wetlands is critical to maintain the integrity of downstream waters -- the steady state assumption captures the behavior of a wetland with a constant, continuous connection to downstream waters, while the transient assumption highlights the potential for intermittent connections to downstream waters that is characteristic of less modified landscapes, and this disconnectivity increases the N retention potential, especially for the smaller, ephemeral wetlands.

Chapter 3 References

Abatzoglou, J.T. *et al.* (2018) 'TerraClimate, a high-resolution global dataset of monthly climate and climatic water balance from 1958-2015', *Scientific data*, 5, p. 170191.

Amado, A.A. *et al.* (4/2018) 'Investigating Hydrologic Connectivity of a Drained Prairie Pothole Region Wetland Complex using a Fully Integrated, Physically-Based Model', *Wetlands*, 38(2), pp. 233–245.

Arheimer, B. and Wittgren, H.B. (2002) 'Modelling nitrogen removal in potential wetlands at the catchment scale', *Ecological engineering*, 19(1), pp. 63–80.

Baron, J.S. *et al.* (2013) 'The interactive effects of excess reactive nitrogen and climate change on aquatic ecosystems and water resources of the United States', *Biogeochemistry*, 114(1), pp. 71–92.

Bertassello, L.E. *et al.* (2018) 'Wetlandscape Fractal Topography', *Geophysical research letters*, 45(14), pp. 6983–6991.

Bertassello, L.E. *et al.* (2020) 'Wetlandscape hydrologic dynamics driven by shallow groundwater and landscape topography', *Hydrological processes*, 34(6), pp. 1460–1474.

Canning, A.D. *et al.* (2021) 'Financial incentives for large-scale wetland restoration: Beyond markets to common asset trusts', *One Earth*, 4(7), pp. 937–950.

Cheng, F.Y. *et al.* (2020) 'Maximizing US nitrate removal through wetland protection and restoration', *Nature*, 588(7839), pp. 625–630.

Cheng, F.Y. and Basu, N.B. (2017) 'Biogeochemical hotspots: Role of small water bodies in landscape nutrient processing', *Water resources research*, 53(6), pp. 5038–5056.

Cohen, M.J. *et al.* (2016) 'Do geographically isolated wetlands influence landscape functions?', *Proceedings of the National Academy of Sciences*, 113(8), pp. 1978–1986.

Cohen, M.J. and Brown, M.T. (2007) 'A model examining hierarchical wetland networks for watershed stormwater management', *Ecological modelling*, 201(2), pp. 179–193.

Creed, I.F. *et al.* (2017) 'Enhancing protection for vulnerable waters', *Nature geoscience*, 10(11), pp. 809–815.

Evenson, G.R. *et al.* (2021) 'Wetland restoration yields dynamic nitrate responses across the Upper Mississippi river basin', *Environmental Research Communications*, 3(9), p. 095002.

Hansen, A.T. *et al.* (2018) 'Contribution of wetlands to nitrate removal at the watershed scale', *Nature geoscience*, 11(2), pp. 127–132.

Hansen, A.T. *et al.* (2021) 'Integrated assessment modeling reveals near-channel management as cost-effective to improve water quality in agricultural watersheds', *Proceedings of the National Academy of Sciences of the United States of America*, 118(28). doi:10.1073/pnas.2024912118.

Hayashi, M., van der Kamp, G. and Rosenberry, D.O. (2016) 'Hydrology of Prairie Wetlands: Understanding the Integrated Surface-Water and Groundwater Processes', *Wetlands* [Preprint]. doi:10.1007/s13157-016-0797-9.

Hayashi, M., van der Kamp, G. and Rudolph, D.L. (6/1998) 'Water and solute transfer between a prairie wetland and adjacent uplands, 1. Water balance', *Journal of Hydrology*, 207(1-2), pp. 42–55.

Jordan, S.J., Stoffer, J. and Nestlerode, J.A. (2011) 'Wetlands as Sinks for Reactive Nitrogen at Continental and Global Scales: A Meta-Analysis', *Ecosystems* , 14(1), pp. 144–155.

Land, M. *et al.* (2016) 'How effective are created or restored freshwater wetlands for nitrogen and phosphorus removal? A systematic review', *Environmental Evidence*, 5(1), p. 9.

Lane, C.R. and D'Amico, E. (2016) 'Identification of Putative Geographically Isolated Wetlands of the Conterminous United States', *JAWRA Journal of the American Water Resources Association*, 52(3), pp. 705–722.

Liebe, J.R. *et al.* (2009) 'Determining watershed response in data poor environments with remotely sensed small reservoirs as runoff gauges', *Water resources research*, 45(7). doi:10.1029/2008wr007369.

Martínez-Espinosa, C. *et al.* (2021) 'Denitrification in wetlands: A review towards a quantification at global scale', *The Science of the total environment*, 754, p. 142398.

Marton, J.M. *et al.* (2015) 'Geographically isolated wetlands are important biogeochemical reactors on the landscape', *Bioscience*, 65(4), pp. 408–418.

McClain, M.E. *et al.* (2003) 'Biogeochemical Hot Spots and Hot Moments at the Interface of Terrestrial and Aquatic Ecosystems', *Ecosystems* , 6(4), pp. 301–312.

Mitsch, W.J. *et al.* (2005) 'Nitrate-nitrogen retention in wetlands in the Mississippi River Basin', *Ecological engineering*, 24(4), pp. 267–278.

Morgan, L.R., Hayashi, M. and Cey, E.E. (2021) 'Land-use comparison of depression-focussed groundwater recharge in the Canadian prairies', *Hydrological processes*, 35(9). doi:10.1002/hyp.14379.

Musolff, A. *et al.* (12/2015) 'Catchment controls on solute export', *Advances in water resources*, 86, pp. 133–146.

Oldham, C.E., Farrow, D.E. and Peiffer, S. (2013) 'A generalized Damköhler number for classifying material processing in hydrological systems', *Hydrology and Earth System Sciences*, 17(3), pp. 1133–1148.

Park, J. *et al.* (2022) 'Seasonality of inundation in geographically isolated wetlands across the United States', *Environmental research letters: ERL [Web site]*, 17(5), p. 054005.

Pekel, J.-F. *et al.* (2016) 'High-resolution mapping of global surface water and its long-term changes', *Nature*, 540(7633), pp. 418–422.

Powers, S.M., Tank, J.L. and Robertson, D.M. (5/2015) 'Control of nitrogen and phosphorus transport by reservoirs in agricultural landscapes', *Biogeochemistry*, 124(1-3), pp. 417–439.

Quin, A., Jaramillo, F. and Destouni, G. (2015) 'Dissecting the ecosystem service of large-scale pollutant retention: The role of wetlands and other landscape features', *Ambio*, 44 Suppl 1(S1), pp. S127–37.

Saunders, D.L. and Kalff, J. (2001) 'Nitrogen retention in wetlands, lakes and rivers', *Hydrobiologia*, 443(1-3), pp. 205–212.

Sloan, C. (1972) *Ground-water hydrology of prairie potholes in North Dakota*. Geological Survey Professional Paper 585-C. U.S. Geological Survey. Available at: https://pubs.usgs.gov/pp/0585c/report.pdf.

Thorslund, J. *et al.* (2017) 'Wetlands as large-scale nature-based solutions: Status and challenges for research, engineering and management', *Ecological engineering* [Preprint]. doi:10.1016/j.ecoleng.2017.07.012.

Tiner, R.W. (2003) 'Geographically isolated wetlands of the United States', *Wetlands*, 23(3), pp. 494–516.

Vanderhoof, M.K., Christensen, J.R. and Alexander, L.C. (2017) 'Patterns and drivers for wetland connections in the Prairie Pothole Region, United States', *Wetlands Ecology and Management*, 25(3), pp. 275–297.

Van Meter, K.J. and Basu, N.B. (2015) 'Signatures of human impact: size distributions and spatial organization of wetlands in the Prairie Pothole landscape', *Ecological applications: a publication of the Ecological Society of America*, 25(2), pp. 451–465.

Vollenweider, R.A. (1975) 'Input-output models', *Schweizerische Zeitschrift fur Hydrologie*, 37(1), pp. 53–84.

Winter, T.C. and LaBaugh, J.W. (2003) 'Hydrologic considerations in defining isolated wetlands', *Wetlands*, 23(3), pp. 532–540.

Wu, Q. and Lane, C.R. (2017) 'Delineating wetland catchments and modeling hydrologic connectivity using lidar data and aerial imagery', *Hydrology and Earth System Sciences*, 21(7), pp. 3579–3595.

Chapter 4

Nevertheless, they persisted: Can hyporheic zones increase the persistence of estrogens in streams?

Chapter 4 Abstract

The presence of estrogens has been linked to adverse ecological effects in surface waters downstream of agricultural and domestic wastewater sources. While laboratory studies suggest that these estrogens should not persist because of fast degradation rates, elevated concentrations in surface waters impacted by agricultural activities are commonly observed. Using a combination of measured data and a stream-hyporheic zone (HZ) model applied to a 100 km reach in a tile-drained catchment, we show that the HZ can increase the persistence of estrogens. Field data reveal high concentrations of sorbed estrogens in sediments and elevated in-stream concentrations during low-flow summer months, suggesting that the HZ acts as a source of estrogens when transport into the streams is minimal. Model results provide further insight into the underlying mechanisms that enable sustained estrogen concentrations in streams, with the HZ acting as a source of dissolved estrogens for 95% of the year. We show that streamwater interactions with the HZ may lead to overall suppression of degradation processes and an increase in the persistence of estrogens. Results suggest that when the model considered exchange in the HZ, approximately 28-49% of estrogen mass remained in the stream ecosystem, while all estrogen mass was degraded in a 100-km reach in the model without the HZ. The mass remaining increased with increasing estrogen sorption coefficient, and this would potentially increase the lag time for lowering estrogen concentrations in surface water bodies even when inputs have ceased. Our findings highlight the importance of including HZ dynamics in estrogen transport models.

4.1 Introduction

Increases in the use of steroidal hormones in agricultural, urban, and industrial (e.g., land application of manure, municipal and industrial wastewater discharge) activities (Jobling et al., 1998; Matthiessen et al., 2006) have been implicated in the development of cancerous tumors and sex changes in fish (Leet et al., 2011; Panter et al., 1998; Vajda et al., 2008), and even the population collapse of certain species within aquatic ecosystems (Coe et al., 2008; Kidd et al., 2007). While early research on hormones primarily focused on urban streams (Khanal et al., 2006; Kolpin et al., 2002; Snyder et al., 2003), streams that drain manure-applied agricultural lands have received more attention in the last decade (Gall et al., 2016; Lafrance & Caron, 2013; Zhao et al., 2010). Indeed, hormones are routinely detected in the 50 million tons of animal manure produced annually in the United States (US), most of which are applied to croplands to meet nutrient demands (USEPA, 2000). Reproductive hormones, like estrogens, have been of particular interest due to the intensification of livestock activities, such that naturally excreted hormones in manure from concentrated animal feeding operations (CAFOs) are being inadvertently transported to surface and groundwater bodies (Alvarez et al., 2013; Gall et al., 2011). Agricultural areas have been estimated to contribute more than 90% of the total estrogen into the environment, as livestock can excrete an order of magnitude more estrogens than humans per capita (Khanal et al., 2006; Raman et al., 2004).

Estrogen loadings from agricultural fields to surface waters are controlled by hydroclimatic conditions (rainfall patterns), landscape characteristics (soil type, topography, presence or absence of tile drainage, etc.), and the properties of the particular estrogen (e.g. sorption coefficients, decay rates) (Gall et al., 2016; Khanal et al., 2006). Based on laboratory studies, most steroidal hormones have moderately large sorption coefficients and short half-lives under aerobic conditions, typically ranging from a few hours to a few days (Bradley & Writer, 2014; Kolpin et al., 2002; Mashtare et al., 2013a; Ying et al., 2002; Zuo et al., 2013). This suggests that their persistence in natural environments should be limited; however, hormones have been consistently detected in soils and streams draining agricultural fields for extended periods of time, even long after manure application and runoff events (Chen et al., 2010; Ciparis et al., 2012; Finlay-Moore et al., 2000; Nichols et al., 1998; Shore et al., 1995). In fact, in a comprehensive survey across US streams, reproductive hormones were detected in over 40% of the samples, and estrogens were the most frequently detected

group of hormones, found in over 20% of sampled streams predominantly in urban and agricultural areas (Kolpin et al., 2002).

This persistence of estrogens in streamwater, despite their fast decay rates, highlights the importance of the interactions of anthropogenic inputs of estrogens with natural hydrologic and biogeochemical processes that can lead to the observed estrogen persistence. For example, Gall et al. (2016) sought to explain higher than expected estrogen loads observed at a tile-drained agroecosystem in the Midwestern US by accounting for the application history of the site and modeling the estrogen accumulation in agricultural soils by considering two decades of manure application. Several field studies have also observed elevated concentrations of estrogen in agricultural streams months after the last manure application (Kjaer et al., 2007; Schoenborn et al., 2015), with some hypothesizing that elevated concentrations were attributed to estrogens desorbing from the streambed sediment. For instance, Zhang et al. (2015) found evidence of endocrine disruption in fish that were chronically exposed to hormones that desorbed from contaminated sediments in agricultural streams. Kolok et al. (2014) provided a conceptual model that described the accumulation and depletion of biologically active compounds like estrogens from sediments in agricultural streams, with streambed sediment acting as a contaminant source during low-flow conditions when the water column is generally "clean", and acting as a sink during high-flow conditions when the water column has contaminants generated during surface runoff events.

While the dual role of the sediments as a source and sink has been demonstrated for nutrients (eg. Schindler & Krabbenhoft, 1998, Zarnetske et al., 2012), there has been little focus on how the source-sink behavior modifies the spatiotemporal persistence of hormones that have been transported to agricultural streams in tile drainage and surface runoff. Indeed, most available stream models used to conduct risk assessments of hormonal compounds do not account for this dynamic source-sink behavior of sediments (Anderson et al., 2012; Arlos et al., 2018; Green et al., 2013; Hannah et al., 2009; Klein, 2004; Williams et al., 2009; X. Zhao & Lung, 2017). One of the only exceptions to this is a modeling study of trenbolone by Ward et al. (2015), where the authors explored how the day-night cycle and interaction with the hyporheic zone (HZ) limited the photodegradation process and consequently led to the persistence of trenbolone in streams at the sub-daily timescale. Thus, there still exists a considerable gap in our understanding of how the unique physicochemical properties of

these nutrients and hormonal compounds contribute to their persistence at different timescales (hourly to decadal). We further argue that the lack of consideration of bi-direction exchanges with the hyporheic zone in most stream models (e.g. the PhATE and GREAT-ER models, c.f. Hannah et al., 2009) can lead to an underestimation of the possible persistence of these estrogens.

The goal of our study is to address this knowledge gap by focusing on the following questions: 1) How do the source-sink dynamics due to the presence of the HZ affect in-stream estrogen concentrations?; 2) Can consideration of HZs in a model explain the persistence of estrogens in stream ecosystems at seasonal and annual timescales?; and 3) How does the potential for estrogens to sorb to the sediment impact their spatial and temporal persistence in the stream network? Our central hypothesis is that persistence of estrogens in the stream network can occur due to exchange of estrogens between the streamwater and the hyporheic zone.

Here, we use a combination of data analysis and modeling to understand the role that exchange dynamics in the hyporheic zone may play in explaining the observed persistence of hormones in a tile-drained agricultural catchment in the Midwestern US. The estrogens considered are estrone (E1), and estradiol (E2), both of which are excreted naturally by livestock. E2 is considered to be the more potent estrogen, and is approximately three times more estrogenic than E1 (Thorpe et al., 2003). E2 has two isomers, 17α- and 17β-estradiol, and degrades to E1 which can further break down into estriol (E3) through aerobic degradation or photodegradation (Adeel et al., 2017; Campbell et al., 2006; Ying et al., 2003). Under anaerobic conditions, however, it has been shown that E1 can be converted back to the more potent estrogen E2 (Mashtare et al., 2013b; Prater et al., 2015). This could lead to an increase in the persistence of E2 under anaerobic streambed sediment conditions. We model both forward and backward reactions between E2 and E1 to understand the persistence of hormones.

4.2 Methods

4.2.1 Field Study and Data Collection

The field data used in this study were collected at Purdue University's Animal Science Research and Education Center (ASREC) located in West Lafayette, Indiana. This field site is a designated CAFO, with more than 6000 livestock units (beef and dairy cattle, poultry, sheep, and swine) and a working

farm comprised of 600 hectares of tile-drained cropland. Although waste management varies by livestock type, the manure from the livestock is generally flushed into a series of primary and second lagoons. Effluent from the lagoons is then land-applied to cropland via solids broadcasting, pivot irrigation, or subsurface injection. Previous work at this site has shown that hormones present in land-applied residuals enter nearby receiving ditches through both tile drainage and surface runoff pathways (Gall et al., 2011).

The data used in this study included sub-daily flow (15-minute) and in-stream estrogen concentrations previously collected at ASREC to characterize hormone dynamics (Gall et al., 2011). Multiple tile drain and drainage ditch locations at the ASREC site have been monitored for flow and sampled for estrogens and nutrients, with the results previously published (Gall et al., 2011, 2015, 2016). For this study, we focused on the water samples collected in one tile drain that fed into the ditch network and one ditch location 1.5 km downstream of the tile drain between January and December in 2009 (locations D3 and S2 in Gall, 2011). This pair of sampling locations were selected to minimize the number of contributing ditches that fed into the network. At both stations, an automated sampler collected 1 L water samples to span both base flow and the rising/recession limb of storm hydrographs (Gall et al., 2010). A total of 555 water samples from the tile drain and 432 from downstream were taken throughout the January-December 2009 sampling period. Concentrations of both E2 isomers (17α- and 17β-estradiol) and E1 were then determined through mass spectrometry analysis from the water samples. We consider the sum of 17α- and 17β-estradiol concentrations as total E2 concentrations. Additional sediment samples were collected at 14 locations along the ditch network, and sorbed estrogen concentrations were determined by mass spectroscopy using sediment samples collected in May and August of 2009. Full sampling and experimental methodology of in-stream samples is described by Gall et al. (2011) and sediment sampling by Mashtare (2013). Note that values below the limit of detection from the mass spectroscopy analysis were treated as zero concentration in the samples, and values between the limits of detection and quantitation (LOQ) were replaced with $LOQ/\sqrt{2}$ (Succop et al., 2004), where LOQ is used to describe the lowest concentration of an analyte that can be reported with a degree of confidence specified by the equipment and quality control protocol.

4.2.2 Model Formulation and Simulations

To quantify the role of the HZ in increasing the persistence of estrogens, we conducted numerical simulations of estrogen transport in a stream-hyporheic system, with and without the presence of the HZ (**Figure 4.1**). We use the term stream and ditch interchangeably in this paper since porewater in the ditch sediment interacts with the ditch water similar to a stream-hyporheic system, and the model we use is what is traditionally used for a stream reach. In fact, in low land agricultural areas, with significant density of tile drains, ditches and streams, the boundaries between ditches and streams is often unclear (Biggs et al., 2017; Clifford & Heffernan, 2018).

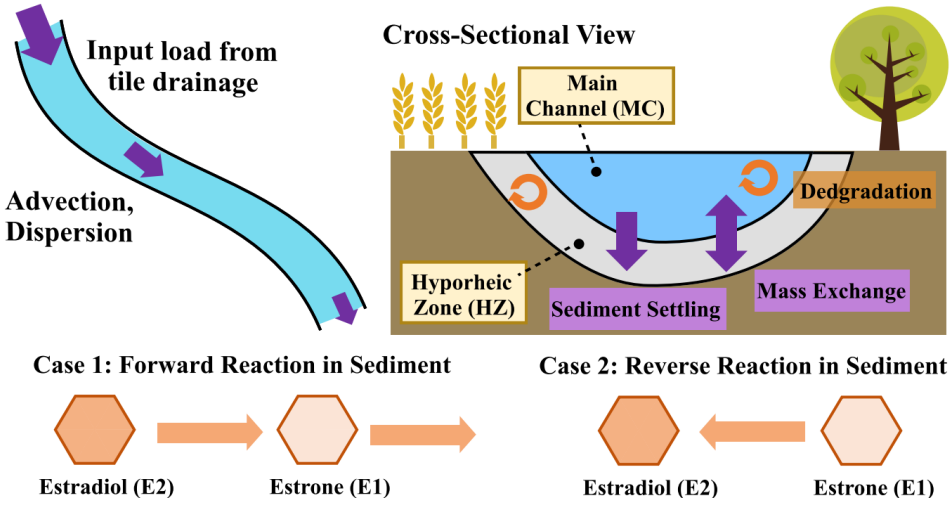

Figure 4.1 Modeling framework depicting physical (purple arrows) and biogeochemical (orange arrows) fluxes between the main channel (MC) and the hyporheic zone (HZ). Case 1 illustrates the forward degradation of E2 to E1 in aerobic conditions and the degradation of E1 to E3 (**Equations 3a and 4a**) while Case 2 shows the reversion of E1 back to E2 in anaerobic conditions (**Equations 3b and 4b**).

Our model formulation is based on the One-Dimensional Transport with Inflow and Storage (OTIS) model that has been extensively used to quantify tracer and contaminant transport along stream networks (Bencala & Walters, 1983; Boano et al., 2014; Runkel, 1998). The OTIS model conceptualizes the HZ as a well-mixed reservoir of finite size (transient storage zone) that is connected to the main channel, and temporarily holds the solute, thereby delaying its downward transport for timescales longer than can be captured by processes of advection and dispersion

(Runkel, 1998). Water and solute exchange between the water column and the transient storage zone is described using a bi-directional first order mass exchange term (with constant α, time^{-1}) that is a lumped representation that describes various complex environmental transport processes between the main stream channel and transient storage zones, including hyporheic exchange (Bencala et al., 2011).

We modified the OTIS model in two specific ways to capture the complexity of processes that are specific to hormone transport in small streams draining agricultural landscapes. First, these streams have high concentrations of suspended sediments (Sassman, 2014; Hodaj et al., 2017), and these get entrapped in the streambed during advective transport of streamwater into the HZ, contributing to high estrogen concentrations in the sediments. Indeed, we found that consideration of an entrapment flux was critical to build up the observed estrogen mass in the sediment. We model this sediment flux as a unidirectional mass exchange process between the main channel and the transient storage. Note that this process represents a combination of net settling (settling - resuspension) of sorbed estrogens and entrapment of fine sediments as water carrying the sediments enters the HZ.

We next modified the OTIS model by considering two interacting species E2 and E1, following Ward et al. (2015). The main biogeochemical processes simulated in our model are the decay of E2 to E1 and E1 to E3 (both in the water column and the porewater of the HZ), and sorption to sediments. Additionally, we also separately simulated the reverse transformation of E1 to E2, a process that has been demonstrated to occur in anaerobic sediments (Prater et al., 2015). We modeled E2 as the aggregated concentrations of 17α- and 17β-E2, since the two isomers behave similarly in the environment (Adeel et al., 2017). Although we modeled both E2 and E1, we focused our analyses on E2 since it is the more potent estrogen (Thorpe et al., 2003).

The following system of coupled partial differential equations were used to describe the stream (**Equations 4.1 and 4.2**) and the HZ (**Equations 4.3 and 4.4**) processes for E2 and E1 (Liu et al., 2019; Ward et al., 2015). Two alternate pathways, which have been both observed in natural systems are simulated separately in the HZ as end-member scenarios: Case 1) degradation of E2 to E1 and E1 to E3 (**Equations 4.3a and 4.4a** respectively); Case 2) transformation of E1 to E2 (**Equations 4.3b and 4.4b** respectively). We define the main channel (MC) as the streamwater and the stream sediment

interacting with the MC as the hyporheic zone (HZ). The evolution of dissolved MC concentrations of E2 and E1 (C_{E2}^{MC} and C_{E1}^{MC}; μg/m^3 of MC) can be described using the following equations:

$$\frac{\partial C_{E2}^{MC}}{\partial t} = -v\frac{\partial C_{E2}^{MC}}{\partial x} + D\frac{\partial^2 C_{E2}^{MC}}{\partial x^2} - \frac{\alpha}{\beta 2}\left(C_{E2}^{MC} - C_{E2}^{HZ}\right) - \frac{k_{E2}^{MC}}{\beta 2} C_{E2}^{MC} - \frac{k_{sed}}{\beta 2}\, K_{d,E2}\, S\, C_{E2}^{MC} \quad \textbf{(4.1)}$$

$$\frac{\partial C_{E1}^{MC}}{\partial t} = -v\frac{\partial C_{E1}^{MC}}{\partial x} + D\frac{\partial^2 C_{E1}^{MC}}{\partial x^2} - \frac{\alpha}{\beta 1}\left(C_{E1}^{MC} - C_{E1}^{HZ}\right) + \frac{k_{E2}^{MC}}{\beta 1} C_{E2}^{MC} - \frac{k_{E1}^{MC}}{\beta 1} C_{E1}^{MC} - \frac{k_{sed}}{\beta 1} K_{d,E1}\, S\, C_{E1}^{MC} \quad \textbf{(4.2)}$$

The differential equations describing the aqueous HZ concentrations of E2 and E1 (C_{E2}^{HZ} and C_{E1}^{HZ}; μg/m^3 of HZ) are:

$$\frac{\partial C_{E2}^{HZ}}{\partial t} = \frac{A}{A_s}\frac{\alpha}{n*R_{E2}}\left(C_{E2}^{MC} - C_{E2}^{HZ}\right) - \frac{k_{E2}^{HZ}}{R_{E2}} C_{E2}^{HZ} + \frac{A}{As}\frac{k_{sed}}{n*R_{E2}} K_{d,E2}\, S\, C_{E2}^{MC} \quad \textbf{(4.3a)}$$

$$\frac{\partial C_{E1}^{HZ}}{\partial t} = \frac{A}{A_s}\frac{\alpha}{R_{E1}}\left(C_{E1}^{MC} - C_{E1}^{HZ}\right) + \frac{k_{E2}^{HZ}}{R_{E1}} C_{E2}^{HZ} - \frac{k_{E1,F}^{HZ}}{R_{E1}} C_{E1}^{HZ} + \frac{A}{As}\frac{k_{sed}}{n*R_{E1}} K_{d,E1}\, S\, C_{E1}^{MC} \quad \textbf{(4.4a)}$$

The differential equations representing the reverse reactions in the HZ (Case 2) are:

$$\frac{\partial C_{E2}^{HZ}}{\partial t} = \frac{A}{A_s}\frac{\alpha}{n*R_{E2}}\left(C_{E2}^{MC} - C_{E2}^{HZ}\right) + \frac{k_{E1,R}^{HZ}}{R_{E2}} C_{E1}^{HZ} + \frac{A}{As}\frac{k_{sed}}{n*R_{E2}} K_{d,E2}\, S\, C_{E2}^{MC} \quad \textbf{(4.3b)}$$

$$\frac{\partial C_{E1}^{HZ}}{\partial t} = \frac{A}{A_s}\frac{\alpha}{n*R_{E1}}\left(C_{E1}^{MC} - C_{E1}^{HZ}\right) - \frac{k_{E1,R}^{HZ}}{R_{E1}} C_{E1}^{HZ} + \frac{A}{As}\frac{k_{sed}}{n*R_{E1}} K_{d,E1} S\; C_{E1}^{MC} \quad \textbf{(4.4b)}$$

where v is the average velocity in the channel (m/d), D is the dispersion coefficient (m^2/d), α is the mass exchange coefficient between the channel and hyporheic zone (1/d), k_{E2}^{MC} is the rate constant of the E2 to E1 degradation pathway in the main channel (1/d), k_{sed} is the net fine sediment flux that includes settling, resuspension and entrapment of suspended solids (1/d), S is the concentration of suspended solids in the water column (kg/L), $K_{d,E2}$ and $K_{d,E1}$ are the sediment-water partition coefficients of E2 and E1 respectively (L/kg), $k_{E1,F}$ is the rate constant for the forward decay pathway of E1 to E3 (1/d), $k_{E1,R}$ is the rate constant for the reverse pathway of E1 to E2 (1/d), A/A_s is the ratio of the cross-sectional area of the main channel to the sediment (m^2/m^2) and R_{E2} and R_{E1} are the retardation factors for E2 and E1, defined as $R = 1 + (\rho_b/n)K_d$ (-). β_{E2} and β_{E1} are conversion factors

that quantify the dissolved fraction of E2 and E1 in the water column in the main channel, where $\beta_2 = (1 + K_{d,E2}S)$ and $\beta_2 = (1 + K_{d,E1}S)$.

The above set of equations were discretized spatially using a finite volume approach and solved numerically with the Crank-Nicolson scheme in MATLAB, with spatial steps of 200 meters and temporal steps of 0.01 days, that were chosen to ensure numerical stability of the model. Each control volume was assumed to be well-mixed and all parameters (such as velocity, chemical properties, etc.) were considered to be spatially homogenous throughout the model space to ensure model stability. The total modelled stream length of 75 km was chosen to be much longer than the modelled stream lengths to avoid numerical artefacts with boundary conditions.

4.2.3 Model Parameters, Inputs and Outputs, and Calibration Methodology

Model parameters were estimated using a combination of literature review, site specific information and manual calibration (**Table 4.1**). Flow measurements were taken at the site and converted to average velocity values based on site-specific flow-velocity relationships (**Supporting Information in Appendix B**) (Sassman, 2014). The median velocity was estimated to be 20 km/d during the low-flow period and 35 km/d during the high flow period from measured field data. Because the other physical parameters of the model - the dispersion coefficient (D), mass exchange coefficient (α), and ratio between the stream and HZ cross-sectional areas (A/A_S) – are difficult to fully parameterize at any site due to their dynamic nature (Marion et al., 2003; Kerr et al., 2013), these values were constrained by a range of literature values of small first-order streams, and then further calibrated within these ranges to best fit the data. Further details on the calibration methodology provided later in the section.

The degradation of E2 and E1 can occur via biotic (aerobic degradation) (Bradley et al., 2009; Lee & Liu, 2002) or abiotic (photodegradation) (Chowdhury et al., 2010; Lin & Reinhard, 2005; Zuo et al., 2013) pathways. In our model, we assumed that photodegradation and biodegradation occurred in the main channel, while only biodegradation occurred in the HZ. The range of biodegradation rate constants ($k_{MC,bio}$ for E2 and E1) were derived from experimental incubation studies from samples collected at the site (**Table 4.1**) (Mashtare et al., 2013a; Mashtare et al., 2013b), while photodegradation rate constants ($k_{MC,photo}$ for E2 and E1) were obtained from literature values (Adeel

et al., 2017; Lin & Reinhard, 2005). The total degradation rates in the main channel ($k_{E2,MC}$ and $k_{E1,MC}$) is the sum of the biodegradation and photodegradation rate constants and was calibrated as an effective parameter that is constant in time as there was insufficient data to capture time-varying rates.

Although suspended sediment concentrations can vary greatly over the year, we calibrated our model to obtain an effective annual value within the bounds of likely values using limited data measured at our study site and a nearby agricultural ditch (Sassman, 2014; Hodaj et al., 2017). Sorption of E2 and E1 to suspended sediments in the water column and bed sediments in the HZ was assumed to occur via linear, reversible sorption processes, with a range of values for the partition coefficient K_d (L/kg) (Lee et al., 2003; Mashtare et al., 2011). The range of partition coefficients for E2 were based on a combination of previously determined parameters using experimental geochemical data derived from samples at the ASREC field site and soils from other agricultural sites (Mashtare, 2013). The range of partition coefficients for E1 was based on literature values as there was insufficient data from the ASREC field site (Chen et al., 2012; Gall et al., 2016). Given the significant uncertainty in estimating site-specific rate constants, we used the range of partition coefficients for model calibration (**Table 4.1**), and the best fit parameter set was used in our simulation scenarios. Although settling of suspended sediments can be a significant flux of E2 and E1 from the main channel to the HZ, suspended sediment concentrations were not measured routinely at the site. We thus estimated it by calibration, and the range of values for calibration (see **Table 4.1**) was based on sporadically measured data at the site (Sassman, 2014; Hodaj et al., 2017). The unidirectional sediment flux constant k_{sed} is a lumped term that encapsulates the sediment settling and resuspension process as well as the entrapment of fine sediments as streamwater flows through the HZ. Since k_{sed} is an effective term that represents multiple processes, we used settling constants ($k_{settling}$ = settling velocity/depth) from literature as an initial starting point for k_{sed}, then further refined the value through model calibration to capture the additional effect of entrapment of fine sediments (**Table 4.1**).

Table 4.1 Parameters used for model calibration, and final calibrated values

Parameter	Variable	Range	Calibrated Value	Units	Source
Hydrological Transport					
Dispersion coefficient in main channel	D	1.9-250	8.6	m^2/s	(Deng et al., 2002; Runkel, 1998)
Mass exchange coefficient	α	0.4-48	1.5	1/d	(Battin et al., 2008)
Ratio of stream/HZ areas	A/As	0.1-1.4	1.4	-	(Bencala & Walters, 1983; Stewart et al., 2011)
Soil bulk density	ρ_b	1100-1500	1300	kg/m^3	(Gall et al., 2016)
Porosity	n	0.3-0.5	0.4	-	(Gall et al.. 2016)
Reaction Rates (Main Channel)					
E2 to E1 in MC (total = photodegradation + biodegradation)	$k_{E2,MC}$	0.25-8.3 (photo) 0.2-3.2 (bio)	2.5 (total)	1/d	(Photo: Adeel et al., 2017; Lin & Reinhard, 2005; Bio: Jürgens et al., 2002; Mashtare et al., 2013a*)
E1 to E3 in MC (total = photodegradation + biodegradation)	$k_{E1,MC}$	0.22-10 (photo) 0.4-5.0 (bio)	12 (total)	1/d	(Photo: Adeel et al., 2017; Lin & Reinhard, 2005; Bio: Jürgens et al., 2002; Mashtare et al., 2013a*)
Reaction Rates (Hyporheic Zone)					
E2 to E1 in HZ	$k_{E2,HZ}$	0.2-3.2	0.9	1/d	(Jürgens et al., 2002; Mashtare et al., 2013a*)
E1 to E3 in HZ	$k_{E1,HZ,F}$	0.4-5.0	0.4	1/d	(Jürgens et al., 2002; Mashtare et al., 2013a*)
E1 to E2 in HZ	$k_{E1,HZ,R}$	0-0.15	0.06	1/d	(Zheng et al., 2012; Mashtare et al., 2013b*)
Solid Phase Parameters					
Suspended solids concentration in MC	S	1-1436	260	mg/L	(Sassman, 2014*; Hodaj et al., 2017)
Net sediment removal rate constant	k_{sed}	0.08 -1800	180	1/d	Range initially estimated as settling velocity/depth (Haan et al., 1994; Liu et al., 2018)
Partition Coefficient of E2	$K_{d,E2}$	3-102	75	L/kg	(Mashtare, 2013*)
Partition Coefficient of E1	$K_{d,E1}$	12-67	65	L/kg	(Chen et al., 2012; Gall et al., 2016*)
Retardation factor of E2 in HZ	R_{E2}	14-443	326	-	Calculated using $R = 1 + (\rho_s/n)K_d$
Retardation factor of E1 in HZ	R_{E1}	53-291	282	-	

* Previously determined site-specific parameters at ASREC field site

To determine how E2 accumulation in the sediment could be affected by changes in the model parameters, we performed a one-at-a-time sensitivity analysis by perturbing each parameter systematically by ±10% (**Table S1** in Supplementary Information in Appendix B) (Pianosi et al., 2016). We found that the ratio of the stream-HZ areas (A/A_s) and the physical transport parameters were the most important (stream velocity, and mass exchange). Among the biogeochemical parameters, the partition coefficient K_d plays a major role in controlling the amount of estrogen that accumulates in the HZ, where a 10% increase leads to a 0.9% increase in E2 mass.

Flow and estrogen concentration data measured at the tile outflow (location D3, Section 2.1) were used as model input, while the same measured at the ditch location S2 was used as the model output. The model was initialized by running it until the model reached a pseudo-steady state such that there was no net accumulation in the sediments in the subsequent years. After initialization, the model was calibrated to monthly aggregated E2 and E1 loads in the ditch, as well as E2 and E1 concentrations measured in the ditch sediment. The metrics percent bias (PBIAS) and r^2 between modelled and measured loads was used for calibration. PBIAS is calculated as $[\Sigma(L_{sim}-L_{obs}) / \Sigma(L_{obs})]* 100\%$, where L_{sim} is the simulated monthly load from the model and L_{obs} is the observed monthly load from the field data. A sequential calibration method was used where E2 in water column and sediment was calibrated first, followed by calibration of E1.

4.2.4 Simulation Scenarios

There are two sets of scenarios that were simulated using the calibrated model to understand the role of the HZ in increasing the persistence of estrogens in the stream ecosystem. We developed models with and without the HZ to isolate the role of the HZ in increasing estrogen persistence. In the first set of scenarios (Scenario 1) we focused on degradation pathways in the HZ, and quantified the mass of estrogens left behind in the stream-sediment system given: (a) Case 1: calibrated model with decay of E2 to E1 to E3 in the HZ (decay rates estimated by model calibration), which is assumed to occur under aerobic conditions; and (b) Case 2: reverse transformation of E1 to E2 in the HZ, which is assumed to occur only under anaerobic conditions. Local conditions in the streambed would determine which pathway is active – given such data was not available at our site we evaluated the impact of both pathways in E2 persistence.

The second set of scenarios (Scenario 2) included exploring the effect of variability in the sorption coefficient K_d and the retardation factor R on the persistence of estrogens. To do this, we varied the retardation factor for E2 by using a range of K_d values (4.4-102 L/kg) based on data collected at the site (Mashtare, 2013). We further held the ratio between the retardation factors of E2 and E1 constant at 1.3, which was the calibrated ratio from Scenario 1a above. A constant ratio is a reasonable assumption, given that differences in retardation factor between sites can be expected to arise due to local sediment characteristics that will most likely affect E2 and E1 similarly. Further, this assumption allows us to isolate the effect of changing the magnitude of the R, while holding the

relationship between the two chemicals constant. We defined two metrics to describe the spatial and temporal persistence of hormones: (1) the Spatial Zone of Influence (SZOI) is defined as the longitudinal distance along the stream over which water column concentrations are decreased to 95% of the input, and the (2) Temporal Zone of Influence (TZOI) is the time it takes for the reach to flush out 95% of the input mass after input loading has ceased. We quantified how SZOI and TZOI change across a continuum of retardation factors.

4.3 Results and Discussion

4.3.1 Seasonal Source-Sink Dynamics of the Hyporheic Zone: Analysis of Field Observations

We compared previously published E2 and E1 concentrations at a single tile drain and ditch location at the ASREC site to understand the downstream propagation of the input pulse from the tile to the ditch location (**Figure 4.2a-d**) (Gall et al., 2011). We separated the year into a low-flow period (July to mid-October) and a high-flow period (mid-October to June), based on an analysis of the flow duration curves at the tile and ditch locations that highlighted significantly greater flows (Wilcox rank sum test, $p < 0.001$) during the high-flow period (median flow of 0.67 m^3/min with an interquartile range (IQR) of 0.35 to 1.44 m^3/min) compared to the low-flow period (median flow of 0.004 m^3/min, IQR of 0 to 0.075 m^3/min) (**Figure S1 in Supporting Information in Appendix B**).

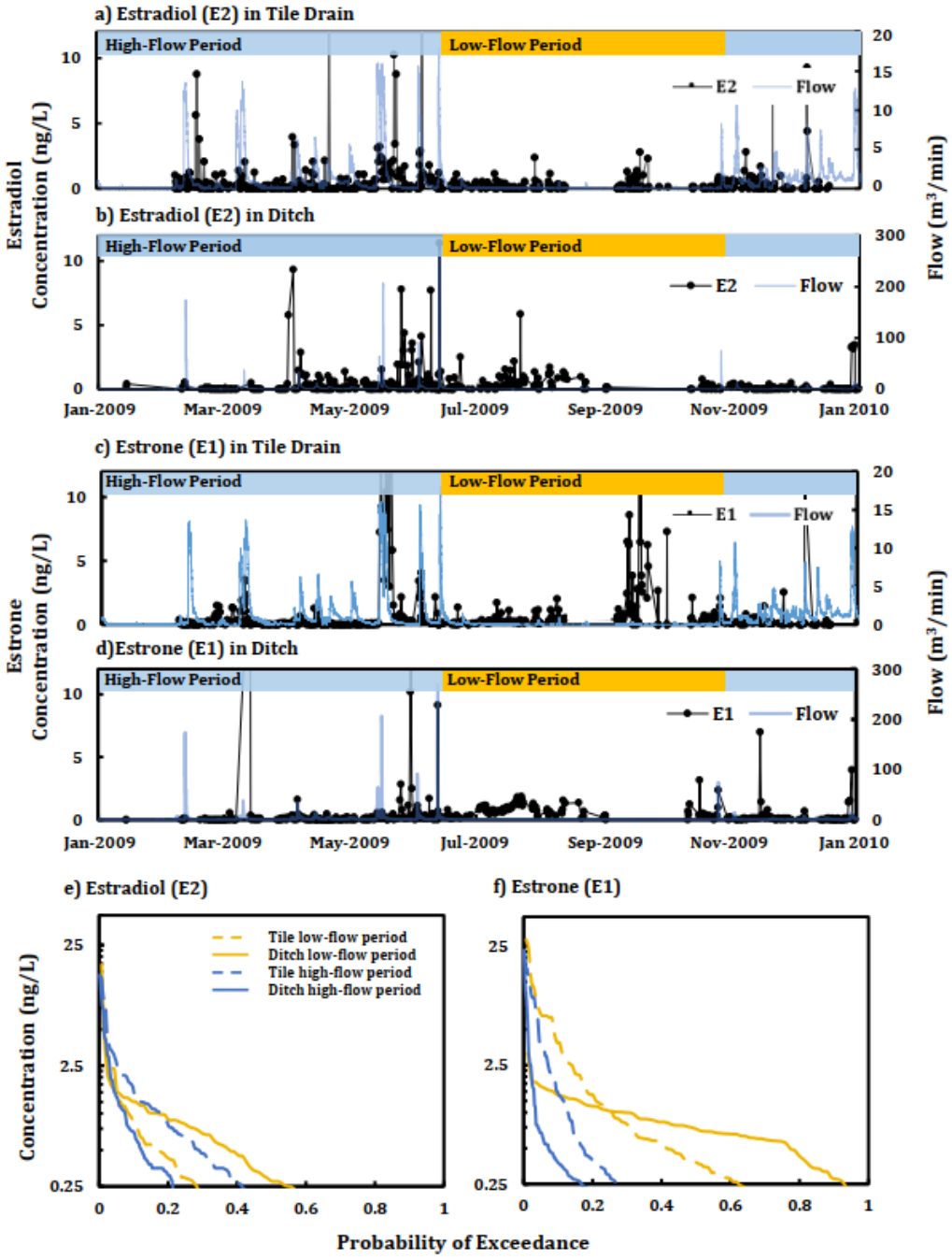

Figure 4.2 Time series of flow and estrogen concentrations of a) E2 in the tile drain and b) E2 in the ditch; c) E1 in the tile drain and d) E1 in ditch. Separation of high and low flow periods are based on mean discharge (see **Figure S1 in Supporting Information**). Exceedance probability plots in tile and ditch for e) E2 and f) E1 in the high- and low-flow period (data from Gall 2011, 2013, 2015).

Aqueous E2 concentrations observed in the tile drain were greater during the high flow period (mean E2 concentration = 0.71 ng/L) compared to the low flow period (mean E2 concentration = 0.50 ng/L) (**Figure 4.2e**), with storm events mobilizing estrogens that had been introduced to the field during irrigation events. In contrast to the tile response, however, ditch E2 concentrations were observed to be higher during the low flow period compared to the high flow period (**Figure 4.2e**). No major surface runoff events were observed during the low flow period (July to October) that could have mobilized hormones and contributed to the consistently higher E2 concentrations. We further found that during the high flow period, aqueous E2 concentrations in the ditch water were lower than the concentrations in the tile drain and this could potentially be attributed to the HZ in the ditch acting as a sink and/or dilution of the ditch flow due to surface runoff events. In contrast, during the low flow period, E2 concentrations in the tile water were lower than concentrations in the ditch water, indicating additional sources of hormones to the ditch. The two other possible sources are (a) desorption from bed sediments, and (b) flow into the ditch section from other tile drains or groundwater flow. It is unlikely that hormone concentrations in groundwater would be high given the high retardation factors in the upland soil matrix – consequently, most estrogens should be relatively immobile in the soil due to sorption (Gall et al., 2016). Thus, desorption from sediments in the ditch is the most likely reason for higher ditch concentrations in the low-flow period and warrants further investigation with modeling. The sorbed concentrations in the ditch sediment during the low-flow period (Mashtare, 2013) were also fairly high (median of 0.10 µg/kg of E2 and an interquartile range of 0.04 to 0.17 µg/kg), thus confirms the potential for the sediment to act as a source of E2 to the streamwater (Kolok et al., 2014).

E1 concentrations observed in the tile drain and the ditch during the high and low flow periods are more difficult to interpret because of the transformation of E1 from E2 (**Figure 4.2f**). In the high flow periods, tile concentrations were observed to be greater than the ditch water concentrations, which are similar trends to those that were observed for E2. However, in contrast to E2, E1 concentrations during low flow periods were observed to be higher than the concentrations during high flow periods, in both tile and ditch waters, possibly due to the greater residence times in the tile and ditch during the low flow periods, allowing more decay from E2 to E1.

To summarize, our data analysis suggests the possibility that streambed sediments may act as a potential source of hormones during low flow periods. Our modeling framework enables us to explore the extent to which observed estrogen chemodynamics can be explained by the sink/source behavior of streambed sediments. Specifically, we will use the model to explore how the streambed can act as a sink when in-stream concentrations are high and as a persistent source when in-stream concentrations are low, as described in the conceptual framework by Kolok et al. (2014).

4.3.2 Model Verification and Sensitivity Analysis

Prior to using the model to explore the questions outlined in Section 1, we needed to first verify if the model broadly captured the range of behaviors observed in the data. Note that there are significant uncertainties in the dataset, including a lack of accounting of all flows into the ditch, which made a rigorous model calibration unfeasible. The model was able to capture both E2 loads in the water column (PBIAS = 9% and $r^2 = 0.56$) and the ditch sediment (PBIAS = 8.7%) (**Figure 4.3a and 4.b**), as well as E1 loads in the water column (PBIAS = 94% and $r^2 = 0.14$) and ditch sediment (PBIAS = -19%) (**Figures 4.3c and 4.d**). Results from January, September, and December were omitted during model fit calculations as there was insufficient data to calculate a representative average load for the month. Model fits were reasonable for E2 in ditch water and sediment, and for E1 in the sediment, but poorer for E1 in the water column. We especially overestimate E1 loads in the main channel in the winter months, and this can be possibly attributed to time varying degradation rates that was not considered in our modelling framework. (**Figure 4.3c and 4.d**). There are a whole range of other assumptions that can be attributed to the poorer fits, including temporally varying mass exchange or biogeochemical parameters, as a function of flow and redox variations. While the model fits can be improved with more site-specific information, the fits are reasonable compared to another study that attempted to deterministically model estrogens at the reach or catchment scale (Green et al, 2013). Estrogens are one of the most poorly studied compounds at the catchment scale, and future work needs to focus on more detailed field-scale data to better constrain parameters in deterministic models. However, given that our goal was not to develop the most detailed model of the system, but to have the model grounded in real data so that it can be used to explore the role of the HZ in quantifying estrogen persistence, the model was considered acceptable for this study.

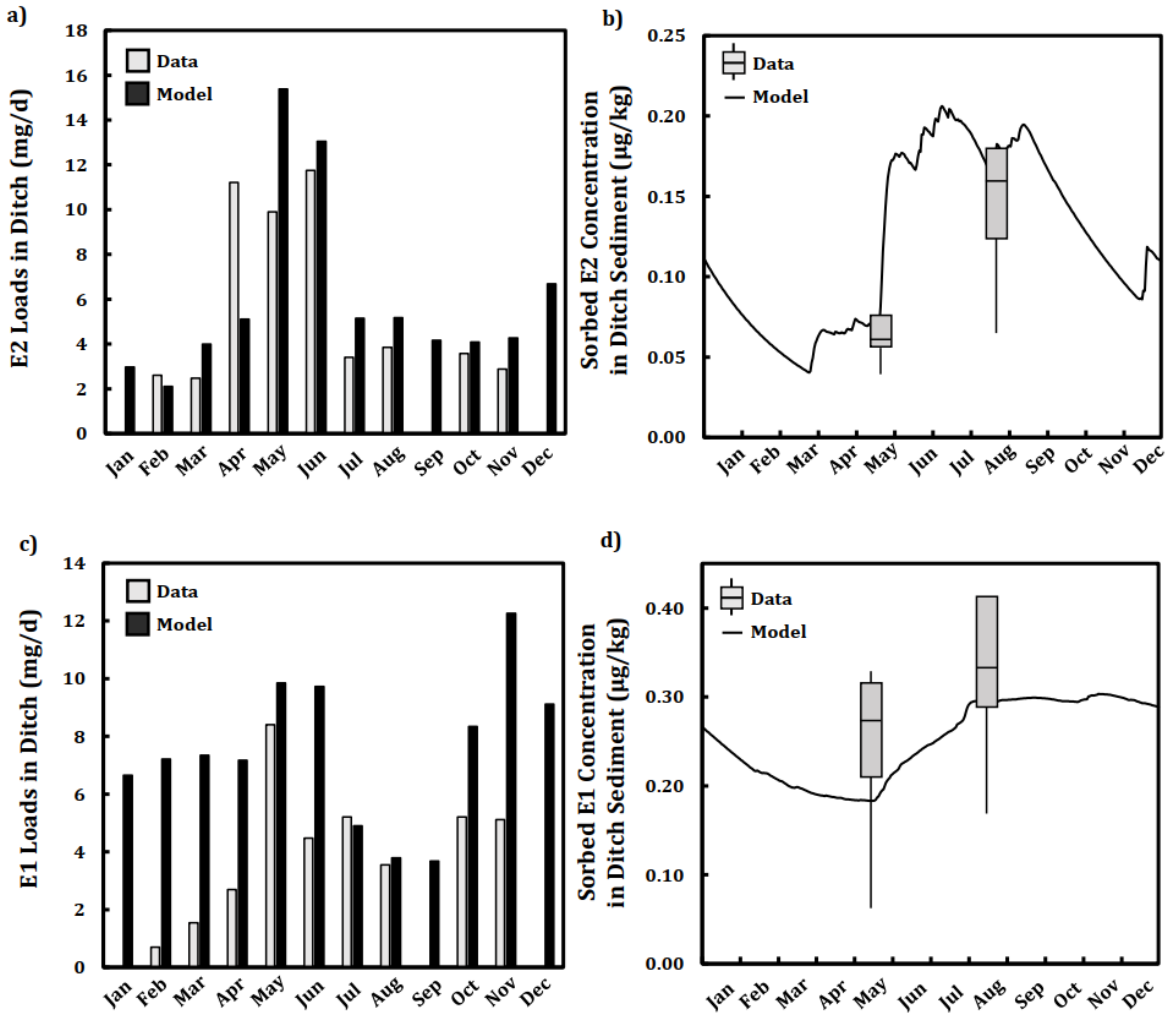

Figure 4.3 Comparison of modeled and measured data for monthly loads in the water column for a) E2 and b) E1. Comparison of modeled and measured concentrations for sorbed c) E2 and d) E1 in the HZ. Center of boxplots indicate median of dataset, edge of boxes indicates the interquartile range, with whiskers showing extreme values.

4.3.3 Source-Sink Dynamics of the Hyporheic Zone

The calibrated model was then used to explore the source-sink function of the HZ as a function of estrogen mass flux between the bed sediment and the water column. There are two fluxes that occur between the water column and the sediment: (1) settling and entrapment of suspended sediments in the HZ (last term of Eqs. 1 and 2) where sediment always acts as a sink, (2) aqueous mass exchange

flux between the bed sediment and the water column (third term on the right hand side of equation 1), where the sediment fluctuates between sink and source behavior. While the settling/entrapment flux is considered in most watershed models (eg SWAT, (Neitsch et al., 2011)), the aqueous mass exchange flux is generally not considered. The aqueous mass exchange flux that occurs as a function of the concentration gradient between pore water in HZ and the main channel, is however, an important source of estrogens especially during low flow periods when there are no landscape sources. Thus, in this section we focused our analysis on the mass exchange flux of E2 between the main channel and the HZ.

We find that porewater E2 concentrations are higher than main channel E2 concentrations (sediments acting as a source) during 95% of the year (white area in **Figure 4.4a and 4.b**). The sediments act as a sink only during 5% of the year and this occurs during large storm events that bring runoff and E2 contributions from the landscape (shaded areas in **Figure 4.4a and 4.b**). The modelled sink events occurred during days with a higher median daily flow of 5285 L/min, compared to source periods with median daily flow of 2165 L/min. Thus, similar to our data analysis, our model results also suggest that the sink behavior occurs during infrequent large storm events, while the source behavior occurs during the more frequent, baseflow conditions. During these times, estrogens sorbed to sediments in the HZ create a persistent source that releases estrogen back into the water column through desorption.

The magnitude of the source-sink behavior is captured in **Figure 4.4b**, where a negative flux indicates that the HZ acts as a sink, while a positive flux indicates that the HZ acts as a source. The magnitude of the exchange fluxes from the water column to the HZ during the short "sink-period" (5% of the year) are large with peak flux values equal to 2050 ng/d/m^2, and median flux equal to 222 ng/d/m^2 (**Figure 4.4b**) This is in contrast to the long "source period" when the flux from the HZ to the streamwater reaches a peak of 503 ng/d/m^2. The large exchange fluxes into the sediment during the "sink-period" suggest that these infrequent, but high-concentration events account for mass accumulation in the sediments during the year (**Figure 4.4c**). It is important, however, to not discount the lower, but more persistent exchange fluxes that occur during most of the year. Despite their smaller magnitudes, these fluxes create a persistent source that can lead to chronic exposure to biota and are thus critically important from an ecosystem health perspective (Söffker & Tyler, 2012).

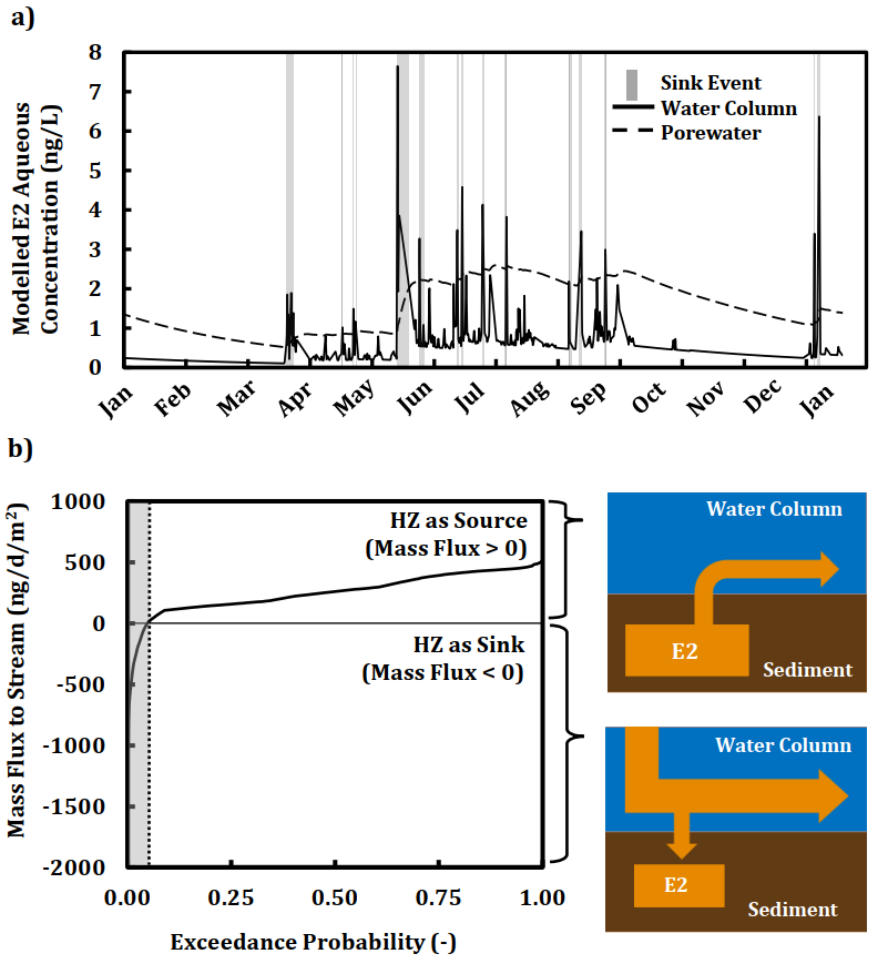

Figure 4.4 Source and sink behavior of hyporheic zone. a) Time series of simulated aqueous E2 concentrations in the main channel and sediment porewater at a cross section 20 km downstream of the input location showing alternating source-sink behavior– shaded grey area show times during the year when concentrations in the main channel are higher than concentration in the porewater, and sediment acts as a sink; these sink periods are associated with higher median flows, whereas the source periods are associated with lower medians flows. b) Exceedance probabilities of the mass exchange flux (= $(C_{HZ} - C_{MC})*\alpha*d$) between the porewater and the main channel. A positive flux implies that sediments act as a source; a negative flux implies that sediments act as a sink. Shaded grey area shows the 5% of the year that HZ acts as sink for estrogen. Note that the magnitude of the fluxes during the short sink period are much greater than the persistent, low fluxes during the longer source period. The results presented are for Case 1 (E2 to E1 degradation pathway active). Model parameters are in **Table 4.1**.

4.3.4 Hyporheic zone homogenizes estrogen concentrations and increases persistence

Model simulations with and without HZ were used to quantify the role of HZ in increasing estrogen persistence (Scenario 1). We found mean aqueous concentrations of E2, averaged across the entire year, to decrease along the reach, as a function of decay rates of E2 and hyporheic processes (**Figure 4.5a**). The presence of HZ leads to an overall slower decay of concentrations since the HZ acts as an additional source of estrogens. Note that, even in the no HZ scenario there is settling and entrapment of suspended sediments and sorbed estrogens from the water column to the sediment. Consideration of the HZ increases the SZOI (see Section 2.4 for definition) of E2 by 54%, from 19 to 30 km, since the HZ acts as an additional source for hormones into the water column (**Figure 4.5a**). Similarly, the presence of the HZ increases the SZOI of E1 by 79%, from 7 to 12 km.

Within-year concentration distributions at a cross section 20-km from the inlet also highlight the effect of the HZ. Specifically, we find that the HZ homogenizes the distribution of E2 concentrations in the stream (**Figure 4.5b**) by decreasing peak concentrations by 30% from 0.73 to 0.5 ng/L and increasing the lower concentrations (**Figure 4.5b**). When HZ was not considered, the concentrations were below the detection limit (7.5 pg/L) for ~27% of the year, in contrast to concentrations being always above the detection limit when HZ was considered (**Figure 4.5b**). We further find that if hyporheic exchange is not considered, the coefficient of variation (CV = standard deviation/mean) of the E2 aqueous concentration timeseries increased from 2.6 at the upstream location to 3.6 within the reach (**Figure 4.5c**). However, when hyporheic exchange is considered, the CV of the concentration timeseries decreases 75% from 1.31 to 0.32 over the same stream reach (**Figure 4.5c**). The reduction of the CV can be attributed to the decreased variability caused by the sediments dampening the extreme concentration – serving as a sink during large storm events, but as a source during the rest of the year.

Next, we explore the effect of the HZ on the total E2 and E1 mass left behind in the stream-sediment system (**Figure 4.5d**). This is important to consider since toxicological assessments have shown that hormones in sediments can have adverse effects on biota (Barel-Cohen et al., 2006; Chen et al., 2010; Zhang et al., 2015). We find that all estrogen coming into the channel is completely degraded within the 100-km reach when the model does not include the HZ. With hyporheic exchange, 28% of

the original estrogen mass remained within the 100-km reach if we considered the E2 to E1 degradation pathway (Scenario 1, Case 1) to be active in the sediment (**Equations 4.3a and 4.4a**), with 40% of the remaining mass as E2 and 60% as E1. However, if the E1 to E2 pathway is active in the sediments (Scenario 1, Case 2), approximately 49% of the input estrogen load (E1 + E2) can persist in the reach (**Equations 4.3b and 4.4b**), and a larger proportion (86% of remaining estrogen mass) of the more potent estrogen E2 remains. Increased mass of estrogens remaining when HZ is considered in the model is somewhat counterintuitive since the prevailing paradigm is that hyporheic zones act as biogeochemical hot spots and remove pollutants from the stream ecosystem through degradation reactions (Gomez-Velez et al., 2015). The reason we observe this phenomenon is because the rate of photodegradation, which occurs along the biotic degradation processes for E2 in the water column, is greater than the aerobic degradation rates that are active in the sediment. Additionally, the presence of the anaerobic transformation of E1 to E2 in the sediment can further increase the amount of E2 in the sediment. Thus, interactions with the sediment suppresses the overall degradation of E2 in the system, and contributes to the observed persistence.

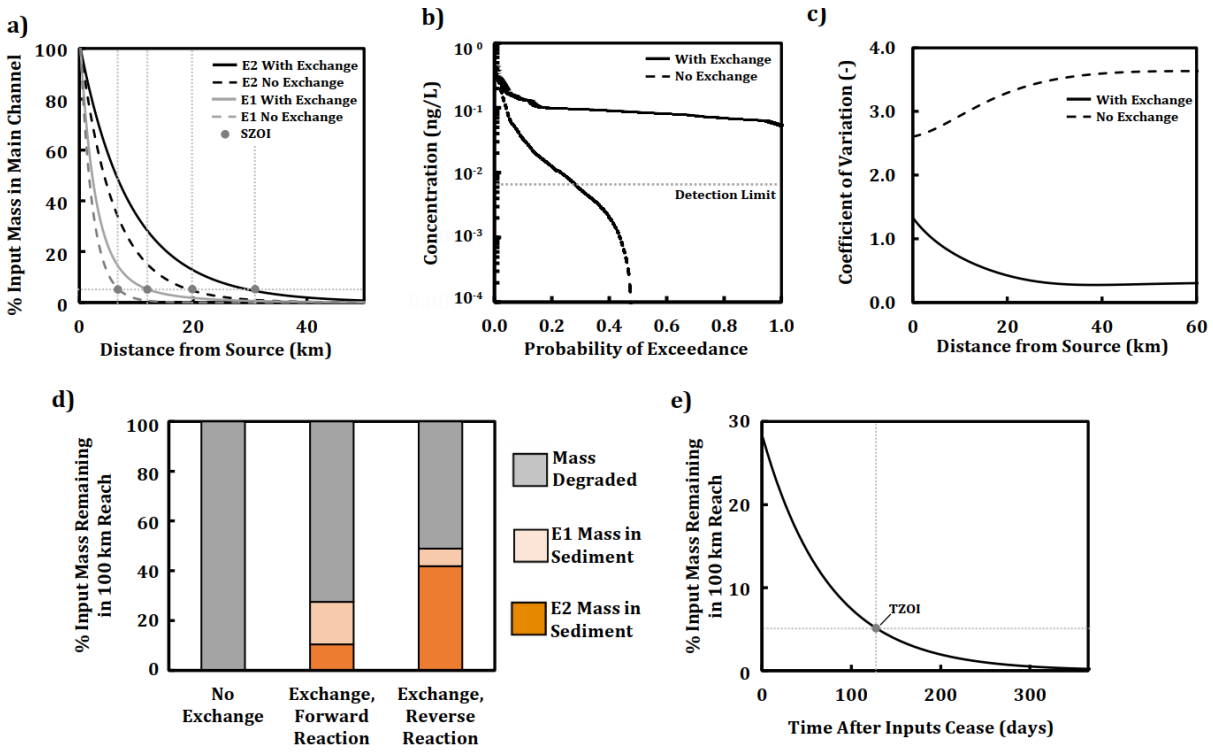

Figure 4.5 Presence of hyporheic zone increases the persistence of estrogens in the stream network: **a)** % Input Mass of E2 and E1 remaining in the main channel -- consideration of HZ increases the spatial zone of influence (SZOI); **b)** Probability of exceedance curves for E2 at 20 km downstream of source with and without HZ; **c)** Coefficient of variation of the E2 decreases due to the influence of HZ; **d)** % Input mass of E2 and E1 remaining within a 100 km reach, when considering forward and reverse reactions in the sediment **e)** % Input mass of E2 and E1 remaining within a 100 km reach plotted against time after input loadings have ceased – shows temporal zone of influence (TZOI). SZOI is defined as the distance required to degrade 95% of the initial mass of E2 and E1 in the main channel -- shown as a horizontal line in a) -- intersection of the line with the curves show the SZOI. TZOI is defined as the time it takes for the system to flush out 95% of the accumulated mass of E2 and E1 after loading has ceased -- shown as a horizontal line in e) -- intersection of the line with the curve shows the TZOI. All model parameters are the same as the calibrated model, and only the reverse reaction is simulated in 5(d), all other simulations consider only the forward reaction.

We further find that after loading into the stream has ceased, it takes 130 days to degrade the mass remaining in a 100-km reach to 5% of the input mass of E2 – this is the TZOI (Section 2.4) for the specific scenario. This is an important metric that captures lag times in system response and allows us to quantify the time it takes for water quality to improve if landscape inputs are ceased (**Figure 4.5e**). In contrast, this time would be approximately 29 hours if we did not consider the HZ; the fast removal

of estrogen is driven by the high photodegradation rates in the water column and the lack of continual release of estrogen from the sediments.

To summarize, we find that there are two ways that the HZ increases the persistence of hormones: (1) alternate source-sink behavior of hormones decreases the variability of instream concentrations and the number of days the concentrations are below the detection limit, and (2) suppression of photodegradation due to interaction with sediments, and reverse transformation of E1 to E2 in the sediment increases the overall mass of hormones remaining in the stream-sediment system.

4.3.5 Trade-offs between spatial zone of influence and temporal persistence

The relative importance of the source-sink function of the sediments, and the resultant persistence of hormones in the stream ecosystems depends on hydrologic factors such as the sediment-water exchange rates (α), and biogeochemical factors, such as the sorption potential of the pollutants and degradation rates in the water column and the sediments. Here, we explored the role of the sorption potentials of E2 and E1, as described by the retardation factor, in controlling the spatial and temporal persistence of pollutants in the stream. The SZOI increased with decrease in R_{E2} (**Figure 4.6a**), as we varied R_{E2} between 20 and 530, and varied R_{E1} proportionally (R_{E2}/R_{E1} = 1.3). This is as expected, since compounds that interact strongly with the sediments having a smaller SZOI due to sorption to the streambed sediment. We found that it takes 56 km of stream channel length to reduce total in-stream mass of E2 and E1 to 95% of the input for R_{E2} = 20, while it takes 23 km to reduce the mass to a similar level when R_{E2}= 530 (**Figure 4.6a**).

Within this smaller SZOI, however, the compound persists longer in time. Indeed, we found that when the model was run for one year, while no mass was left behind in the stream sediment system for the lowest *R* values, 63% of the mass was left behind for the highest *R* value (**Figure 4.6b**). The mass left behind impacts the ability of the stream to recover when the loading has ceased, a factor that is captured well in the TZOI parameter. We find that the TZOI is greater for compounds with higher *R*, and lower for compounds with lower *R* (**Figure 4.6c**). This occurs because of two reasons: (1) there is more mass left behind in the system for compounds with higher R, and thus it takes longer to flush out, and (2) rates of flushing and degradation are also suppressed in compounds with higher R due to their lower concentrations in the aqueous phase. Thus, we find that the SZOI and TZOI values

of a compound behave in opposite ways – with increasing retardation factors the SZOI decreases from 58 to 23 km, while the TZOI increases from 34 to 323 days (**Figure 4.6d**). Note that due to lower interaction of the HZ, the total estrogen mass in simulations with low *R* has already degraded to <5% of input mass after one year, and the TZOI does not exist in the scenarios with R of 20 and 120.

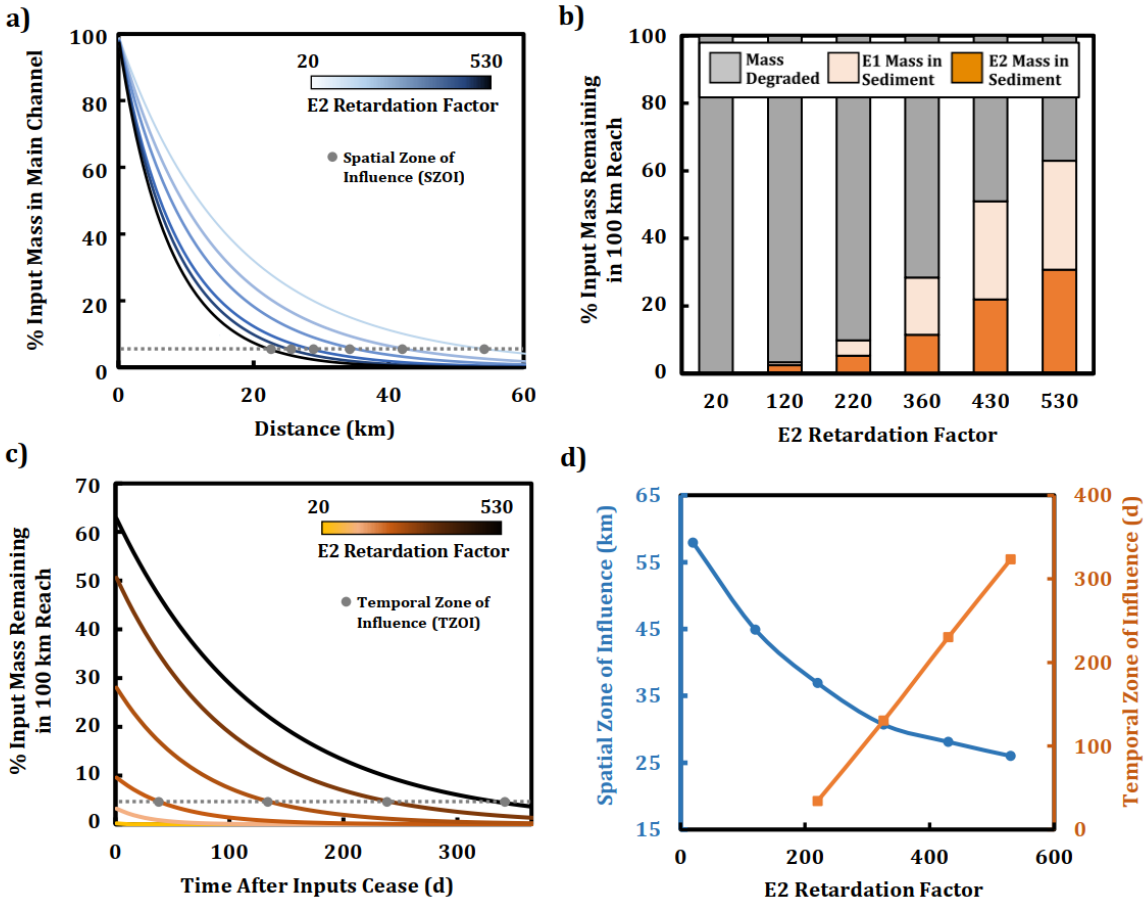

Figure 4.6 Spatial and temporal persistence as a function of retardation factor: (a) Mass of E2 and E1 in the main channel (MC) as % of the input mass, plotted against distance from the input location – SZOI, indicated by grey circles, decreases with increase in R (b) % mass of E2 and E1 remaining in the 100-km reach right after input is ceased (time zero in the next plot), (c) % mass of E2 and E1 remaining in the 100-km reach plotted against time after input loadings have ceased – TZOI, indicated by grey circles, increases with increase in *R*, (d) TZOI increases with increase with *R*, but SZOI decreases with increase in *R*. All model parameters except for sorption coefficients are the same as the calibrated model, with only forward reaction (Case 1) being simulated (**Table 4.1**). Figure presents R_{E2} values, while R_{E2}/R_{E1} ratio was maintained at 1.3 across all simulations.

Finally, while SZOI and TZOI relate to the occurrence of a pollutant in the water column and is governed by its sorption-desorption properties, the overall persistence of the chemical in the stream-sediment system is controlled to a large part by the ratio of its biogeochemical rates in the water column and the sediment zone. For chemicals with much lower decay rates in the water column than in the sediments (e.g. nitrate), HZs perform their expected function of enhanced biogeochemical transformation and decreased persistence. However, for chemicals in which decay rates in the water column are greater than those in the sediment, the HZ likely increases the persistence of the chemicals in the stream ecosystem. Our study thus highlights the need to consider the hyporheic zone as a complex control point of contaminant transport rather than a biogeochemical hotspot characterized by greater reactivity, as is often the norm. The bi-directionality of estrogen transport and their enhanced persistence due to hyporheic exchange must be considered when characterizing the fate of estrogens and related compounds in agricultural ecosystems.

4.4 Conclusions

The last decade has seen a tremendous increase in research on the role of the HZ on the removal of pollutants from the river network, thus reducing pollutant loads to downstream waters and protecting water quality (Gomez-Velez et al., 2015; Harvey et al., 2013; Kaushal et al., 2008; Stewart et al., 2011; Zarnetske et al., 2011). The most interesting finding of our study is that this might not necessarily be true for all compounds. The HZ can act both as a sink and a source, and for certain chemicals with high sorption potentials, like estrogens, interactions with the HZ can contribute to their increased persistence in the stream network. This helps explain, at least partially, why estrogens are detected consistently in surface water bodies, despite their short half-lives.

We hypothesized that for estrogens, the HZ suppresses the overall decay in the stream channel by three primary mechanisms. First, estrogens have a high affinity for sediments in the HZ that act as a sink for both dissolved and sorbed estrogen on suspended sediments during high flow events, but a source during the rest of the year when stream concentrations are lower. Second, photodegradation is the primary decay pathway for estrogens in streamwater, but estrogens in sediments are unable to photodegrade, and thus soroption of sediments reduces the overall degradation of the estrogens in the

channel. Finally, estrogens are redox sensitive, such that while E2 degrades to E1 under aerobic conditions, the reverse pathway can be active during anaerobic conditions. This leads to the persistence of E2 in the stream sediment, rather than conversion to E1 which is 10 times less estrogenic than E2.

Our analysis of field data on estrogen concentrations in a tile-drain and a ditch within the same reach showed more persistent concentrations of estrogens in the ditch compared to the tile, with higher concentrations during the low flow period compared to the high flow period. This observation, coupled with high concentrations of sorbed estrogen in sediments, suggests that the HZ acts as a source of estrogens in the summer months. We further developed a stream-hyporheic zone (HZ) model and using model results show that the HZ can act as a stronger estrogen sink during high-flow periods and a greater source during low-flow periods. Our model is able to quantify how interactions with the HZ may increase the mass of estrogens remaining in the stream network Specifically, for our calibrated model we show that approximately 28-49% of the estrogens remain in a 100 km reach over a 2-year period when exchange was considered, compared to all mass being degraded with no exchange. Increasing sorption potential of the estrogen increases the mass remaining within the stream ecosystem, and the potential lag time for lowering concentrations when inputs have ceased. Finally, we define two terms – the spatial zone of influence (SZOI) and the temporal zone of influence (TZOI). The TZOI captures the lag time of the system to recover when input has ceased, while the SZOI quantifies the distance from the source at which the pollutant signal disappears under persistent loading. We find that with increase in the sorption potential of the pollutant, captured by higher retardation factors, the SZOI decreases while the TZOI increases. Notably, although a lower SZOI suggests that a smaller section of the stream will be impacted by persistent hormone concentrations, a higher TZOI implies that the affected portion of the stream takes longer to recover when the input loading has ceased. We find TZOI values to range between 34 to 323 days, which is much shorter than the decadal timescales of recovery than have been predicted at the watershed scale (Gall et al., 2016) – highlighting that although streams can build up legacy pollutants, they might have faster flushing and recovery times than soils.

Our results highlight the importance of considering bidirectional exchange between the hyporheic zone and the water column while modeling hormone transport along stream networks. Stream

network models that describe transport of reactive solutes often do not consider the presence of the HZ (e.g. the PhATE and GREAT-ER models, c.f. Hannah et al., 2009), or when they do the interaction is unidirectional (e.g. SWAT, Neitsch et al., 2011), or the models only have the sediment acting as a sink for stream pollutants (Gomez-Velez et al., 2015). This finding challenges the existing paradigm that HZs only act as sinks for contaminants. The HZs *can* often act as sinks for solutes like nitrate that undergo microbial decay processes in the HZ. But for solutes like estrogen for which photodegradation rates are higher than the microbial decay processes, consideration of HZ might contribute to lower effective reaction rates in the stream channel. The model we developed, of course, has multiple limitations, including simplifications related to seasonally constant velocities, mean suspended sediment concentrations, and temporally constant degradation rates. Future work should involve studying lateral and horizontal fluxes in a stream reach more comprehensively to understand how the source-sink behavior switches both at a single location, and in multiple reaches along a stream network. Despite its limitations, the model allows us, for the first time, to show that not including HZs in stream network models might lead to an overestimation of estrogen decay in streams.

Our finding that hyporheic exchange can increase the environmental persistence of compounds, while focused on estrogens, also applies to other redox-sensitive compounds, such as steroidal hormones (testosterone, trenbolone, etc.), pesticides (Barber et al., 2013; Casey et al., 2004; Jaffé, 1991; Stoeckel et al., 2012; Ward et al., 2015) and phosphorus (P). For example, phosphorus is known to sorb to sediments under aerobic conditions and desorb under anaerobic conditions (Katsev et al., 2006; Jarvie et al., 2005; Kim et al., 2003; Mortimer, 1942). Thus, phosphorus in stream sediments can act as a source of bioavailable phosphorus in the water column during low-flow summer months when biological activity, high stream temperatures, and low water levels can lead to the development of anoxia and algal blooms (Christensen et al., 1990; Young & Huryn, 1999). While sediment sorption/desorption and hyporheic processes have been incorporated into some stream P models (e.g. Vilmin et al., 2015; Kim et al., 2006; Wade et al., 2002), there are still gaps in our understanding of how sediment P buffering modifies catchment scale transport of dissolved reactive P. In a recent extensive review, Simpson et al. (2021) emphasized the need to better quantify the time scales of phosphorus attenuation in streams by understanding how P sorption/desorption processes are modulated by hyporheic exchange.

The hyporheic zone has been traditionally conceptualized as a biogeochemical reaction hot spot for pollutants – our work challenges that paradigm and highlights that it is important to consider these landscape elements as both sinks and sources, as a function of changing hydrology. Given the important role of the stream network in modulating pollutant delivery from the landscape, it is critically important to understand and quantify the role of the hyporheic zone, and incorporate its effect appropriately in stream network models.

Chapter 4 References

Adeel, M., Song, X., Wang, Y., Francis, D., & Yang, Y. (2017). Environmental impact of estrogens on human, animal and plant life: A critical review. *Environment International*, *99*, 107–119. https://doi.org/10.1016/j.envint.2016.12.010

Alvarez, D. A., Shappell, N. W., Billey, L. O., Bermudez, D. S., Wilson, V. S., Kolpin, D. W., et al. (2013). Bioassay of estrogenicity and chemical analyses of estrogens in streams across the United States associated with livestock operations. *Water Research*, *47*(10), 3347–3363. https://doi.org/10.1016/j.watres.2013.03.028

Anderson, P. D., Johnson, A. C., Pfeiffer, D., Caldwell, D. J., Hannah, R., Mastrocco, F., et al. (2012). Endocrine disruption due to estrogens derived from humans predicted to be low in the majority of U.S. surface waters. *Environmental Toxicology and Chemistry*, *31*(6), 1407–1415. https://doi.org/10.1002/etc.1824

Arlos, M. J., Parker, W. J., Bicudo, J. R., Law, P., Hicks, K. A., Fuzzen, M. L. M., et al. (2018). Modeling the exposure of wild fish to endocrine active chemicals: Potential linkages of total estrogenicity to field-observed intersex. *Water Research*, *139*, 187–197. https://doi.org/10.1016/j.watres.2018.04.005

Barber, L. B., Keefe, S. H., Brown, G. K., Furlong, E. T., Gray, J. L., Kolpin, D. W., et al. (2013). Persistence and Potential Effects of Complex Organic Contaminant Mixtures in Wastewater-Impacted Streams. *Environmental Science & Technology*, *47*(5), 2177–2188. https://doi.org/10.1021/es303720g

Barel-Cohen, K., Shore, L. S., Shemesh, M., Wenzel, A., Mueller, J., & Kronfeld-Schor, N. (2006). Monitoring of natural and synthetic hormones in a polluted river. *Journal of Environmental Management*, *78*(1), 16–23. https://doi.org/10.1016/j.jenvman.2005.04.006

Battin, T. J., Kaplan, L. A., Findlay, S., Hopkinson, C. S., Marti, E., Packman, A. I., et al. (2008). Biophysical controls on organic carbon fluxes in fluvial networks. *Nature Geoscience*, *1*(2), 95–100. https://doi.org/10.1038/ngeo101

Bencala, K. E., Gooseff, M. N., & Kimball, B. A. (2011). Rethinking hyporheic flow and transient storage to advance understanding of stream-catchment connections. *Water Resources Research*, *47*(3), W00H03. https://doi.org/10.1029/2010WR010066

Bencala, K. E., & Walters, R. A. (1983). Simulation of solute transport in a mountain pool-and-riffle stream: A transient storage model. *Water Resources Research*, *19*(3), 718–724. https://doi.org/10.1029/WR019i003p00718

Biggs, J., von Fumetti, S., & Kelly-Quinn, M. (2017). The importance of small waterbodies for biodiversity and ecosystem services: implications for policy makers. *Hydrobiologia*, *793*(1), 3–39. https://doi.org/10.1007/s10750-016-3007-0

Boano, F., Harvey, J. W., Marion, A., Packman, A. I., Revelli, R., Ridolfi, L., & Wörman, A. (2014). Hyporheic flow and transport processes: Mechanisms, models, and biogeochemical implications. *Reviews of Geophysics*, *52*(4), 603–679. https://doi.org/10.1002/2012RG000417

Bradley, P. M., & Writer, J. H. (2014). Effect of Light on Biodegradation of Estrone, 17β -Estradiol, and 17α-Ethinylestradiol in Stream Sediment. *JAWRA Journal of the American Water Resources Association*, *50*(2), 334–342. https://doi.org/10.1111/jawr.12157

Bradley, P. M., Barber, L. B., Chapelle, F. H., Gray, J. L., Kolpin, D. W., & McMahon, P. B. (2009). Biodegradation of 17β-estradiol, estrone and testosterone in stream sediments. *Environmental Science & Technology*, *43*(6), 1902–1910.

Campbell, C. G., Borglin, S. E., Green, F. B., Grayson, A., Wozei, E., & Stringfellow, W. T. (2006). Biologically directed environmental monitoring, fate, and transport of estrogenic endocrine disrupting compounds in water: A review. *Chemosphere*, *65*(8), 1265–1280. https://doi.org/10.1016/j.chemosphere.2006.08.003

Casey, F. X. M., Hakk, H., Šimůnek, J., & Larsen, G. L. (2004). Fate and Transport of Testosterone in Agricultural Soils. *Environmental Science & Technology*, *38*(3), 790–798. https://doi.org/10.1021/es034822i

Chen, T. C., Chen, T. S., Yeh, K. J., Lin, Y. C., Chao, H. R., & Yeh, Y. L. (2012). Sorption of estrogens estrone, 17β-estradiol, estriol, 17α-ethinylestradiol, and diethylstilbestrol on sediment affected by different origins. *Journal of Environmental Science and Health, Part A*, *47*(12), 1768–1775. https://doi.org/10.1080/10934529.2012.689225

Chen, T.-S., Chen, T.-C., Yeh, K.-J. C., Chao, H.-R., Liaw, E.-T., Hsieh, C.-Y., et al. (2010). High estrogen concentrations in receiving river discharge from a concentrated livestock feedlot. *Science of The Total Environment*, *408*(16), 3223–3230. https://doi.org/10.1016/j.scitotenv.2010.03.054

Chowdhury, R. R., Charpentier, P., & Ray, M. B. (2010). Photodegradation of Estrone in Solar Irradiation. *Industrial & Engineering Chemistry Research*, *49*(15), 6923–6930. https://doi.org/10.1021/ie901796x

Christensen, P. B., Nielsen, L. P., Sørensen, J., & Revsbech, N. P. (1990). Denitrification in nitrate-rich streams: Diurnal and seasonal variation related to benthic oxygen metabolism. *Limnology and Oceanography*, *35*(3), 640–651. https://doi.org/10.4319/lo.1990.35.3.0640

Ciparis, S., Iwanowicz, L. R., & Voshell, J. R. (2012). Effects of watershed densities of animal feeding operations on nutrient concentrations and estrogenic activity in agricultural streams. *Science of The Total Environment*, *414*, 268–276. https://doi.org/10.1016/j.scitotenv.2011.10.017

Clifford, C. C., & Heffernan, J. B. (2018). Artificial Aquatic Ecosystems. *Water*, *10*(8), 1096. https://doi.org/10.3390/w10081096

Coe, T. S., Hamilton, P. B., Hodgson, D., Paull, G. C., Stevens, J. R., Sumner, K., & Tyler, C. R. (2008). An Environmental Estrogen Alters Reproductive Hierarchies, Disrupting Sexual Selection in Group-Spawning Fish. *Environmental Science & Technology*, *42*(13), 5020–5025. https://doi.org/10.1021/es800277q

Deng, Z.-Q., Bengtsson, L., Singh, V. P., & Adrian, D. D. (2002). Longitudinal Dispersion Coefficient in Single-Channel Streams. *Journal of Hydraulic Engineering*, *128*(10), 901–916. https://doi.org/10.1061/(ASCE)0733-9429(2002)128:10(901)

Finlay-Moore, O., Hartel, P. G., & Cabrera, M. L. (2000). 17β-Estradiol and Testosterone in Soil and Runoff from Grasslands Amended with Broiler Litter. *Journal of Environmental Quality*, *29*(5), 1604–1611. https://doi.org/10.2134/jeq2000.00472425002900050030x

Gall, H. E., Jafvert, C. T., & Jenkinson, B. (2010). Integrating hydrograph modeling with real-time flow monitoring to generate hydrograph-specific sampling schemes. *Journal of Hydrology*, *393*(3), 331–340. https://doi.org/10.1016/j.jhydrol.2010.08.028

Gall, H. E., Sassman, S. A., Lee, L. S., & Jafvert, C. T. (2011). Hormone Discharges from a Midwest Tile-Drained Agroecosystem Receiving Animal Wastes. *Environmental Science & Technology*, *45*(20), 8755–8764. https://doi.org/10.1021/es2011435

Gall, H. E., Sassman, S. A., Lee, L. S., & Jafvert, C. T. (2015). Comparison of export dynamics of nutrients and animal-borne estrogens from a tile-drained Midwestern agroecosystem. *Water Research*, *72*, 162–173. https://doi.org/10.1016/j.watres.2014.08.041

Gall, H. E., Basu, N. B., Mashtare, M. L., Rao, P. S. C., & Lee, L. S. (2016). Assessing the impacts of anthropogenic and hydro-climatic drivers on estrogen legacies and trajectories. *Advances in Water Resources*, *87*, 19–28. https://doi.org/10.1016/j.advwatres.2015.10.012

Gomez-Velez, J. D., Harvey, J. W., Cardenas, M. B., & Kiel, B. (2015). Denitrification in the Mississippi River network controlled by flow through river bedforms. *Nature Geoscience*, *8*(12), 941–945. https://doi.org/10.1038/ngeo2567

Green, C., Williams, R., Kanda, R., Churchley, J., He, Y., Thomas, S., et al. (2013). Modeling of Steroid Estrogen Contamination in UK and South Australian Rivers Predicts Modest Increases in Concentrations in the Future. *Environmental Science & Technology*, *47*(13), 7224–7232. https://doi.org/10.1021/es3051058

Haan, C. T., Barfield, B. J., & Hayes, J. C. (1994). *Design hydrology and sedimentology for small catchments*. San Diego, Calif: Academic Press.

Hannah, R., D'Aco, V. J., Anderson, P. D., Buzby, M. E., Caldwell, D. J., Cunningham, V. L., et al. (2009). Exposure assessment of 17α-ethinylestradiol in surface waters of the United States and Europe. *Environmental Toxicology and Chemistry*, *28*(12), 2725–2732. https://doi.org/10.1897/08-622.1

Harvey, J. W., Böhlke, J. K., Voytek, M. A., Scott, D., & Tobias, C. R. (2013). Hyporheic zone denitrification: Controls on effective reaction depth and contribution to whole-stream mass balance: Scaling hyporheic flow controls on stream denitrification. *Water Resources Research*, *49*(10), 6298–6316. https://doi.org/10.1002/wrcr.20492

Hodaj, A., Bowling, L. C., Frankenberger, J. R., & Chaubey, I. (2017). Impact of a two-stage ditch on channel water quality. *Agricultural Water Management*, *192*, 126–137. https://doi.org/10.1016/j.agwat.2017.07.006

Jaffé, R. (1991). Fate of hydrophobic organic pollutants in the aquatic environment: A review. *Environmental Pollution*, *69*(2), 237–257. https://doi.org/10.1016/0269-7491(91)90147-O

Jarvie, H. P., Jürgens, M. D., Williams, R. J., Neal, C., Davies, J. J. L., Barrett, C., & White, J. (2005). Role of river bed sediments as sources and sinks of phosphorus across two major eutrophic UK river basins: the Hampshire Avon and Herefordshire Wye. *Journal of Hydrology*, *304*(1), 51–74. https://doi.org/10.1016/j.jhydrol.2004.10.002

Jobling, S., Nolan, M., Tyler, C. R., Brighty, G., & Sumpter, J. P. (1998). Widespread Sexual Disruption in Wild Fish. *Environmental Science & Technology*, *32*(17), 2498–2506. https://doi.org/10.1021/es9710870

Jürgens, M. D., Holthaus, K. I. E., Johnson, A. C., Smith, J. J. L., Hetheridge, M., & Williams, R. J. (2002). The potential for estradiol and ethinylestradiol degradation in english rivers. *Environmental Toxicology and Chemistry*, *21*(3), 480–488. https://doi.org/10.1002/etc.5620210302

Katsev, S., Tsandev, I., L'Heureux, I., & Rancourt, D. G. (2006). Factors controlling long-term phosphorus efflux from lake sediments: Exploratory reactive-transport modeling. *Chemical Geology*, *234*(1–2), 127–147. https://doi.org/10.1016/j.chemgeo.2006.05.001

Kaushal, S. S., Groffman, P. M., Mayer, P. M., Striz, E., & Gold, A. J. (2008). Effects of Stream Restoration on Denitrification in an Urbanizing Watershed. *Ecological Applications*, *18*(3), 789–804. https://doi.org/10.1890/07-1159.1

Kerr, P. C., Gooseff, M. N., & Bolster, D. (2013). The significance of model structure in one-dimensional stream solute transport models with multiple transient storage zones – competing vs. nested arrangements. *Journal of Hydrology*, *497*, 133–144. https://doi.org/10.1016/j.jhydrol.2013.05.013

Khanal, S. K., Xie, B., Thompson, M. L., Sung, S., Ong, S.-K., & van Leeuwen, J. (Hans). (2006). Fate, Transport, and Biodegradation of Natural Estrogens in the Environment and Engineered Systems. *Environmental Science & Technology*, *40*(21), 6537–6546. https://doi.org/10.1021/es0607739

Kidd, K. A., Blanchfield, P. J., Mills, K. H., Palace, V. P., Evans, R. E., Lazorchak, J. M., & Flick, R. W. (2007). Collapse of a fish population after exposure to a synthetic estrogen. *Proceedings*

of the National Academy of Sciences, *104*(21), 8897–8901. https://doi.org/10.1073/pnas.0609568104

Kim, L.-H., Choi, E., & Stenstrom, M. K. (2003). Sediment characteristics, phosphorus types and phosphorus release rates between river and lake sediments. *Chemosphere*, *50*(1), 53–61. https://doi.org/10.1016/S0045-6535(02)00310-7

Kim, K., Kalita, P. K., Bowes, M. J., & Eheart, J. W. (2006). Modeling of river dynamics of phosphorus under unsteady flow conditions. *Water Resources Research*, *42*(7). https://doi.org/10.1029/2005WR004210

Kjaer, J., Olsen, P., Bach, K., Barlebo, H. C., Ingerslev, F., Hansen, M., & Sørensen, B. H. (2007). Leaching of Estrogenic Hormones from Manure-Treated Structured Soils. *Environmental Science & Technology*, *41*(11), 3911–3917. https://doi.org/10.1021/es0627747

Klein, M. (2004). Advisory Opinion on the Exposure Assessment for Substances based on Geo-Referenced Computer Models FKZ 360 12 007. Fraunhofer-institut for Molecular Biology und Applied Ecology. Retrieved from http://www.great-er.org/files/great-er_fraunhofer_advisory_opinion.pdf

Kolok, A. S., Sellin Jeffries, M. K., Knight, L., Snow, D. D., & Bartelt-Hunt, S. L. (2014). The Hourglass: A Conceptual Framework for the Transport of Biologically Active Compounds from Agricultural Landscapes. *JAWRA Journal of the American Water Resources Association*, *50*(2), 266–274. https://doi.org/10.1111/jawr.12158

Kolpin, D. W., Furlong, E. T., Meyer, M. T., Thurman, E. M., Zaugg, S. D., Barber, L. B., & Buxton, H. T. (2002). Pharmaceuticals, hormones, and other organic wastewater contaminants in US streams, 1999-2000: A national reconnaissance. *Environmental Science & Technology*, *36*(6), 1202–1211.

Lafrance, P., & Caron, E. (2013). Impact of recent manure applications on natural estrogen concentrations in streams near agricultural fields. *Environmental Research*, *126*, 208–210. https://doi.org/10.1016/j.envres.2013.05.008

Lee, H. B., & Liu, D. (2002). Degradation of 17β-Estradiol and its Metabolites by Sewage Bacteria. *Water, Air, and Soil Pollution*, *134*(1–4), 351–366. https://doi.org/10.1023/A:1014117329403

Lee, L. S., Strock, T. J., Sarmah, A. K., & Rao, P. S. C. (2003). Sorption and Dissipation of Testosterone, Estrogens, and Their Primary Transformation Products in Soils and Sediment. *Environmental Science & Technology*, *37*(18), 4098–4105. https://doi.org/10.1021/es020998t

Leet, J. K., Gall, H. E., & Sepúlveda, M. S. (2011). A review of studies on androgen and estrogen exposure in fish early life stages: effects on gene and hormonal control of sexual differentiation: Androgen and estrogen exposure in fish early life stages. *Journal of Applied Toxicology*, *31*(5), 379–398. https://doi.org/10.1002/jat.1682

Lin, A. Y.-C., & Reinhard, M. (2005). Photodegradation of common environmental pharmaceuticals and estrogens in river water. *Environmental Toxicology and Chemistry*, *24*(6), 1303–1309. https://doi.org/10.1897/04-236R.1

Liu, Y., Zarfl, C., Basu, N. B., Schwientek, M., & Cirpka, O. A. (2018). Contributions of catchment and in-stream processes to suspended sediment transport in a dominantly groundwater-fed catchment. *Hydrology and Earth System Sciences*, *22*(7), 3903–3921. https://doi.org/10.5194/hess-22-3903-2018

Liu, Y., Zarfl, C., Basu, N. B., & Cirpka, O. A. (2019). Turnover and legacy of sediment-associated PAH in a baseflow-dominated river. *Science of The Total Environment*, *671*, 754–764. https://doi.org/10.1016/j.scitotenv.2019.03.236

Marion, A., Zaramella, M., & Packman, A. I. (2003). Parameter Estimation of the Transient Storage Model for Stream–Subsurface Exchange. *Journal of Environmental Engineering*, *129*(5), 456–463. https://doi.org/10.1061/(ASCE)0733-9372(2003)129:5(456)

Mashtare, M. (2013). Fate of 17α-Estradiol, 17β-Estradiol, and Estrone in Agricultural Soils and Sediments (Dissertation). *Purdue University*. Retrieved from https://docs.lib.purdue.edu/open_access_dissertations/6

Mashtare, M., Khan, B., & Lee, L. S. (2011). Evaluating stereoselective sorption by soils of 17α-estradiol and 17β-estradiol. *Chemosphere*, *82*(6), 847–852. https://doi.org/10.1016/j.chemosphere.2010.11.021

Mashtare, M., Green, D. A., & Lee, L. S. (2013a). Biotransformation of 17α- and 17β-estradiol in aerobic soils. *Chemosphere*, *90*(2), 647–652. https://doi.org/10.1016/j.chemosphere.2012.09.032

Mashtare, M., Lee, L. S., Nies, L. F., & Turco, R. F. (2013b). Transformation of 17α-Estradiol, 17β-Estradiol, and Estrone in Sediments Under Nitrate- and Sulfate-Reducing Conditions. *Environmental Science & Technology*, 130619144051009. https://doi.org/10.1021/es4008382

Matthiessen, P., Arnold, D., Johnson, A. C., Pepper, T. J., Pottinger, T. G., & Pulman, K. G. T. (2006). Contamination of headwater streams in the United Kingdom by oestrogenic hormones from livestock farms. *Science of The Total Environment*, *367*(2), 616–630. https://doi.org/10.1016/j.scitotenv.2006.02.007

Mortimer, C. H. (1942). The exchange of dissolved substances between mud and water in lakes. *The Journal of Ecology*, *30*(1), 147. https://doi.org/10.2307/2256691

Neitsch, S., Arnold, J., Kiniry, J., & Williams, J. (2011). *Soil and Water Assessment Tool Theoretical Documentation Version 2009* (No. TR-406). Temple, Texas: USDA-ARS Grassland, Soil and Water Research Laboratory. Retrieved from https://swat.tamu.edu/media/99192/swat2009-theory.pdf

Nichols, D. J., Daniel, T. C., Edwards, D. R., Moore, P. A., & Pote, D. H. (1998). Use of grass filter strips to reduce 17β-estradiol in runoff from fescue-applied poultry litter. *Journal of Soil and Water Conservation*, *53*(1), 74–77.

Panter, G. H., Thompson, R. S., & Sumpter, J. P. (1998). Adverse reproductive effects in male fathead minnows (Pimephales promelas) exposed to environmentally relevant concentrations of the natural oestrogens, oestradiol and oestrone. *Aquatic Toxicology*, *42*(4), 243–253. https://doi.org/10.1016/S0166-445X(98)00038-1

Pianosi, F., Beven, K., Freer, J., Hall, J. W., Rougier, J., Stephenson, D. B., & Wagener, T. (2016). Sensitivity analysis of environmental models: A systematic review with practical workflow. *Environmental Modelling & Software*, *79*, 214–232. https://doi.org/10.1016/j.envsoft.2016.02.008

Prater, J. R., Horton, R., & Thompson, M. L. (2015). Reduction of estrone to 17 β-estradiol in the presence of swine manure colloids. *Chemosphere*, *119*, 642–645. https://doi.org/10.1016/j.chemosphere.2014.07.072

Raman, D. R., Williams, E. L., Layton, A. C., Burns, R. T., Easter, J. P., Daugherty, A. S., et al. (2004). Estrogen Content of Dairy and Swine Wastes. *Environmental Science & Technology*, *38*(13), 3567–3573. https://doi.org/10.1021/es0353208

Runkel, R. L. (1998). *One-Dimensional transport with inflow and storage (OTIS): A solute transport model for streams and rivers* (Water Resources Investigations Report No. 98–4018). Denver, Colorado: US Geological Survey.

Sassman, S. (2014). *A new passive surface water flux meter for simultaneous measurement of contaminant and water fluxes in streams and rivers* (PhD Dissertation). Purdue University, West Lafayette.

Schindler, J. E., & Krabbenhoft, D. P. (1998). The hyporheic zone as a source of dissolved organic carbon and carbon gases to a temperate forested stream. *Biogeochemistry*, *43*(2), 157–174. https://doi.org/10.1023/A:1006005311257

Schoenborn, A., Kunz, P., & Koster, M. (2015). Estrogenic activity in drainage water: a field study on a Swiss cattle pasture. *Environmental Sciences Europe*, *27*, 17. https://doi.org/10.1186/s12302-015-0047-4

Shore, L. S., Correll, D. L., & Chakraborty, P. K. (1995). Relationship of fertilization with chicken manure and concentrations of estrogens in small streams. Retrieved from http://agris.fao.org/agris-search/search.do?recordID=US9616776

Simpson, Z. P., McDowell, R. W., Condron, L. M., McDaniel, M. D., Jarvie, H. P., & Abell, J. M. (2021). Sediment phosphorus buffering in streams at baseflow: A meta-analysis. *Journal of Environmental Quality*, *n/a*(n/a). https://doi.org/10.1002/jeq2.20202

Snyder, S. A., Westerhoff, P., Yoon, Y., & Sedlak, D. L. (2003). Pharmaceuticals, Personal Care Products, and Endocrine Disruptors in Water: Implications for the Water Industry. *Environmental Engineering Science*, *20*(5), 449–469. https://doi.org/10.1089/109287503768335931

Söffker, M., & Tyler, C. R. (2012). Endocrine disrupting chemicals and sexual behaviors in fish – a critical review on effects and possible consequences. *Critical Reviews in Toxicology*, *42*(8), 653–668. https://doi.org/10.3109/10408444.2012.692114

Stewart, R. J., Wollheim, W. M., Gooseff, M. N., Briggs, M. A., Jacobs, J. M., Peterson, B. J., & Hopkinson, C. S. (2011). Separation of river network-scale nitrogen removal among the main channel and two transient storage compartments. *Water Resources Research*, *47*(10), n/a-n/a. https://doi.org/10.1029/2010WR009896

Stoeckel, J. A., Morris, J., Ames, E., Glover, D. C., Vanni, M. J., Renwick, W., & González, M. J. (2012). Exposure Times to the Spring Atrazine Flush Along a Stream-Reservoir System1. *JAWRA Journal of the American Water Resources Association*, *48*(3), 616–634. https://doi.org/10.1111/j.1752-1688.2011.00633.x

Succop, P. A., Clark, S., Chen, M., & Galke, W. (2004). Imputation of Data Values That are Less Than a Detection Limit. *Journal of Occupational and Environmental Hygiene*, *1*(7), 436–441. https://doi.org/10.1080/15459620490462797

Thorpe, K. L., Cummings, R. I., Hutchinson, T. H., Scholze, M., Brighty, G., Sumpter, J. P., & Tyler, C. R. (2003). Relative Potencies and Combination Effects of Steroidal Estrogens in Fish. *Environmental Science & Technology*, *37*(6), 1142–1149. https://doi.org/10.1021/es0201348

USEPA. (2000). *Proposed regulations to address water pollution from concentrated animal feeding operations* (No. EPA 833-F-00-016). Washington, DC: Office of Water.

Vajda, A. M., Barber, L. B., Gray, J. L., Lopez, E. M., Woodling, J. D., & Norris, D. O. (2008). Reproductive Disruption in Fish Downstream from an Estrogenic Wastewater Effluent. *Environmental Science & Technology*, *42*(9), 3407–3414. https://doi.org/10.1021/es0720661

Vilmin, L., Aissa-Grouz, N., Garnier, J., Billen, G., Mouchel, J.-M., Poulin, M., & Flipo, N. (2015). Impact of hydro-sedimentary processes on the dynamics of soluble reactive phosphorus in the Seine River. *Biogeochemistry*, *122*(2), 229–251. https://doi.org/10.1007/s10533-014-0038-3

Wade, A. J., Whitehead, P. G., & Butterfield, D. (2002). The Integrated Catchments model of Phosphorus dynamics (INCA-P), a new approach for multiple source assessment in heterogeneous river systems: model structure and equations. *Hydrology and Earth System Sciences*, *6*(3), 583–606. https://doi.org/10.5194/hess-6-583-2002

Ward, A. S., Cwiertny, D. M., Kolodziej, E. P., & Brehm, C. C. (2015). Coupled reversion and stream-hyporheic exchange processes increase environmental persistence of trenbolone metabolites. *Nature Communications*, *6*, 7067. https://doi.org/10.1038/ncomms8067

Williams, R. J., Keller, V. D. J., Johnson, A. C., Young, A. R., Holmes, M. G. R., Wells, C., et al. (2009). A national risk assessment for intersex in fish arising from steroid estrogens. *Environmental Toxicology and Chemistry*, *28*(1), 220–230. https://doi.org/10.1897/08-047.1

Ying, G.-G., Kookana, R. S., & Ru, Y.-J. (2002). Occurrence and fate of hormone steroids in the environment. *Environment International*, *28*(6), 545–551.

Ying, G.-G., Kookana, R. S., & Dillon, P. (2003). Sorption and degradation of selected five endocrine disrupting chemicals in aquifer material. *Water Research*, *37*(15), 3785–3791. https://doi.org/10.1016/S0043-1354(03)00261-6

Young, R. G., & Huryn, A. D. (1999). Effects of Land Use on Stream Metabolism and Organic Matter Turnover. *Ecological Applications*, *9*(4), 1359–1376. https://doi.org/10.1890/1051-0761(1999)009[1359:EOLUOS]2.0.CO;2

Zarnetske, J. P., Haggerty, R., Wondzell, S. M., & Baker, M. A. (2011). Dynamics of nitrate production and removal as a function of residence time in the hyporheic zone. *Journal of Geophysical Research: Biogeosciences*, *116*(G1). https://doi.org/10.1029/2010JG001356

Zarnetske, J. P., Haggerty, R., Wondzell, S. M., Bokil, V. A., & González-Pinzón, R. (2012). Coupled transport and reaction kinetics control the nitrate source-sink function of hyporheic zones. *Water Resources Research*, *48*(11), n/a-n/a. https://doi.org/10.1029/2012WR011894

Zhang, Y., Krysl, R. G., Ali, J. M., Snow, D. D., Bartelt-Hunt, S. L., & Kolok, A. S. (2015). Impact of Sediment on Agrichemical Fate and Bioavailability to Adult Female Fathead Minnows: A Field Study. *Environmental Science & Technology*, *49*(15), 9037–9047. https://doi.org/10.1021/acs.est.5b01464

Zhao, S., Zhang, P., Melcer, M. E., & Molina, J. F. (2010). Estrogens in streams associated with a concentrated animal feeding operation in upstate New York, USA. *Chemosphere*, *79*(4), 420–425. https://doi.org/10.1016/j.chemosphere.2010.01.060

Zhao, X., & Lung, W.-S. (2017). Modeling the fate and transport of 17β-estradiol in the South River watershed in Virginia. *Chemosphere*, *186*, 780–789. https://doi.org/10.1016/j.chemosphere.2017.08.058

Zheng, W., Li, X., Yates, S. R., & Bradford, S. A. (2012). Anaerobic Transformation Kinetics and Mechanism of Steroid Estrogenic Hormones in Dairy Lagoon Water. *Environmental Science & Technology*, *46*(10), 5471–5478. https://doi.org/10.1021/es301551h

Zuo, Y., Zhang, K., & Zhou, S. (2013). Determination of estrogenic steroids and microbial and photochemical degradation of 17α-ethinylestradiol (EE2) in lake surface water, a case study. *Environmental Science: Processes & Impacts*, *15*(8), 1529–1535. https://doi.org/10.1039/C3EM00239J

Chapter 5

Fluctuating Water Tables Enhance Carbon-Nitrogen Cycling in Humid Agroecosystems

5.1 Introduction

The critical zone, defined as the layer of Earth's surface that begins at the vegetation canopy, encompasses the soil and groundwater in the subsurface, and ends at the bedrock, is a region of intense biogeochemical activity (Billen et al., 2009; Guo & Lin, 2016). Within the critical zone, the water table acts as the interface between the saturated and unsaturated zone of the soil and plays a key role in landscape-scale nutrient cycling by modulating biogeochemical conditions and transporting solutes (Winter et al., 2015). By spanning both the groundwater aquifer (a reducing environment) and the unsaturated zone (an oxidizing environment), this interface can support a gradient of aerobic and anaerobic microbial communities that perform a wide range of biogeochemical functions (Hefting et al., 2004; Jost et al., 2010).

The position of the water table has been shown to be a major influence on the biogeochemical processes in the soil column. For example, Szymczycha et al. (2017) found that the vadose zone thickness (i.e. the water table depth) is a strong control on nitrogen cycling in the subsurface: when the water table is high, the low dissolved oxygen and increased DOC availability at the water table greatly increases the extent of denitrification in the soil. Vidon (2017) synthesized studies linking water table depth to greenhouse gas emissions and found that higher CO_2 production in wetter soils with a high water table may be suppressed after a rain event due to widespread anoxic conditions, whereas a dry soil with a low water table may experience an increase of CO_2 fluxes after the same rain event.

The fluctuations of the water table also have a role in enhancing reactivity in the critical zone. The wetting and re-wetting of the unsaturated zone has been shown to result in a burst of enhanced microbial activity as opposed to steady conditions (Birch, 1960; Baldwin & Mitchell, 2000; Reverey et al., 2016; Wang et al., 2018). This effect has been attributed to the fluctuating water table carrying organic substrates to deeper parts of the subsurface, as well as creating oxic and anoxic zones that can support the growth of both aerobic and anaerobic microbial populations (Rühle et al., 2015). In another study, CO_2 emissions were found to be enhanced during periods of soil water drainage due to increased aerobic respiration compared to a static water table scenario (Pronk et al., 2020). Additionally, the rate at which the water table fluctuates can also impact biogeochemical processes. In an experimental study, Haberer et al. (2012) observed that gradual fluctuations in the water table allow more oxygen to be transferred to groundwater than rapid fluctuations. This phenomenon may

have significant implications for the intensity of precipitation controlling the redox state and the biogeochemical processes around the water table.

The position and fluctuations of the water table are strongly influenced by climate, soil type, and landscape position. Precipitation and temperature are the dominant external forcings that control the water balance of the soil column and thus the height of the water table (Tamea et al., 2009). The properties of the underlying soil will also determine how the water table responds to climate forcings. For example, soils with low specific yields will have water tables that fluctuate more than those with higher specific yields under the same rainfall (McLaughlin et al., 2014). In addition to the above environmental controls, human management practices control the behavior of the water table. In agroecosystems with high water tables, tile drains are commonly installed in the subsurface to maintain a set water table depth to prevent crops from drowning (David et al., 2009). More recently, controls on tile drainage have been used to prevent the unrestricted leaching of nutrients into streams and to encourage biogeochemical processes such as denitrification in the subsurface (Ng et al., 2002).

Given the importance of the water table in controlling biogeochemical processing, and the variability in the water table depth across the landscape, it is important to develop an explicit framework that can describe the coupling between water table fluctuations and biogeochemical processes. There are numerous models that have been developed to describe the biogeochemical processes in soils. In a review of over 250 CN models developed in the last century, Manzoni and Porporato (2009) found that there has been a shift towards more complex models in recent literature, but that this shift has not always been followed by improved model performance. Even amongst these models, very few of them couple CN directly to water table fluctuations. Common approaches to CN processes in soils either model the shallow soil layers close to the surface, or assume a deep water table that does not interact with the upper layers of the soil. Indeed, one of the most prominent CN models in literature, DNDC, was only updated recently to incorporate fluctuating water tables (Smith et al., 2020).

Existing CN biogeochemical models typically have complex biogeochemical modules with highly simplified hydrologic representation. To better understand the role of dynamic water tables on CN processes, the purpose of this study will be to develop a point scale model that explicitly links the fluctuations of the water table and carbon-nitrogen cycling. Specifically, the overall objective of this

study will be to better understand how the management of the water table can affect the stores of N in the soil, as well as how the aqueous and gaseous fluxes of N are modified. To avoid the issues of equifinality in a highly complex model, the modeling approach taken will be to develop a parsimonious but balanced representation of the soil. One such parsimonious framework is the stochastic CN model by Poporato et al. (2003) developed for (semi-)arid systems without any water table interactions. This model has been successfully applied in multiple studies of semi-arid ecosystems to develop relationships for probability distribution functions of carbon and nitrogen pools as a function of stochastic rainfall and soil biogeochemical processing rates in arid systems (e.g. Porporato et al., 2003; S. Manzoni et al., 2004; Botter et al., 2008; Batlle-Aguilar et al., 2011).

5.2 Model Description and Development

In this study, we will develop a modeling framework for CN dynamics in humid systems by combining two existing models: 1) the stochastic C-N model developed by Porporato et al. (2003) for grassland systems in (semi-) arid climates, and 2) a stochastic soil moisture model that describes water table fluctuations in humid ecosystems as a function of soil characteristics and random climate forcings (Laio et al., 2009). The existing Laio et al. model will be described in Section **5.2.1**, the existing Porporato et al. will be described in **Section 5.2.2**, and the coupling and modifications of the two models in **Section 5.2.3**.

5.2.1 Stochastic Soil Moisture Models for Humid Climates

The spatiotemporal movement of water within the vadose zone can be described by the Richards' equation (Freeze, 1971). However, because there is not a closed-form solution of the equation and it is computationally expensive to solve the Richards' equation numerically, simplified conceptual models are often used to approximate the flow of water in the unsaturated zone (Mein & Larson, 1973; Salvucci & Entekhabi, 1994). One such framework is the stochastic soil moisture model developed by Laio et al. (2009), which discretizes the vadose zone in a more parsimonious manner. Instead of a continuous soil moisture profile, the Laio et al. model conceptualizes the soil column as three distinct moisture zones: the low moisture zone (LMZ, the unsaturated zone where the soil saturation s is variable and typically less than field capacity s_{fc}), the high moisture zone (HMZ, where water content is at field capacity s_{fc}) and the saturated zone (STZ, the groundwater and capillary

fringe where $s = 1$). Using this approach, probability density functions can be developed for water table positions as a function of climatic and soil characteristics and to explore how variations in model parameterization can affect the water table behavior.

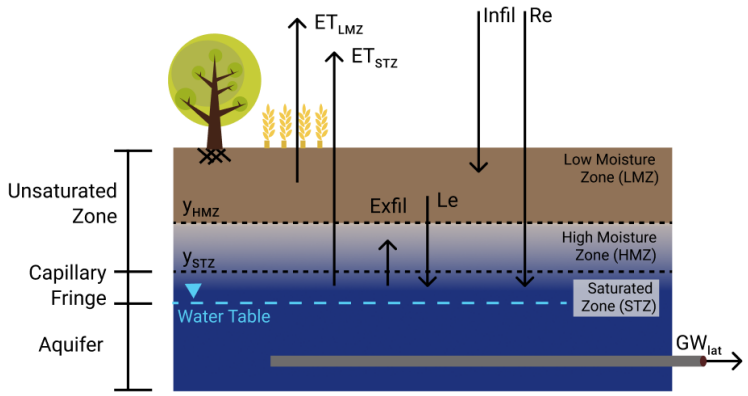

Figure 5.1 Hydrologic fluxes of the soil column based on the Laio et al. (2009) model. Fluxes of the low moisture zone and the saturated zone shown here. The low moisture zone is where the saturation is typically below field capacity, the high moisture zone is the transition zone between field capacity and full saturation, and the saturated zone contains the capillary fringe and underlying aquifer. ET is evaportranspiration, Inil is infiltration to the unsaturated zone, Re is the direct recharge to the saturated zone, Le is the leakage of water from the unsaturated to the saturated zone, Exfil is the exfiltration of water to the high moisture zone to replace water that was transpired, and GW_{lat} is the lateral groundwater flow.

The stochasticity of the system is driven by a random rainfall process, which is modeled as a Poisson process to describe event frequency (with λ as the mean number of days between events), and an exponential distribution to describe the intensity of the rain (with α the mean depth of water during a rain event at a daily scale) (Rodriguez-Iturbe et al., 1999).

The potential evapotranspirative demand of the soil column (*PET*) is first determined for use as the upper limit of actual ET (described in sections below). *PET* is approximated using a sinusoid function to simulate seasonal peaks following McLaughlin et al. (2014):

$$PET_t = PET_{min} + \omega \sin\left(\pi \frac{DOY}{365}\right) \tag{5.1}$$

where *PET* on day *t* is a function of a daily minimum PET value (PET_{min}), *DOY* is the Julian day of year, and ω is a scaling factor used to calibrate the PET such that the annual PET matches recorded PET estimates of the region.

Water Balance of the Water Table

The position of the HMZ-STZ boundary (i.e. the capillary fringe, y_{STZ}) is defined by the following water balance equation:

$$S_y \frac{dy_{STZ}}{dt} = Re(t) - ET_{wt}(y_{wt}) - Exfil\,(y_{wt}) \pm GW_{Lat}(y_{wt}) \quad (5.2)$$

where *Sy* is the specific yield of the soil [-], *Re* is the recharge to the water table [L/T], ET_w is the direct ET losses from the water table [L/T], *Exfil* is the exfiltration losses due to capillary rise of water that replaces the ET losses in the HMZ [L/T] and GW_{lat} is the lateral groundwater flow [L/T].

Recharge to the Saturated Zone

The primary processes in which the saturated zone is recharged is through infiltration of rainfall and the redistribution of water from the unsaturated zone. How the recharge process is represented depends on the presence of the low moisture zone. When the water table is close to the surface (i.e. the LMZ has not formed), the recharge to the STZ is equal to the precipitation flux P **(Equation 5.3a**). Because the HMZ has saturations at or greater than field capacity, it is assumed that the unsaturated hydraulic conductivity is sufficiently high at daily timescales to allow for instantaneous redistribution of water to the STZ. When the LMZ is present, the downward water flux to the saturated zone is suppressed due to reduced hydraulic conductivities (because of low soil moisture conditions) and is represented by the leakage flux from the LMZ (**Equation 5.3b**, full leakage equation shown in next section). The conditions when the LMZ forms is described in a later section.

$$Re = P(\alpha, \lambda) \quad (5.3a)$$

$$Re = Le(s) \quad (5.3b)$$

Root Uptake from Saturated Zone

The uptake of water by plants is a key ecohydrological process that regulates the water table dynamics. In reality, the root-groundwater interaction is a complex bi-directional process. Roots uptake groundwater, thereby lowering the water table (Naumburg et al,, 2005). On the other hand, the water table can potentially affect the growth of the plant roots - for example, prolonged saturation of

the roots can lead to anoxia and death of plants (Ho et al., 2004). In the Laio et al. model, it is assumed that the plants in these humid agroecosystems are adapted to these hydrologic conditions and are also managed to avoid overwatering. Additionally, the diel patterns of transpiration are ignored as the model is run at a daily scale. Finally, the roots are assumed to have an exponential distribution of biomass *r(z)* with an average rooting depth *b* [L], where *z* is some depth [L]. Thus, uptake can be expressed as:

$$ET_{wt} = PET \int_{-\infty}^{y_{STZ}} r(z)dz = PET\, e^{y_{STZ}/b} \tag{5.4}$$

where *PET* is the potential evapotranspiration [L/T], y_{STZ} is the depth to the saturation zone [L], and *b* is the mean root depth [L]. The formulation for root uptake is the same in shallow and deep conditions, but note that exfiltration is a function of water table depth and average plant root depth and will converge to zero deeper in the soil column due to the lack of roots.

Exfiltration from Saturated Zone

Exfiltration from the STZ is the upward flux of water due to capillary rise. In a soil column, this capillary rise is driven by the need to replace water that was removed through evapotranspiration from the HMZ.

$$Exfil(y_{STZ}) = PET\left(1 - e^{y_{STZ}/b}\right) \tag{5.5}$$

In the case where the LMZ is formed, the total exfiltration flux is reduced as there is no capillary flux in the LMZ.

$$Exfil(y_{STZ}, y_{HMZ}) = PET\left(e^{y_{HMZ}/b} - e^{y_{STZ}/b}\right) \tag{5.6}$$

Lateral Groundwater Fluxes

The lateral movement of water can be induced by the head gradient due to factors such as topographic changes or groundwater extraction. The flow of groundwater can be expressed generally with a simplified version of Darcy's law:

$$GW_{Lat} = k_{sat}\frac{dy}{dL} = k_{lat}\,(y_{STZ} - y_o) \tag{5.7}$$

where k_{sat} is the saturated hydraulic conductivity of the soil [L/T], $dy = (y_{STZ} - y_o)$ is the head gradient between the saturated zone and a reference head potential [L], dL is the distance to a reference point (e.g. tile outlet) [L], and k_{lat} is a proportionality constant based on k_{sat} and dL [1/T].

Location of the High Moisture Zone

As the saturated zone lowers, the upper portion of the soil begins to drain below full saturation and thus the high moisture zone forms ($S_{fc} < S_{HMZ} < 1$). If the soil column continues to dry, the saturated zone will eventually hit some critical depth y_c such that the ground surface is at field capacity. Any further lowering of the saturated zone will cause the upper boundary of the HMZ (i.e. the HMZ-LMZ boundary) to lower and also cause the low moisture zone to form, where the soil can go below field capacity.

The location of the HMZ-LMZ boundary (y_{HMZ}) is a function of soil moisture properties, the position of the HMZ-STZ boundary (y_{STZ}) and the critical depth y_c (approximated using soil texture and mean root depth, see Laio et al., 2009 for complete details):

$$y_{HMZ}(y_{STZ}) \begin{cases} 0 & if\ y\ \geq y_c\,, \\ \left(1 - A^{\frac{3}{4}}\right)(y - y_c) - \frac{A^2\left(1 - A^{-\frac{1}{4}}\right)}{-y_c + \psi_{fc} - \psi_s}(y - y_c)^2 & if - 5b\ + \psi_{fc} - \psi_s\ \leq y <\ y_c\,, \\ y_{STZ} - \psi_{fc} + \psi_s & if\ y\ <\ -5b\ + \psi_{fc} - \psi_s \end{cases} \tag{5.8}$$

where $A = \frac{\psi_{fc} - \psi_s - y_c}{\psi_{fc} - \psi_s - y_c - 5b}$ and $\psi_{fc} = \psi_s\, {S_{fc}}^{-1/m}$. This is a numerical approximation of the Richards' equation for the HMZ, where the HMZ does not form until the water table falls below the critical depth y_c, increases dynamically until it reaches the end of the estimated root zone (-5b +ψ_{fc}-ψ_s),and then remains at a constant distance from the saturated zone beyond that point (Laio et al, 2009).

Water Balance of the Low Moisture Zone

The water balance equation is used to capture the soil moisture dynamics in the low moisture zone, is described below following Rodriguez-Iturbe (1999):

$$n\,|y_{HMZ}|\frac{ds}{dt} = I(s,t) - ET(s) - L(s) \tag{5.9}$$

where n is the porosity [-], $|y_{HMZ}|$ is the size of the low moisture zone (i.e. the depth to the high moisture-low moisture zone boundary) [L], $I(s)$ is the recharge from infiltrated rain [L/T], $L(s)$ is leakage to the high moisture zone [L/T], and $ET_{lm}(s)$ is the evapotranspiration flux from the low moisture zone [L/T]. When the low moisture zone is present, $I(s)$ equals precipitation, and **Equation 5.3a** representing recharge to the saturated zone is replaced with **Equation 5.3b**.

Leakage in this low moisture zone describes vertical percolation of water to the deeper moisture zones under unit gradient conditions, and is described as:

$$L(s) = \frac{k_{sat}}{e^{\beta(1-s_{fc})}-1}\left[e^{\beta(s-s_{fc})} - 1\right] \tag{5.10}$$

where k_{sat} is the hydraulic conductivity of the soil [L/T], β modifies the leakage process as a function of soil texture where $\beta = 2p+4$ and p is the pore size distribution index. In this formulation, leakage only occurs when the low moisture zone is above field capacity S_{fc} and approaches k_{sat} near full saturation.

Actual evapotranspiration from the low moisture zone was then modelled as the remaining evapotranspirative demand after accounting for ET from the water table ($PET_{lm} = PET - ET_{wt}$). A reduction term is applied based on the current saturation in the low moisture zone, such that there is no ET after the soil dries below the wilting point (S_w). Thus, ET in the LMZ is modeled as:

$$ET_{lm} = PET_{lm}\left(\frac{s-s_w}{s_{fc}-s_w}\right) \tag{5.11}$$

5.2.2 Stochastic CN Cycling Modeling

Soil moisture and nutrient cycling are intricately linked through complex feedbacks and non-linear processes. Process-based biogeochemical models often discretize soil C and N into different pools to account for different rates of decomposition. For example, Century (Parton et al., 1988), DNDC (Li et al., 1994), CLM-BGC (Lawrence et al., 2011), use active/labile and passive/recalcitrant pools of carbon and nitrogen to distinguish components of the soil that have varying degrees of susceptibility

to decomposition. The use of discrete pools is a way to simplify the entire distribution of soil quality in a finite manner (Manzoni et al., 2009).

Here, we adapt the C-N modelling framework of Porporato et al. (2003) which was specifically developed to quantify the ecohydrologic feedbacks between point-scale soil moisture dynamics with the carbon and nitrogen cycles in a parsimonious manner. The model has been used to quantify probability density functions of the nutrient pools and fluxes as a function of different climate regimes in arid systems to characterize how the average and variance of state variables respond to climatic forcings (D'Odorico et al., 2010). For example, in arid systems, the stochastic nature of rainfall can result in predictable biogeochemical behaviour such as the gradual accumulation of organic matter or the intermittent leaching of nitrate (Tamea et al., 2009).

In the Porporato et al. model, the authors conceptualize the soil to be made up of three carbon pools (litter C_L, microbial biomass C_b, and humus C_H) and five nitrogen pools (litter N_L, microbial biomass N_b, humus N_H, ammonium N^+, and nitrate N^-). Nonlinear differential equations are written for each of these pools, and these equations are coupled to the equations for water fluxes developed by Rodriguez-Iturbe et al. (1999) in their model for arid systems. The biogeochemical processes captured in the model include decomposition, mineralization, immobilization, plant uptake, and leaching (**Figure 5.2**). The carbon and nitrogen cycles are coupled through C-N ratios of the various pools and thus can account for stoichiometric limitations of processes in the C and N cycles. In the following section, the key equations and processes of the base Porporato et al. CN model is briefly described.

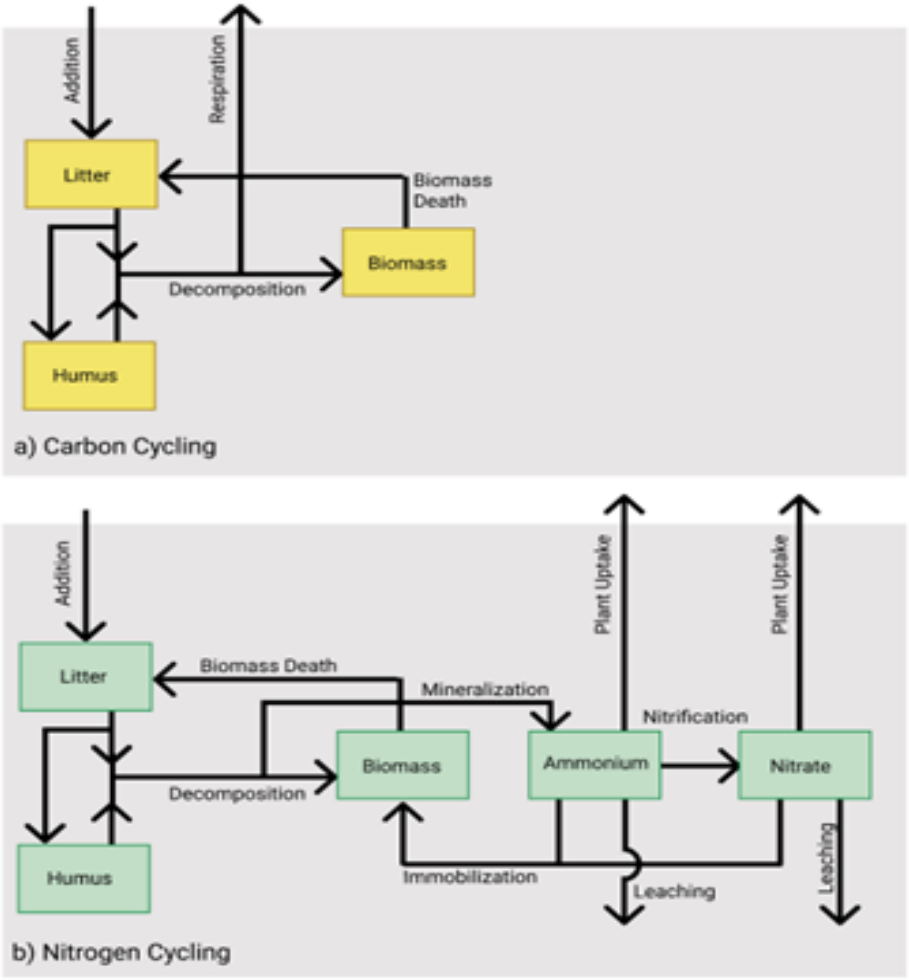

Figure 5.2 a) Carbon and b) nitrogen pools and fluxes in the Porporato et al. (2003) modelling framework

Carbon-Nitrogen Cycling in the Litter Pool

The litter pool represents the fraction of soil organic matter that is more labile and susceptible to decomposition. The mass balance equation of carbon in the litter pool, C_L expressed as concentrations relative to the soil system (mass per unit volume soil), can be written as:

$$\frac{dC_L}{dt} = ADD + BD - DEC_L \tag{5.12}$$

where *ADD* is the addition of external litter input, *BD* is the biomass death and DEC_L is the decomposition of the litter. The primary source of carbon into the soil column is through the addition of plant material and residues (the *ADD* flux). This plant material is considered to be more degradable and thus only added to the litter pool. The secondary source of carbon into the litter pool is from biomass death (*BD*), where a fraction of the microbial biomass returns to the litter pool, described using a first order rate constant: $BD = k_{bd}C_b$.

The loss of carbon in the litter pool is driven by microbial decomposition (DEC_L) and can be represented by the following:

$$DEC_L = C_L\,[k_L\, C_b \varphi\, f_d(s)] \tag{5.13}$$

The decomposition flux is dependent on both the concentration of C in the litter pool C_L and microbes C_b. The rate at which litter decomposes can be described by the rate constant k_L [L^3/M/T]. This rate constant is an effective rate of decomposition of different organic material. Additionally, the decomposition process is mediated by environmental conditions. First, scarcity of nitrogen in the soil can reduce the decomposition rate in the soil and microbes cannot acquire enough nitrogen through immobilization. This non-dimensional factor φ is further described under the Mineralization and Immobilization section. Additionally, decomposition can be suppressed due to excess or low soil moisture conditions, with a peak at field capacity:

$$f_d(s) = \begin{cases} \frac{s}{s_{fc}}, & s < s_{fc} \\ \frac{s_{fc}}{s}, & s \geq s_{fc} \end{cases} \tag{5.14}$$

Nitrogen cycling in the litter pool N_L can be represented by the same fluxes as the carbon litter equation and using C/N ratios of the appropriate pool from where the flux originates:

$$\frac{dN_L}{dt} = \frac{ADD}{(C/N)_{add}} + \frac{BD}{(C/N)_b} - \frac{DEC_L}{(C/N)_L} \tag{5.15}$$

Carbon-Nitrogen Cycling in the Humus Pool

The carbon in the humus pool, C_H expressed as concentrations relative to the soil system (mass per unit volume soil), is represented by the following mass balance equation:

$$\frac{dC_H}{dt} = r_h DEC_L - DEC_h \tag{5.16}$$

where r_h is the fraction of the litter decomposition flux that forms humus [-], and mass is lost through humus decomposition DEC_h . Similarly to the litter pool, the decomposition of humus is modeled as:

$$DEC_H = C_H \left[k_H C_b \varphi f_d(s)\right] \tag{5.17}$$

where the only difference is the rate constant for humus decomposition k_H [L^3/M/T].

The corresponding mass balance of the nitrogen content of the humus pools (N_H) can be written as:

$$\frac{dN_H}{dt} = \frac{r_h DEC_L}{(C/N)_H} - \frac{DEC_h}{(C/N)_H} \tag{5.18}$$

Given that the CN ratio of humus is assumed constant, this equation does not need to be solved, and can be determined from the carbon humus equation.

Carbon-Nitrogen Cycling in the Microbial Biomass Pool

The carbon content of the microbial biomass (C_b) is written as:

$$\frac{dC_b}{dt} = (1 - r_h - r_r)DEC_L + (1 - r_r)DEC_h - BD \tag{5.19}$$

The microbial biomass grows by incorporating carbon through the decomposition of the humus and litter pools. A fraction of the carbon is lost via respiration to CO_2 production (r_r), which is assumed constant in this model. Finally, the microbial biomass pool decreases via biomass death *BD*, and is defined by the rate constant $k_{bd.}$

The nitrogen content of the microbial biomass (N_b) is similar to the carbon content, with some modifications due to new processes:

$$\frac{dN_b}{dt} = (1 - r_h - r_r)\frac{DEC_L}{(C/N)_L} + (1 - r_r)\frac{DEC_h}{(C/N)_H} - \frac{BD}{(C/N)_b} - \Phi \tag{5.19}$$

Like carbon, nitrogen is incorporated into the microbial biomass pool through the decomposition of the litter and humus pools, and is lost via biomass death. Each of these fluxes are converted to nitrogen based on the stoichiometric ratios. The term Φ represents the net mineralization (or ammonification) or immobilization and is described in the next section.

Mineralization and Immobilization

The process of mineralization and immobilization (Φ) is dependent on the nitrogen availability in the soil in relation to the stoichiometric needs of the microbial biomass (i.e. to maintain a constant $(C/N)_b$ ratio). There will be net mineralization ($+\Phi$) when there is an abundance of organic N after decomposition and production of inorganic N; conversely, there will be net immobilization ($-\Phi$) where the microbes use inorganic N to meet their N demands. Thus, the net mineralization/immobilization flux is written as:

$$\Phi = DEC_H\left[\frac{1}{(C/N)_H} - \frac{1-r_r}{(C/N)_b}\right] + DEC_L\left[\frac{1}{(C/N)_L} - \frac{r_h}{\left(\frac{C}{N}\right)_H} - \frac{1-r_r-r_h}{(C/N)_b}\right] \tag{5.20}$$

Or expanded as:

$$\Phi = \varphi\, f_d(s) C_b\left\{k_H\, C_H\left[\frac{1}{(C/N)_H} - \frac{1-r_r}{(C/N)_b}\right] + k_L\, C_L\left[\frac{1}{(C/N)_L} - \frac{r_h}{\left(\frac{C}{N}\right)_H} - \frac{1-r_r-r_h}{(C/N)_b}\right]\right\} \tag{5.21}$$

Here, if the inner term of the brackets of **Equation 5.21** are positive, there is sufficient organic N for mineralization to occur, while a negative term results in immobilization is required to maintain the stoichiometric needs of the microbes. The term φ is a reduction term of the decomposition rate due to insufficient N, and can be written as:

$$\varphi = \frac{-\left(k_i^+ N^+ + k_i^- N^-\right)}{k_H C_H\left[\frac{1}{(C/N)_H} - \frac{1-r_r}{(C/N)_b}\right] + k_L C_L\left[\frac{1}{(C/N)_L} - \frac{r_h}{(C/N)_H} - \frac{1-r_r-r_h}{(C/N)_b}\right]} \tag{5.22}$$

In the case of immobilization (Φ is negative), the products are partitioned into ammonium and nitrate based on the constants k^+_i and k^-_i, and is written as:

$$\begin{cases} IMM^+ = \dfrac{k_i^+ N^+}{k_i^+ N^+ + k_i^- N^-} |\Phi| \\ IMM^- = \dfrac{k_i^- N^-}{k_i^+ N^+ + k_i^- N^-} |\Phi| \end{cases} \tag{5.23}$$

Cycling of the Mineral Nitrogen Pools

The mass balances of ammonium and nitrate have very similar dynamics and share similar fluxes and can be written as:

$$\frac{dN^+}{dt} = MIN - IMM^+ - NIT - LE^+ - UP^+ \tag{5.24}$$

$$\frac{dN^-}{dt} = NIT - IMM^- - LE^- - UP^- - DEN \tag{5.25}$$

Nitrification (*NIT*) is the production of nitrate via microbial processes and can be expressed as:

$$NIT = N^+ [k_n C_b f_n(s)] \tag{5.26}$$

where $f_n(s)$ [-] is the reduction factor that suppresses the nitrification rate constant k_n [L^3/M/T] under non-ideal moisture conditions. It is assumed the $fn(s)$ is at its peak at field capacity where there is sufficient oxygen for the aerobic process. Increases of saturation will result in anoxic conditions, while decreases of saturation will result in access limitation between the microbes and ammonium. Thus, *fn* can be expressed as:

$$f_n(s) = \begin{cases} \dfrac{s}{s_{fc}}, & s < s_{fc} \\ \dfrac{1-s}{1-s_{fc}}, & s \geq s_{fc} \end{cases} \tag{5.27}$$

Leaching is the downward transport of mineral N via percolation, and thus is dependent on the hydrologic leakage flux $L(s)$. Leaching is modeled as

$$LE^{\pm} = a^{\pm} \frac{L(s)}{sn\, Z_r} N^{\pm} \tag{5.28}$$

where $a^{\pm}$ is related to the solubility coefficients of ammonium and nitrate [-], and snZ_r represents the volume of water in the soil column [L].

Plant uptake of mineral N can be modeled as the summation of the passive ($UP^{\pm}{}_p$) and active uptake ($UP^{\pm}{}_a$). The passive uptake is the transport of N simply via the transpiration flux and can be written as:

$$UP_p^{\pm} = a^{\pm} \frac{ET(s)}{sn\, Z_r} N^{\pm} \tag{5.29}$$

The active uptake component is dependent on the plant N demands ($DEM^{\pm}$), and represents the extra uptake of mineral N via a diffusive flux driven by a concentration gradient:

$$UP_a^{\pm} = \begin{cases} 0 & if\ DEM^{\pm} - UP_p^{\pm} < 0 \\ k_u\, N^{\pm} & if\ k_u\, N^{\pm} < DEM^{\pm} - UP_p^{\pm} \\ DEM^{\pm} - UP_p^{\pm} & if\ k_u\, N^{\pm} > DEM^{\pm} - UP_p^{\pm} > 0 \end{cases} \tag{5.30}$$

The first case represents the case when the nitrogen demands are already provided by the passive uptake flux. The second case occurs when passive uptake is insufficiently low and allows for the full active uptake based on the rate constant k_u. The final case occurs when passive uptake is still low, but the active uptake component will be limited by the actual plant needs.

5.2.3 Connecting the Hydrologic and CN Modules

Denitrification

Denitrification is a key process in anoxic environments and thus is a necessary addition to the modelling framework due to the prevalence of saturated conditions. A variety of models can be used to represent denitrification at different levels of complexity. In a review of over fifty models, Heinen (2006) identified common variables used to modulate the actual rate of denitrification: an inherent denitrification rate constant, nitrate availability, water content, soil temperature, and pH, where the dependency of denitrification on each of these environmental conditions can be described with a

range of nonlinear functions. To match the data availability and general model structure, we use describe denitrification as a function of water content and nitrogen availability:

$$DEN = k_d\, f_s\, f_N\, N^- \tag{5.31}$$

$$f_s = \begin{cases} 0 & S < S_t \\ \left(\frac{S - S_t}{1 - S_t}\right)^w & S_t \leq S \end{cases} \tag{5.32}$$

$$f_N = \frac{N^-}{K_N + N^-} \tag{5.33}$$

where S is the saturation [-], S_t is a saturation value when $fs = 0$, w is a shape factor, and K_N is the half-saturation constant [M/L^3].

As part of the model result analyses, we estimate how denitrification is partitioned into N_2 and N_2O. We use the following saturation-partitioning relationship used in CENTURY (Parton et al., 1996):

$$N_2 \,/\, N_2O = \frac{1.4}{13^{\frac{17}{13^{2.2\,s}}}} \tag{5.34}$$

where s is the saturation of the soil [-]. This relationship, used in the model CENTURY, was an empirically fitted function using observed gas fluxes from different soil types. This function is a monotonically increasing function that approaches zero below 40% saturation (i.e. full N_2O production), and approaches 1 at full saturation (i.e. full N_2 production).

Vertical Discretization of CN Cycling

In the previous formulation of the CN model (Porporato et al, 2003), the water table was assumed to be at some depth that does not interact with the unsaturated zone due to arid conditions. Additionally, the carbon and nitrogen pools were all assumed to be confined within some static depth *Zr* that represents the unsaturated zone as the model domain. However, in humid conditions, the water table fluctuates and consequently affects the size of the unsaturated zone. Mass accounting of the carbon and nitrogen pools become difficult due to the changing domain of the unsaturated zone.

Thus, to avoid numerical artifacts of modeling CN pools in moisture zones that may not be present, we instead split the carbon-nitrogen pools into smaller pools associated with different soil horizons (O, A and B soil horizons at 0-10 cm, 10-60 cm and 60-250 cm respectively) and their physical boundaries are static. Each C and N pool in the horizons are represented by the same mass balance equations, but may have different soil moisture values. In particular, the soil moisture content of each horizon ($s_{O\ horizon}$, $s_{A\ horizon}$,$s_{B\ horizon}$) is calculated in one of two ways: 1) if the soil horizon is completely within a hydrologic zone (LMZ, HMZ, STZ), then the soil moisture content of that horizon is equal to the current moisture content of that zone; 2) if the soil horizon comprises of more than one moisture zone, then the weighted average of the moisture content of the different moisture zones is used. Consequently, each mass balance equation of C and N were split into three equations (e.g. C_L becomes $C_{L,\ O\ horizon}$, $C_{L,\ A\ horizon,}$ $C_{L,\ B\ horizon}$).

5.2.4 Model Parameterization and Simulation

The typical physical properties of a sandy loam soil was assumed for the simulation (**Table 5.1**). The O, A, and B soil horizons were assigned thicknesses of 10, 50, and 190 cm, for a total soil column of 250 cm. To isolate the effects of the fluctuating water table and avoid issues of equifinality, the CN cycling parameters (**Table 5.1**) were independent of soil horizon and depth. Assigning different parameters based on soil horizon would require further calibration to observed values in the field.

Table 5.1 Soil properties related to the hydrologic model

Parameter	Symbol	Value
Porosity	n	0.44
Hydraulic Conductivity	$Ksat$	0.125 m/d
Rooting Depth	b	0.3 m
Specific Yield	Sy	0.19
Soil matric potential	ψ_s	0.2 m
Field Capacity	s_{fc}	0.57
Wilting Point	s_w	0.26
k_{lat}	k_{lat}	1.7×10^{-4} 1/d
Thickness of O Horizon	h_O	0.1m
Thickness of A Horizon	h_A	0.5m
Thickness of B Horizon	h_B	2.4m

Table 5.2 Parameters related to biogeochemical model

Parameter	Symbol	Value
Carbon:Nitrogen of Litter	$(C/N)_{ADD}$	58
Carbon:Nitrogen of Litter	$(C/N)_L$	22
Carbon:Nitrogen of Biomass	$(C/N)_b$	11.5
Fraction dissolved ammonium	a^+	0.05
Fraction dissolved nitrate	a^-	1
Denitrification rate constant	k_{den}	0.001 1/d
Nitrification rate constant	k_{nit}	0.06 $m^3/d/gC$
Biomass death rate constant	k_{bd}	0.0085 1/d
Humification rate constant	k_h	2.5E-6 $m^3/d/gN$
Fraction as respiration	r_r	0.6
Fraction as humus	r_h	0.25
Plant ammonium demand	DEM^+	0.2 $gN/m^3/d$
Plant nitrate demand	DEM^-	0.5 $gN/m^3/d$
Half-saturation constant of nitrate	K_N	10 mgN/L
Ammonium immobilization proportionality constant	ki^+	1 $m^3/d/gC$
Nitrate immobilization proportionality constant	ki^-	1 $m^3/d/gC$

The model was implemented using a forward Euler numerical scheme with a time step of 0.1d to ensure numerical stability. The model was run for 500 years, with the analysis only using the results in the latter 300 years to avoid the impact of the model spin-up period. Two scenarios were explored in this chapter: **Scenario 1** where the soil had no lateral groundwater fluxes and **Scenario 2** where a large groundwater flux was imposed to artificially lower the groundwater table and simulate the effect of tile drainage.

5.3 Results and Discussion

5.3.1 Linkages Between Water Table Fluctuations and Nitrogen Cycling

We first simulated a soil column with no lateral groundwater fluxes to isolate the effects of the given climatic regime on the carbon-nitrogen cycles (**Figure 5.3**). This model run (Scenario 1) had an average water table depth of 0.18 m below the ground surface (**Figure 5.3a**), with the soil near full saturation for extended periods of time. The primary water losses in this scenario are through evapotranspiration and saturation-excess runoff, with no lateral groundwater flux.

The organic nitrogen pools represent the largest and most stable stores of N within the soil column, with the total humus N averaging 170 g N/m^3 soil (coefficient of variation CV = 0.06) and the total litter N averaging 46 g N/m^3 soil (CV = 0.05) (**Figures 5.3b and c**). The magnitudes of the organic N

pools in the model are in line with soil samples taken in agricultural soils in southern Ontario (Yang and Kay, 2001). In contrast, the average concentration of ammonium was 7.6 g N/m^3 soil (CV = 0.38) and nitrate was 3.7 x 10^{-2} g N/m^3 (CV = 1.83).

While the total mass of the N pools were dominated by the largest soil horizon (horizon B, deeper than 0.6 m below the ground) when looking at the entire soil column, there are distinct gradients of N by depth. In general, all organic N pools had the highest concentrations nearest to the ground surface, consistent with the location of the external N inputs. The litter N had more variable concentrations in the O and A horizons due to the episodic loading of fertilizer and the subsequent transportation pathways to biomass N and inorganic N (**Figure 5.3c**).

The patterns of inorganic N concentrations differed from the organic pools, where the model showed consistently higher ammonium concentrations and some episodic spikes of nitrate in the A horizon (from 0.1 to 0.6 m below the ground) (**Figures 5.3e and f**). The higher ammonium concentration in the A horizon is indicative of high mineralization rates due to the abundance of organic N, and a relatively low rate of nitrification from the anaerobic conditions. There were periodic spikes of nitrate production that can be directly attributed to periods of a lower water table, which allows for the production of nitrate via nitrification. However, the presence of nitrate in the soil column is limited due to the high rates of denitrification promoted by near saturated conditions.

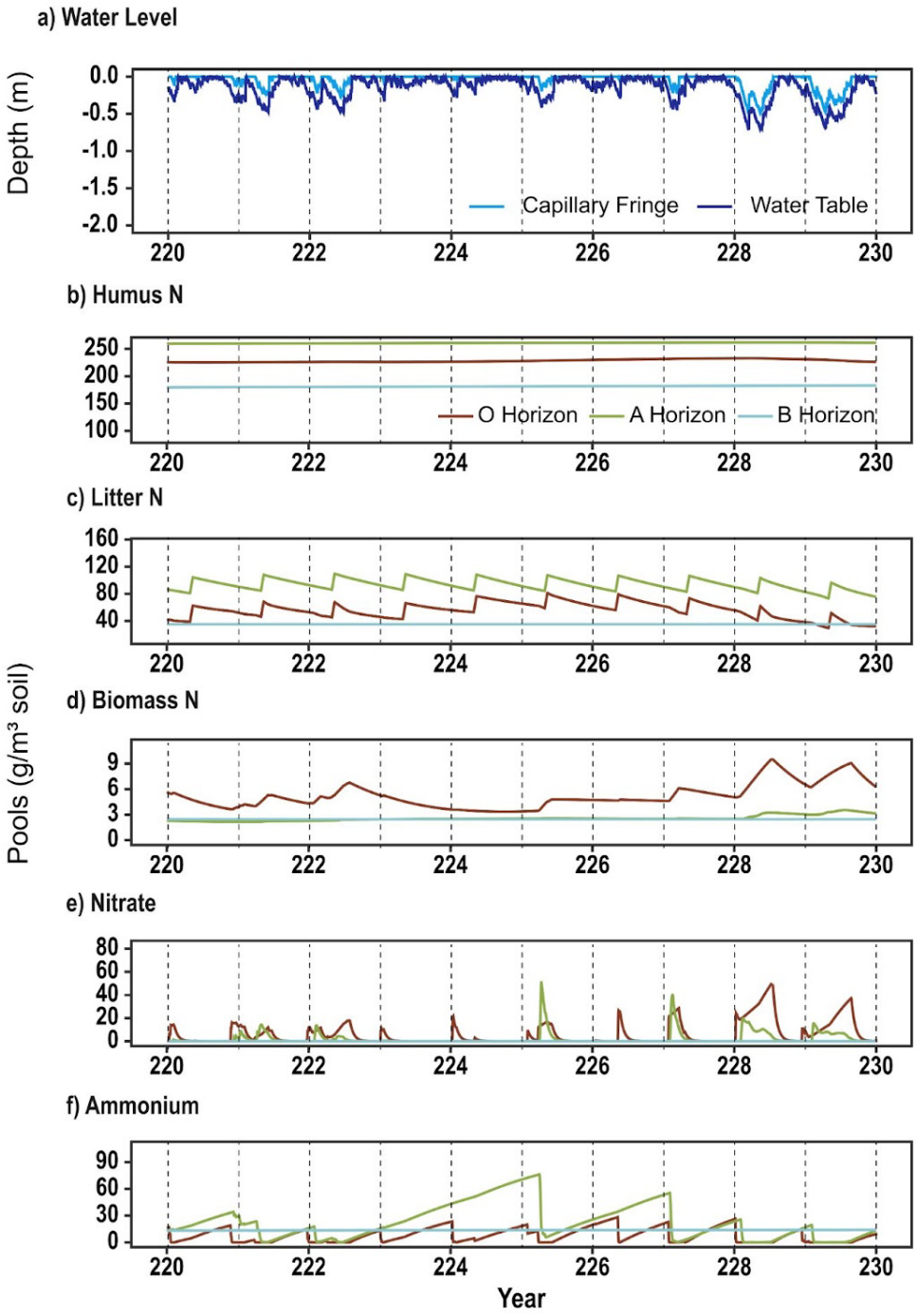

Figure 5.3 Time series of nitrogen pools for Scenario 1 with limited lateral drainage and a high water table (mean depth of 0.18 m below ground surface).

The second set of model runs (Scenario 2) simulates the effects of an artificially lowered water table (mean depth of 0.91 m below the ground surface) by increasing the lateral groundwater flux (**Figure 5.4**) - all other climatic and soil parameters remained the same as Scenario 1. Similar to Scenario 1, the organic pools of nitrogen in Scenario 2 remain the most stable and largest pools of nitrogen in the soil column. The humus pool is relatively stable (190 g N/m3 soil; CV = 0.06), while the litter and biomass N are slightly more variable (35.6 g N/m^3 soil with CV = 0.15, and 0.73 g N/m^3 soil with CV = 0.43 respectively). The litter N concentrations continue to be increased seasonally by fertilizer inputs and is consequently transformed to biomass N via decomposition (**Figures 5.4c and d**). Finally, the ammonium and nitrate pools were the most variable pools of N in the soil column, with CVs of 1.1 and 0.68 respectively.

To compare between the two scenarios, the median concentrations of the various N pools of each horizon were calculated (**Figure 5.5**). Here, we see the role of increased decomposition in the O and A horizons due to less saturation in the drained scenario, with lower concentrations in all three horizons for the humus and litter N. The range of humus N concentrations across the soil horizons were more narrow in the drained scenario, (ranging from 153 to 170g N/m^3 soil), whereas the undrained case had a much wider range (ranging from 120 to 252 g N/m^3 soil).

As expected, the abundance of oxygen in the soil column in Scenario 2 promotes high nitrification rates and limited denitrification, resulting in low ammonium and high nitrate concentrations - for example in the A horizon, the drained case resulted in an 8.6 g N/m^3 soil (or 34 mg/L of porewater) increase in median nitrate concentrations and a reduction of 1.2 g N/m^3 soil (or 4.7 mg/L of porewater) in median ammonium concentrations. The time series shows that while ammonium can temporarily build up in the soil, it can quickly be oxidized into nitrate when the water table lowers.

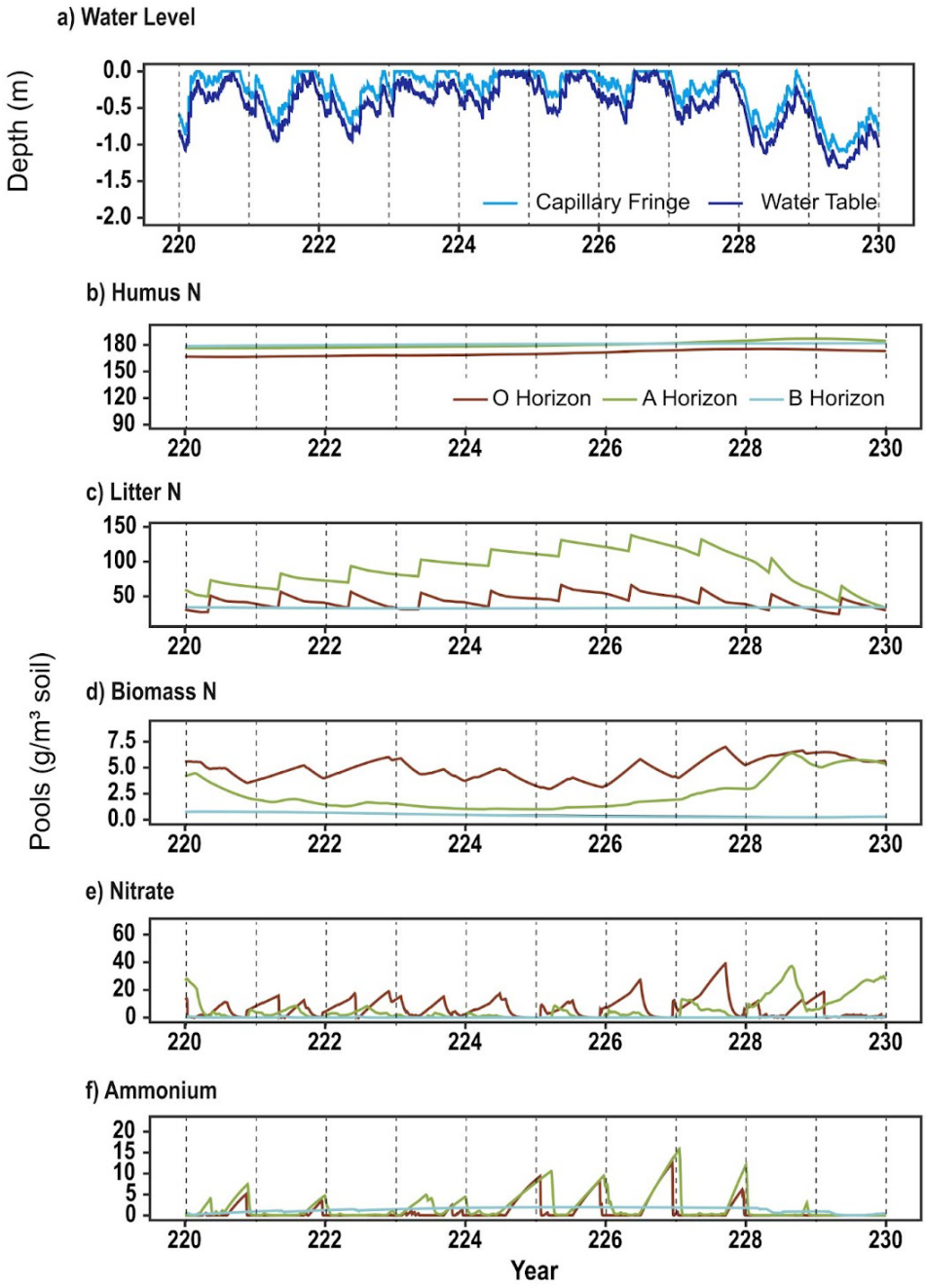

Figure 5.4 Time series of nitrogen pools for Scenario 2 with greater lateral drainage and a lower water table (mean depth of 0.91 m below ground surface)

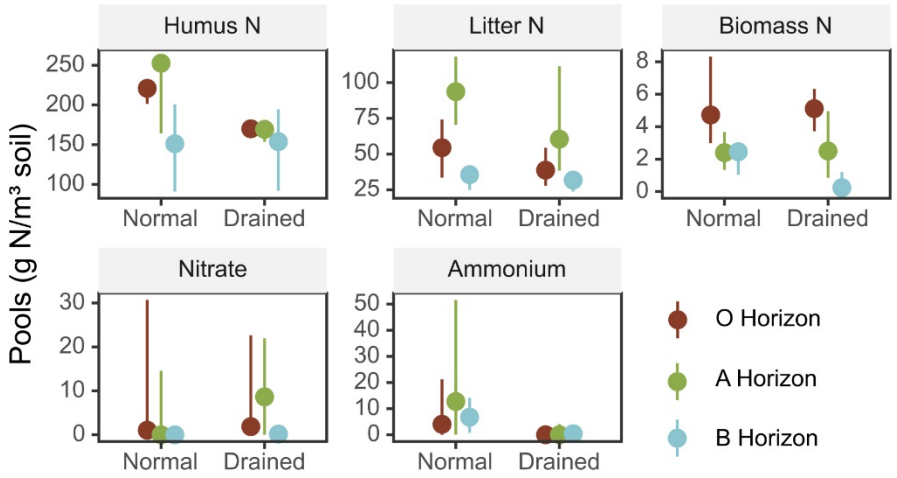

Figure 5.5 Comparison of N pool concentrations of Scenario 1 (Normal) and Scenario 2 (Drained). Colors indicate soil horizon; Point shows the median value across the time series and the whisker extents show the 5th and 95th percentiles.

5.3.2 The Effect of Water Table Management on Nitrogen Fluxes

The two major fluxes of concern with respect to nitrate are nitrification and denitrification (**Figure 5.6**). Here, we can see that nitrogen and denitrification are more balanced in the first scenario, where the soil column is typically between near saturation or at saturation which allows for a near-balance between the two fluxes (nitrification:denitrification ratio of 1.1). In contrast, there is a much greater difference in the nitrification and denitrification fluxes in the drained scenario (nitrification:denitrification ratio of 1.8)

Finally, an estimate of the products of the denitrification flux was estimated for the two model scenarios (**Figure 5.7**). The undrained case (Scenario 1) produced substantially more N_2, with a small fraction of N_2O (2 % of total gas fluxes). While the total denitrification flux in the drained soil was lower, N_2O was a slightly larger proportion of the flux (7%), and larger in magnitude than in Scenario A. It should be noted that while the water table was nearly a meter deeper in the drained case, the soil column was predominantly saturated (depth weighted average of 0.9) and tending towards N_2 production rather than N_2O. In fact, N_2O production in the models are essentially limited to the O and A horizons, which only constitute approximately 20% of the soil depth.

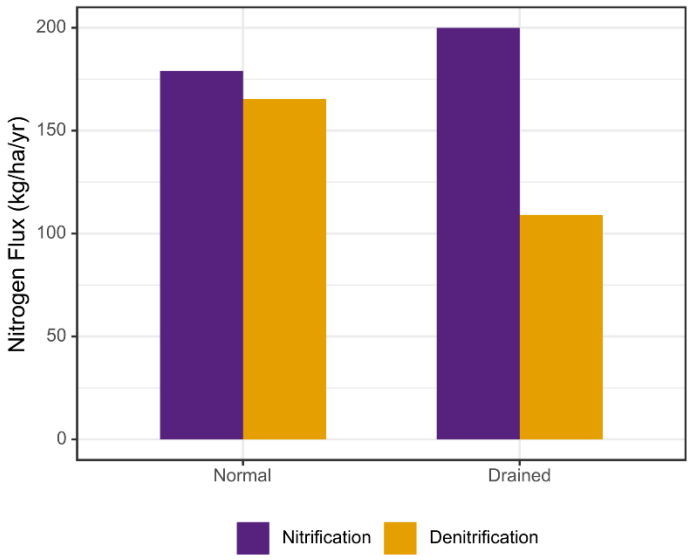

Figure 5.6 Comparison of denitrification and nitrification fluxes

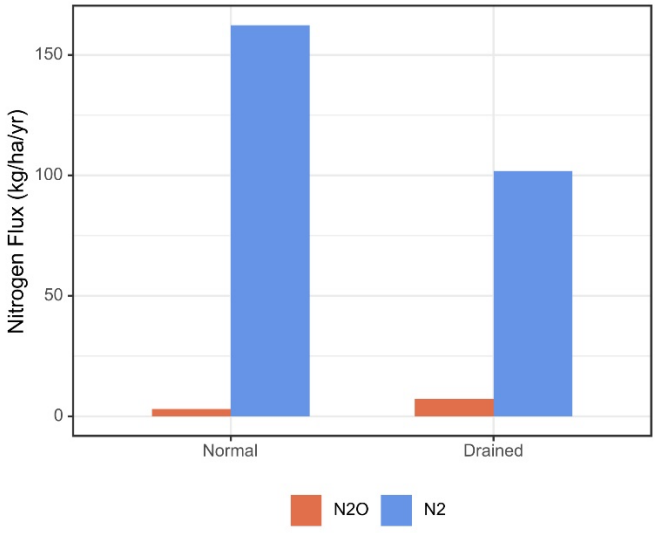

Figure 5.7 N_2O and N_2 production in the soil column.

5.4 Conclusions and Next Steps

This chapter focused primarily on the coupling of the Porporato et al. (2003) carbon-nitrogen model and Laio et al. (2009) humid water balance model into a framework that can be applied to humid

agroecosystems. Preliminary analysis showed that the position of the water table has a large role in controlling the nitrogen fluxes and partitioning within the soil system but there remains significant opportunities to use the model to explore how human management of agroecosystems can affect CN dynamics while considering the ecohydrological interactions of climate, soil, and vegetation. Ultimately, we need to better understand the trade-offs between soil health, water quality, as well as greenhouse gas emissions. Below, I outline several paths forward to further the work beyond the model development stage to address these concerns.

More Rigorous Validation of Model

While it is not common to have water table fluctuations, CN pools, as well as the aqueous and gaseous fluxes all measured at a single agricultural field site, there is an opportunity to calibrate the model to existing time series data for several of the state variables. This would allow us to constrain the model better and focus on the remaining model processes that are difficult to measure in the field.

Exploring the Range of Soil-Climate Interaction

In this chapter, the analysis was focused only on one type of soil, whereas there exists a wide range of soil textures in agroecosystems. More importantly, the role of soil texture is known to have a strong role in controlling the position and fluctuations of the water table. Similarly, the role of climate (rainfall patterns characterized by frequency and intensity, as well as changing ET dynamics) also have a direct effect on the water table. Thus the feedbacks between a range of soil types and climate forcings and CN cycling in these humid agroecosystems should still be explored.

Adapting the Model to Different Landscape Factors

While the model here was used to simulate the effect of artificial drainage and the lowering of the water table, this modelling framework can be easily adapted to other scenarios as well. For example, the model could be used to simulate low and high locations of the watershed (i.e. saturated areas such as riparian regions close to the stream or on top of the hillslope that has thick unsaturated zones) to better understand the role of these different areas on CN cycling within the landscape.

Chapter 5 References

Baldwin, D. S., & Mitchell, A. M. (2000). The effects of drying and re-flooding on the sediment and soil nutrient dynamics of lowland river–floodplain systems: a synthesis. *Regulated Rivers: Research & Management*, *16*(5), 457–467. https://doi.org/10.1002/1099-1646(200009/10)16:5<457::AID-RRR597>3.0.CO;2-B

Batlle-Aguilar, J., Brovelli, A., Porporato, A., & Barry, D. A. (2011). Modelling soil carbon and nitrogen cycles during land use change. A review. *Agronomy for Sustainable Development*, *31*(2), 251–274. https://doi.org/10.1051/agro/2010007

Billen, G., Thieu, V., Garnier, J., & Silvestre, M. (2009). Modelling the N cascade in regional watersheds: The case study of the Seine, Somme and Scheldt rivers. *Agriculture, Ecosystems & Environment*, *133*(3), 234–246. https://doi.org/10.1016/j.agee.2009.04.018

Birch, H. F. (1960). Nitrification in soils after different periods of dryness. *Plant and Soil*, *12*(1), 81–96. https://doi.org/10.1007/BF01377763

Botter, G., Daly, E., Porporato, A., Rodriguez-Iturbe, I., & Rinaldo, A. (2008). Probabilistic dynamics of soil nitrate: Coupling of ecohydrological and biogeochemical processes. *Water Resources Research*, *44*(3), W03416. https://doi.org/10.1029/2007WR006108

David, M. B., Grosso, S. J. D., Hu, X., Marshall, E. P., McIsaac, G. F., Parton, W. J., et al. (2009). Modeling denitrification in a tile-drained, corn and soybean agroecosystem of Illinois, USA. *Biogeochemistry*, *93*(1–2), 7–30. https://doi.org/10.1007/s10533-008-9273-9

Freeze, R. A. (1971). Three-Dimensional, Transient, Saturated-Unsaturated Flow in a Groundwater Basin. *Water Resources Research*, *7*(2), 347–366. https://doi.org/10.1029/WR007i002p00347

Guo, L., & Lin, H. (2016). Critical Zone Research and Observatories: Current Status and Future Perspectives. *Vadose Zone Journal*, *15*(9). https://doi.org/10.2136/vzj2016.06.0050

Haberer, C. M., Rolle, M., Cirpka, O. A., & Grathwohl, P. (2012). Oxygen Transfer in a Fluctuating Capillary Fringe. *Vadose Zone Journal*, *11*(3). https://doi.org/10.2136/vzj2011.0056

Hefting, M., Clément, J. C., Dowrick, D., Cosandey, A. C., Bernal, S., Cimpian, C., et al. (2004). Water table elevation controls on soil nitrogen cycling in riparian wetlands along a European climatic gradient. *Biogeochemistry*, *67*(1), 113–134. https://doi.org/10.1023/B:BIOG.0000015320.69868.33

Heinen, M. (8/2006). Simplified denitrification models: Overview and properties. *Geoderma*, *133*(3-4), 444–463.

Ho, M. D., McCannon, B. C., & Lynch, J. P. (2004). Optimization modeling of plant root architecture for water and phosphorus acquisition. *Journal of Theoretical Biology*, *226*(3), 331–340.

Jost, D., Winter, J., & Gallert, C. (2010). Distribution of aerobic motile and non-motile bacteria within the capillary fringe of silica sand. *Water Research*, *44*(4), 1279–1287. https://doi.org/10.1016/j.watres.2010.01.001

Laio, F., Tamea, S., Ridolfi, L., D'Odorico, P., & Rodriguez-Iturbe, I. (2009). Ecohydrology of groundwater-dependent ecosystems: 1. Stochastic water table dynamics. *Water Resources Research*, *45*(5), n/a-n/a. https://doi.org/10.1029/2008WR007292

Manzoni, S., Porporato, A., D'Odorico, P., Laio, F., & Rodriguez-Iturbe, I. (2004). Soil nutrient cycles as a nonlinear dynamical system. *Nonlin. Processes Geophys.*, *11*(5/6), 589–598. https://doi.org/10.5194/npg-11-589-2004

Manzoni, Stefano, & Porporato, A. (2009). Soil carbon and nitrogen mineralization: Theory and models across scales. *Soil Biology and Biochemistry*, *41*(7), 1355–1379. https://doi.org/10.1016/j.soilbio.2009.02.031

McLaughlin, D. L., Kaplan, D. A., & Cohen, M. J. (2014). A significant nexus: Geographically isolated wetlands influence landscape hydrology. *Water Resources Research*, *50*(9), 7153–7166. https://doi.org/10.1002/2013WR015002

Mein, R. G., & Larson, C. L. (1973). Modeling infiltration during a steady rain. *Water Resources Research*, *9*(2), 384–394. https://doi.org/10.1029/WR009i002p00384

Naumburg, E., Mata-Gonzalez, R., Hunter, R. G., McLendon, T., & Martin, D. W. (2005). Phreatophytic vegetation and groundwater fluctuations: a review of current research and application of ecosystem response modeling with an emphasis on great basin vegetation. *Environmental Management*, *35*(6), 726–740.

Ng, H. Y. F., Tan, C. S., Drury, C. F., & Gaynor, J. D. (2002). Controlled drainage and subirrigation influences tile nitrate loss and corn yields in a sandy loam soil in Southwestern Ontario. *Agriculture, Ecosystems & Environment*, *90*(1), 81–88. https://doi.org/10.1016/S0167-8809(01)00172-4

Parton, W. J., Mosier, A. R., Ojima, D. S., Valentine, D. W., Schimel, D. S., Weier, K., & Kulmala, A. E. (1996). Generalized model for N2 and N2O production from nitrification and denitrification. *Global Biogeochemical Cycles*, *10*(3), 401–412.

Porporato, A., D'Odorico, P., Laio, F., & Rodriguez-Iturbe, I. (2003). Hydrologic controls on soil carbon and nitrogen cycles. I. Modeling scheme. *Advances in Water Resources*, *26*(1), 45–58.

Pronk, G. J., Mellage, A., Milojevic, T., Smeaton, C. M., Engel, K., Neufeld, J. D., et al. (2020). Carbon turnover and microbial activity in an artificial soil under imposed cyclic drainage and imbibition. *Vadose Zone Journal: VZJ*, *19*(1). https://doi.org/10.1002/vzj2.20021

Reverey, F., Grossart, H.-P., Premke, K., & Lischeid, G. (2016). Carbon and nutrient cycling in kettle hole sediments depending on hydrological dynamics: a review. *Hydrobiologia*, *775*(1), 1–20. https://doi.org/10.1007/s10750-016-2715-9

Rodriguez-Iturbe, I., Porporato, A., Ridolfi, L., Isham, V., & Coxi, D. R. (1999). Probabilistic modelling of water balance at a point: the role of climate, soil and vegetation. In *Proceedings of the Royal Society of London A: Mathematical, Physical and Engineering Sciences* (Vol. 455, pp. 3789–3805). The Royal Society.

Rühle, F. A., Netzer, F. von, Lueders, T., & Stumpp, C. (2015). Response of Transport Parameters and Sediment Microbiota to Water Table Fluctuations in Laboratory Columns. *Vadose Zone Journal*, *14*(5). https://doi.org/10.2136/vzj2014.09.0116

Salvucci, G. D., & Entekhabi, D. (1994). Explicit expressions for Green-Ampt (delta function diffusivity) infiltration rate and cumulative storage. *Water Resources Research*, *30*(9), 2661–2663. https://doi.org/10.1029/94WR01494

Smith, W., Grant, B., Qi, Z., He, W., VanderZaag, A., Drury, C. F., & Helmers, M. (2020). Development of the DNDC model to improve soil hydrology and incorporate mechanistic tile drainage: A comparative analysis with RZWQM2. *Environmental Modelling & Software*, *123*, 104577.

Szymczycha, B., Kroeger, K. D., Crusius, J., & Bratton, J. F. (2017). Depth of the vadose zone controls aquifer biogeochemical conditions and extent of anthropogenic nitrogen removal. *Water Research*, *123*, 794–801. https://doi.org/10.1016/j.watres.2017.06.048

Tamea, S., Laio, F., Ridolfi, L., D'Odorico, P., & Rodriguez-Iturbe, I. (2009). Ecohydrology of groundwater-dependent ecosystems: 2. Stochastic soil moisture dynamics. *Water Resources Research*, *45*(5), n/a-n/a. https://doi.org/10.1029/2008WR007293

Wang, J., Bogena, H. R., Vereecken, H., & Brüggemann, N. (2018). Characterizing Redox Potential Effects on Greenhouse Gas Emissions Induced by Water-Level Changes. *Vadose Zone Journal*, *17*(1). https://doi.org/10.2136/vzj2017.08.0152

Winter, J., Ippisch, O., & Vogel, H.-J. (2015). Dynamic Processes in Capillary Fringes. *Vadose Zone Journal*, *14*(5), 0. https://doi.org/10.2136/vzj2015.04.0059

Chapter 6

Conclusions and Perspectives

6.1 Summary of Major Contributions

The work presented in this thesis explored multiple reactive interfaces across different spatiotemporal scales to further our understanding of the controls and functionality of reactive interface behaviour.

The first research objective was to quantify the role of wetlands in retaining nitrogen across the United States. Through the use of novel spatial datasets of N surplus and wetland locations, I showed that wetlands retain approximately 860 ktons of N/yr in the US. Here, I further demonstrated that there was a large spatial disconnect between N sources (e.g. agricultural hotspots) and N sinks (wetlands), which resulted in lower estimates of total N retention compared to previous studies that did not have such spatial resolution in their models. Simulating different management strategies, this work also showed the value of restoring wetlands in the landscape specifically in locations of high N surplus – a 10% increase in existing wetland area would double current wetland N removal, and provide nearly 40 times more N removal than the scenario with random wetland restoration and agricultural land protection.

The second research objective focused on quantifying how wetland size and climate interact to modulate the retention of N. In this chapter, I used a novel approach of incorporating remotely sensed wetland extent data with a coupled hydrologic-N retention model to quantify the wetland N retention across eight different wetlandscapes in the US. I showed that incorporating transient hydrologic conditions can increase N retention estimates compared to the steady-state models that are commonly used at watershed scales. This effect was more apparent in smaller, isolated wetlands, and in drier climates, where the lower fraction of outflow limited the loss of N and increased the time for denitrification in the wetland.

The third research objective was to quantify the role of the hyporheic zone (HZ) on the spatiotemporal persistence of estrogens in an agricultural stream. Here, I developed a new deterministic contaminant transport model for estrogen in the stream-HZ system. The model showed that the temporal persistence of estrogens in the stream increases with more interaction with the hyporheic zone. The HZ acts as a temporary storage for sorbed estrogen and inhibits photodegradation during high loading events, and can then act as an internal source in the stream during low loading periods.

Finally, the fourth objective was to develop a coupled carbon-nitrogen model that focuses on the interactions between the water table and the nutrient cycles. We show how consideration of water table fluctuations can heavily influence the redox sensitive processes in the C-N cycles, and change the export of nitrogen in its aqueous and gaseous forms.

6.2 Future Research Directions

Reactive interfaces are increasingly recognized as ‘nature-based solutions’ that can help modulate agricultural contaminants and increase the water quality of the landscape. While interest in the construction, management, or restoration of these ecosystems increases, there is still a need to understand how these reactive interfaces behave under different conditions and how best to optimize their functionality. Here, I will list some possible extensions of my current work:

Wetlands and Wetlandscapes

Within this thesis, we focus on how several wetland characteristics affect their ability to retain N: size, proximity to N sources, and water partitioning (as driven by climate and size). However, there

remains many other wetland characteristics that could affect N retention in wetlands. For example, watershed position, extreme flow events (e.g. fill and spill dynamics), synchronicity of seasonal hydrologic and biogeochemical processes, are all factors that should be explored at watershed scales to better inform the management and protection of the wetlandscape.

While wetlands provide myriad hydrologic, biogeochemical, and ecological benefits, different wetlands provide different benefits. In this thesis, I focus primarily on the water quality benefits of wetlands, but relatively little work has focused on the tradeoffs between optimal wetland functions (e.g. N retention vs. flood buffering vs. greenhouse gas emissions). A direct extension of my current work would be to couple the models of several different wetland functions. These coupled models can be used to explore if there exists wetland types that can provide multiple ecosystem benefits, or what combination of wetland types should be protected/restored within the wetlandscape.

Of course, nitrogen is not the only agricultural contaminant of concern. For example, phosphorus is another common contaminant that wetlands can retain but the relative controls of P retention remain uncertain. The development of parallel analyses to the work in this thesis could provide further insight on how wetlands affect P cycling in the landscape. Additionally, there would also be an opportunity to combine these models to better understand how different wetlands modify N:P ratios.

Hyporheic Zones as Sources

The model developed in this thesis focused on simplistic boundary conditions to better understand the effects of point source loading from a tile drain or upstream loading. In reality, estrogens can enter the stream network through overland flow as a distributed load, which can have additional effects on the spatiotemporal dynamics of estrogen in the stream. Further refinements to the modelling framework could be added to account for this non-point source loading, as well as building up a river network model. These modifications would be useful for quantifying the cumulative effect of estrogen contamination within a watershed, where multiple source zones and pathways exist.

Finally, estrogens have many similarities to other redox sensitive and multi-phase agricultural contaminants such as other steroidal hormones, pesticides, and phosphorus. The modelling framework developed here can be translated to these other contaminants to quantify how the source-sink behaviour of the hyporheic zone can affect their persistence in the stream network. This

knowledge is essential as the presence of these contaminants downstream can have severe ecological effects (e.g. development of algal blooms due to P, developmental issues of downstream fish due to prolonged exposure to steroidal hormones).

Appendices

Appendix A

Supplemental Information for Chapter 2

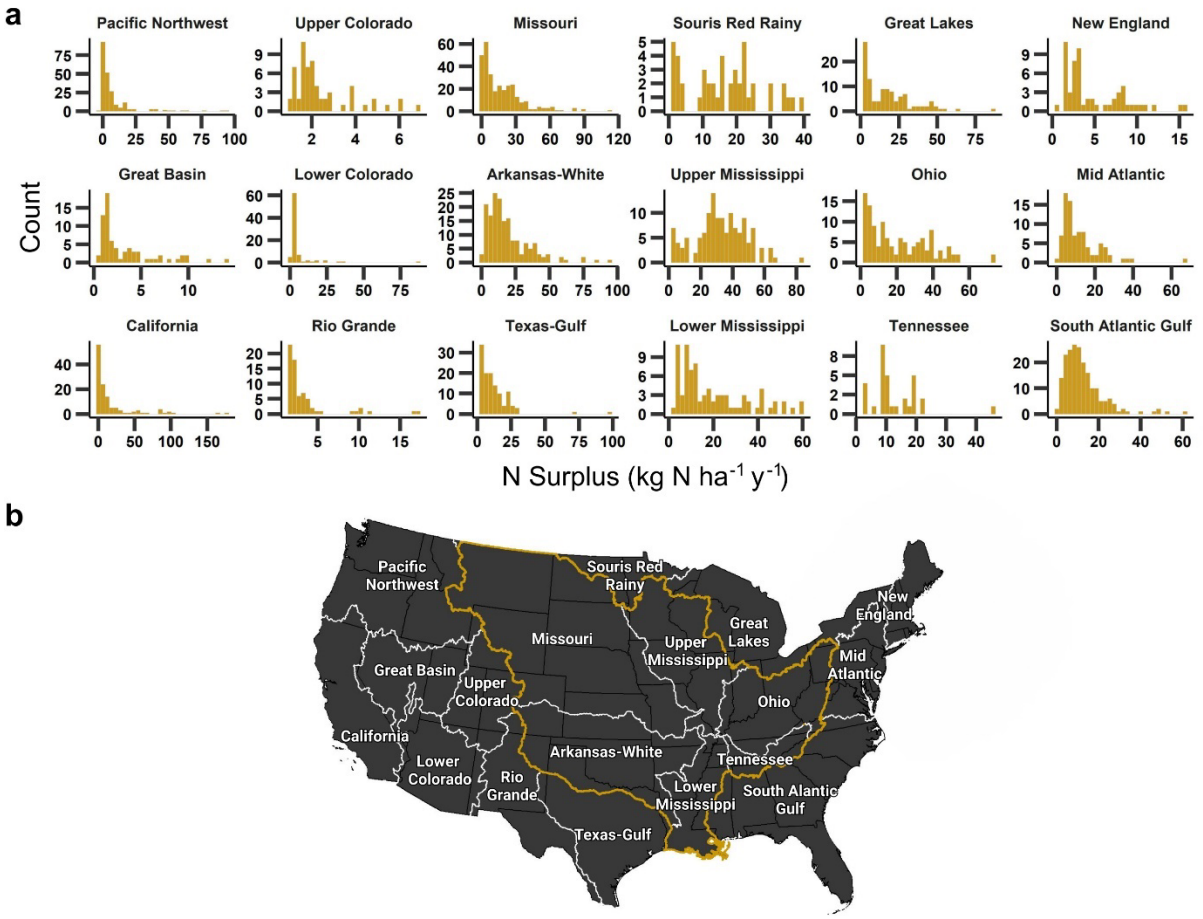

Extended Data Fig. 1 | Nitrogen surplus distributions across the U.S. hydrologic regions. (**a**) Histograms of N surplus by hydrologic region. The counts in the histograms refer to individual HUC-8 watersheds within the hydrologic regions. (**b**) Map of hydrologic regions defined by the U.S. Geological Survey. Boundaries of the Mississippi River Basin are drawn in yellow.

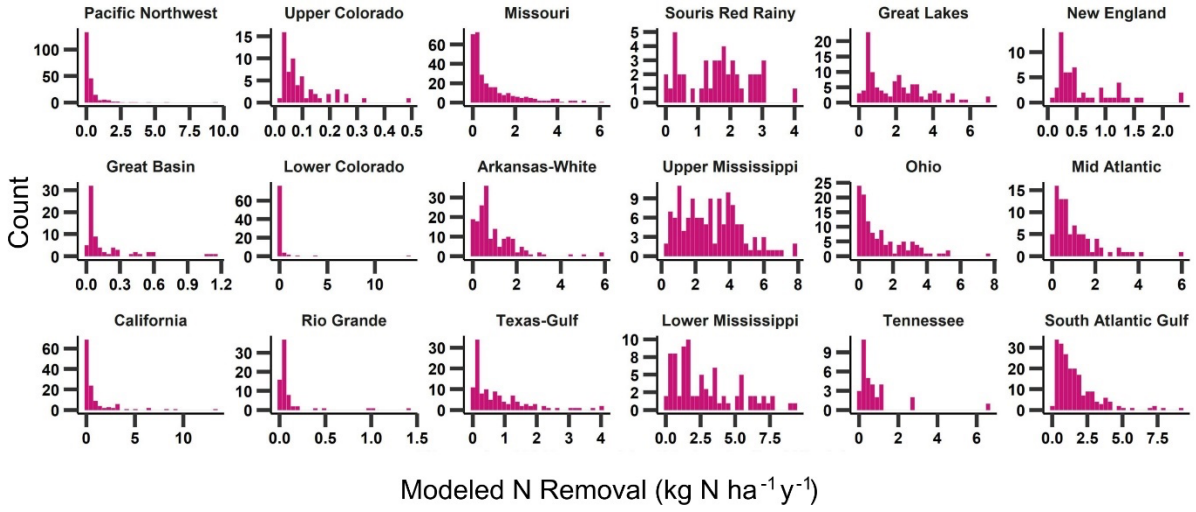

Extended Data Fig. 2 | Histograms of modeled N removal by hydrologic region. The counts in the histograms refer to individual HUC-8 watersheds within the hydrologic regions. See **Extended Data Fig. 1b** for region locations

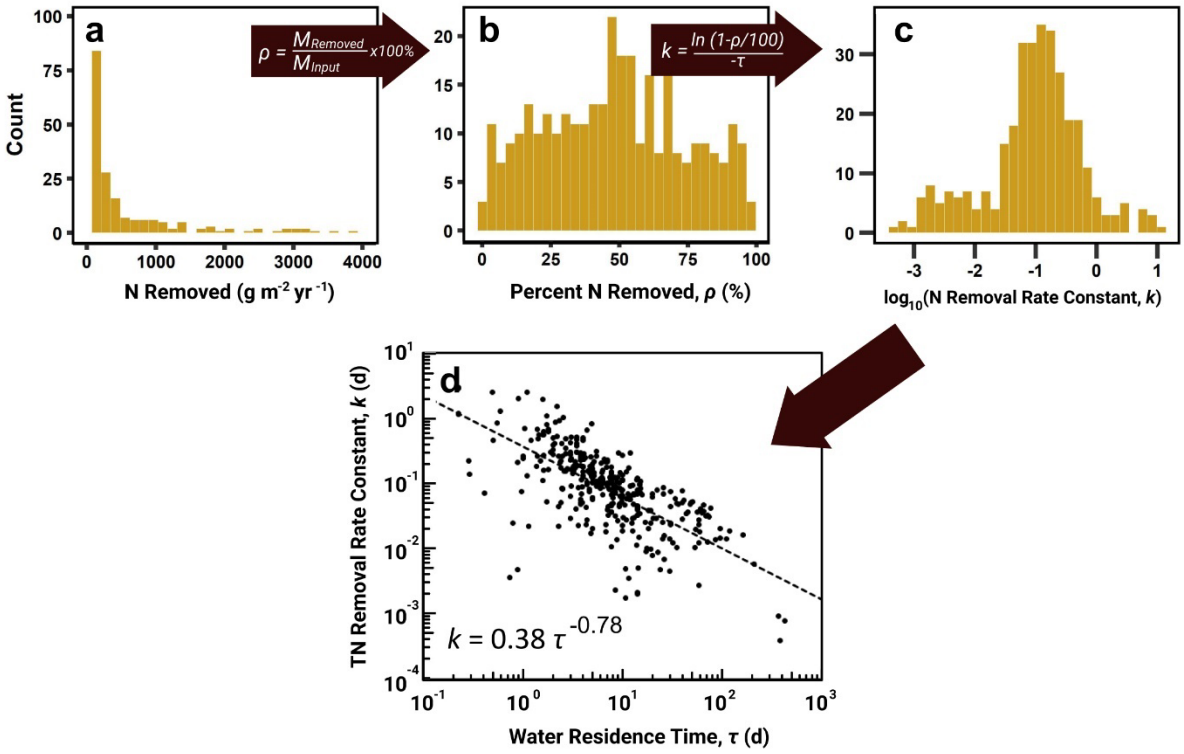

Extended Data Fig. 3 | Analysis of empirical data used by Cheng and Basu (2017) to develop the k-τ relationship used in our study. (a) Histogram of N removed at the individual wetland scale. Data were obtained from a global meta-analysis of 178 wetlands; (b) N removal efficiency, $\boldsymbol{\rho}$, calculated as the ratio between N removal and N inputs to the wetland; (c) N removal rate constant k [T^{-1}] estimated as a function of $\boldsymbol{\rho}$ and empirically based estimates of wetland residence times, τ [T], assuming that N removal within the wetland follows first-order kinetics; (d) A strong inverse relationship was found between k and wetland residence time τ. This relationship between size and N removal rate constants allows us, in the current work, to more accurately upscale to the continental scale than has previously been achieved.

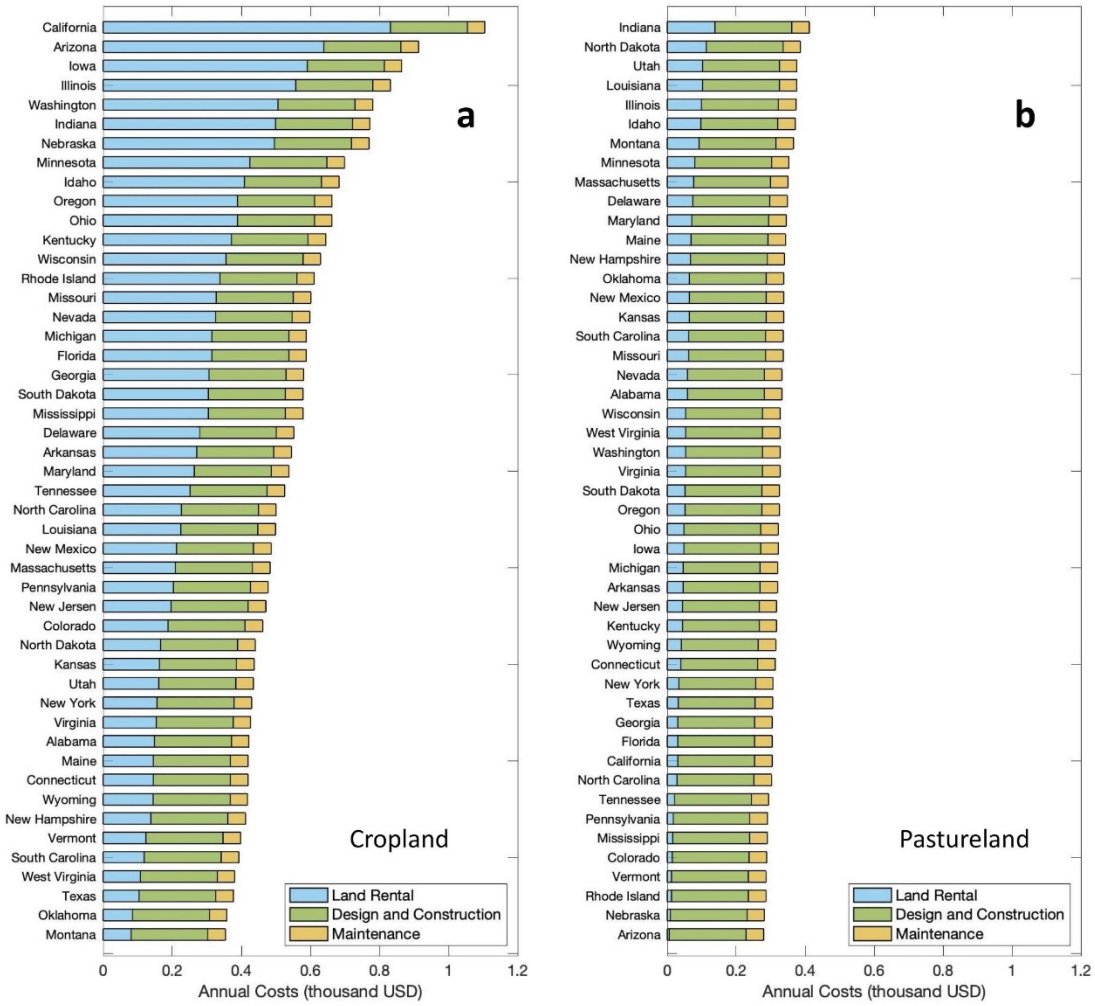

Extended Data Fig. 4 | Costs of wetland restoration. Estimated costs for restoration of a 1-hectare wetland in 48 states across the contiguous U.S. on (a) cropland and (b) pastureland. While construction and maintenance costs are considered to be constant across states, land rental costs vary by state and by land use. Costs are annualized over a 50-year management horizon.

Extended Data Table 1 | N surplus and wetland N removal magnitudes for a subset of nitrate-impacted watersheds. Note that the estimated wetland N removal rates, normalized by wetland area (kg ha^{-1} y^{-1}), reported here are approximately an order of magnitude lower than the measured wetland N removal rates from empirical meta-analyses (Extended Data Fig. 3). This difference arises because the studied wetlands have higher N inputs than those typical of many wetlands across the country due to the spatial disconnect between N source areas and wetland dense regions (Fig. 3). The targeted restoration scenarios presented are for a 10% increase in wetland area across the U.S. Uncertainty bounds for additional wetland N removal from targeted restoration scenario based on 95% confidence interval from Monte Carlo analysis.

Watershed Name	Drainage Area (km^2)	Landscape N Surplus (ktons y^{-1})	Riverine N Load (ktons y^{-1})	Current Wetland Area (km^2)	Current Wetland N Removal (ktons y^{-1})	Current Wetland N Removal (% of N Surplus)	Current Wetland N Removal (% of Riverine N Load)	Current Area-normalized Wetland N Removal (kg ha^{-1} y^{-1})	Targeted Restoration Scenario, Additional Wetland N Removal (ktons y^{-1})	Targeted Restoration Scenario, Additional Wetland N Removal (% of Riverine N Load)
Mississippi River (St. Francisville)	2,935,570	6,117	868	145,324	322	5%	37%	22.1	467 ± 239	54%
Ohio River (Dam 53)	527,424	1,093	298	18,286	47	4%	16%	25.8	83 ± 41	28%
Susquehanna River (Congress St. Park)	71,221	135	46	2,195	4	3%	10%	20.5	9.9 ± 4.8	22%
Illinois River (Valley City)	68,820	222	104	3,022	10	5%	10%	33.7	9.3 ± 6.4	9%
Maumee River (Waterville)	16,275	82	29	899	4	5%	13%	42.1	7.0 ± 3.6	24%
Iowa River (Wapello)	32,386	162	57	1,363	6	4%	11%	45.6	5.4 ± 2.6	10%

Extended Data Table 2 | Ranges of parameters used in the Monte Carlo simulations of wetland N removal. Ranges for parameters in Eqs. 3 and 4 are based on 95% confidence intervals around fitted parameters.[3] Range for wetland catchment ratios is obtained from the geometric standard deviation around a geometric mean based on calculated ratios from more than 30,000 wetlands.[43] Range for the proportion of N surplus reaching wetlands is based on literature values.[2,52]

Variable	Range	Reference
Constant in SA-τ relationship (a in Eq.3)	1.48 to 1.62	*(3)*
Exponent in SA-τ relationship (b in Eq.3)	0.21 to 0.25	*(3)*
Constant in τ-k relationship (c in Eq.4)	0.31 to 0.45	*(3)*
Exponent in τ-k relationship (d in Eq.4)	-0.86 to -0.7	*(3)*
Wetland catchment-wetland area ratio	3 to 20	*(43)*
Proportion of N surplus reaching wetlands	0.3 to 0.5	*(2, 52)*

Appendix B
Supplemental Information for Chapter 4

Introduction

The supporting information here contains Text 1 (Flow-Velocity relationships), Table S1 (results from sensitivity analysis), and Figure S1 (Exceedance plots of seasonal flow)

Text S1.

Flow measurements were taken at ASREC and converted to average velocity values based on site-specific flow-stage-velocity relationships (Sassman, 2014). The data showed significantly lower flows between June and October compared to the rest of the year at ASREC (Figure S1), and thus we separated the year into the low-flow season (late-June to mid-October) and the high-flow season (January to late-June and mid-October to December). To ensure numerical stability, we chose to use the mean velocity for each season rather than having a time-varying velocity component in the model. Channel flow (Q, ft^3/s) as a function of velocity (V, ft/s) is described as (Sassman, 2014):

$0.35 < V < 1.6$: $\quad V = \dfrac{Q + 22.3}{6}$

$V \geq 1.6$: $\quad V = \dfrac{Q + 445.6}{278}$

Table S1. Percent change in estrogen mass in sediment from base case using a 10% perturbation of parameters

	E2 Mass in Sediment		E1 Mass in Sediment	
	-10% Perturbation	**+10% Perturbation**	**-10% Perturbation**	**+10% Perturbation**
V	-1.70	1.70	-0.66	0.67
D	-0.05	0.05	-0.05	0.05
α	-0.42	0.43	0.23	-0.21
A/As	9.18	-7.50	11.12	-9.09
$k_{d,E2}$	-1.05	0.87	0.45	-0.38
$k_{d,E1}$	0.00	0.00	-1.22	1.03
S	-0.62	0.57	-0.66	0.64
k_{sed}	-0.60	0.55	-0.66	0.64
$k_{E2,MC}$	0.41	-0.40	0.01	-0.01
$k_{E2,HZ}$	0.68	-0.67	-0.41	0.41
$k_{E2,HZ}$	0.00	0.00	0.74	-0.64
$k_{E1,HZ,F}$	0.00	0.00	0.08	-0.08

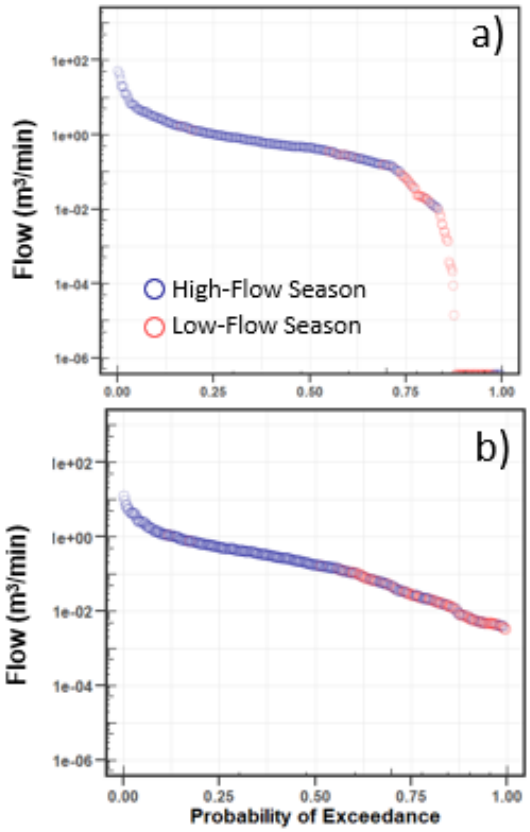

Figure S1. Probability of exceedance curve for flow in the (a) stream and (b) tile drain showing distinct flow regimes in the growing (high-flow) season between July to mid-October and non-growing (low-flow) season between mid-October to June.

Appendix C
Repositories for Data and Model Code

Chapter 2 Repository

Nitrogen mass balance data was obtained from the TREND-nitrogen dataset, available through the PANGAEA Data Publisher. The National Wetlands Inventory dataset was retrieved from the US-FWS (fws.gov/wetlands). The Watershed Boundary Dataset used for HUC-8 boundaries was retrieved from the U.S. Geological Survey website (usgs.gov/core-science-systems/ngp/ngtoc/watershed-boundary-dataset). U.S. Geological Survey water quality data were retrieved from Oelsner, G.P. et al. 2017. "Water-Quality Trends in the Nation's Rivers and Streams, 1972–2012—Data Preparation, Statistical Methods, and Trend Results." *Scientific Investigations Report*. https://doi.org/10.3133/sir20175006.

The MATLAB software used for the present analysis is available from Mathworks (https://www.mathworks.com/); R (version 3.5.2) used for geospatial analysis is available from the R Core Team (https://www.r-project.org/). Code for the estimation of current wetland N removal, wetland restoration scenarios and cost analysis are available at https://github.com/landscape-ecohydrology/optimizing_wetland_restoration_in_nature

Chapter 4 Repository

Datasets for this research can be found in these in-text data citations: Gall et al., 2011, Gall et al., 2015, Gall et al., 2016. The base code for the model can be found at https://github.com/landscape-ecohydrology/stream-hormone-persistence

Note that Chapters 3 and 5 have not been published and do not have a public repository yet. Code and data can be made available upon request, or with the future published articles.